HAL
open science

Pre-breakdown and breakdown phenomena in air along insulating solids

Laure Tremas

To cite this version:

Laure Tremas. Pre-breakdown and breakdown phenomena in air along insulating solids. Electric power. Université Grenoble Alpes, 2017. English. NNT : 2017GREAT117 . tel-03825751

HAL Id: tel-03825751

https://theses.hal.science/tel-03825751v1

Submitted on 23 Oct 2022

HAL is a multi-disciplinary open access archive for the deposit and dissemination of scientific research documents, whether they are published or not. The documents may come from teaching and research institutions in France or abroad, or from public or private research centers.

L'archive ouverte pluridisciplinaire **HAL**, est destinée au dépôt et à la diffusion de documents scientifiques de niveau recherche, publiés ou non, émanant des établissements d'enseignement et de recherche français ou étrangers, des laboratoires publics ou privés.

Communauté
UNIVERSITÉ Grenoble Alpes

THÈSE

Pour obtenir le grade de

DOCTEUR DE LA COMMUNAUTE UNIVERSITE GRENOBLE ALPES

Spécialité : **Génie Electrique**

Arrêté ministériel : 25 mai 2016

Présentée par

Laure TREMAS

Thèse dirigée par **Olivier LESAINT**
codirigée par **Nelly BONIFACI**

préparée au sein du **G2Elab**
dans **l'École Doctorale EEATS**

Pre-breakdown and breakdown phenomena in air along insulating solids

Thèse soutenue publiquement le **04/12/2017**,
devant le jury composé de :

M. Emmanuel ODIC
Professeur à SUPELEC, Paris, Rapporteur
M. Eric MOREAU
Professeur à l'Université de Poitiers, Rapporteur
M. Serge AGNEL
Professeur à l'Université Montpellier 2, Président
M. Olivier LESAINT
Directeur de recherche au CNRS-G2Elab, Directeur de thèse
Mme. Nelly BONIFACI
Chargé de recherche au CNRS-G2Elab, Co-Encadrant de thèse
Mme. Brigitte OHL
Ingénieur de recherche à Schneider Electric, Examinateur

Remerciements

Je tiens d'abord à remercier toutes les personnes qui m'ont accompagnée pendant ces trois ans au G2Elab. Plus particulièrement mon directeur de thèse Olivier Lesaint qui m'a toujours encadrée avec beaucoup de patience et m'a beaucoup appris. Je tiens également à remercier Nelly Bonifaci qui a toujours été là pour moi que ce soit scientifiquement ou moralement. Je n'oublierai jamais les journées passées ensemble au CNRS dans la cage de Faraday. Sans l'œil de Nelly mes travaux n'auraient pas pu avancer si vite !
Merci également à tous les doctorants pour les pauses et les moments passés ensemble : Priscillia, Clara, Raphaël, Nathan, Joko, Florian et sans oublier Rachelle (doctorante de cœur).
Merci à Julien, Jean-Paul, Jean-Luc et Christophe pour leurs disponibilités.

Je remercie également les personnes qui m'ont accompagnée chez Schneider Electric. Un grand merci à Brigitte Ohl qui a su me guider tout en m'apportant tout le soutien nécessaire lors de ces trois années. Merci pour toutes les connaissances que j'ai pu acquérir à tes côtés ainsi que ta bienveillance.
Je voudrais particulièrement remercier Giovanni et Yvon pour avoir réalisé un grand nombre de mes échantillons.
Merci à l'équipe matériaux : Florence, Delphine, Clémence, Patrice, Stéphane, Yara, Vincent, David, Marie, Marie-Hélène, Laurent ainsi que Marilyn.
Merci aux personnes qui m'ont accompagnée scientifiquement au cours de ces trois années : François, Romain, Abdou, Mehrdad et Raimmund.

Merci tout particulièrement à ma famille et mes amis.

A mes parents et ma sœur pour leur soutien pendant mes longues études et leurs conseils. Je tiens également à remercier ma grand-mère d'avoir toujours été présente. Merci à Vikas d'avoir partagé ces trois années intenses avec moi.

A mes amis pour tous ces moments passés ensemble : Lucie et Quentin, Evan, Thomas, Marine, Tagaroa, Frédéric, Laurence et Max.

Et plus particulièrement :
Elodie pour toutes nos aventures/voyages (on n'oubliera pas l'épisode Air Caraïbes) et pour ton soutien inconditionnel au fil des années.
Inès pour être restée à Grenoble avec moi (j'aurais été perdue sans toi !) et à qui je peux toujours me confier. Et bien sûr pour nos folles séances de gym !

Contents

Introduction **5**

Chapter 1: State of the art for creeping discharge over solid insulator **8**

1. Context 9
    1.1. Electrical network 9
    1.2. Insulation test methods and device validation 10
    1.3. Insulating materials 11
    1.4. Problem associated with the use of solid insulators 13
2. Discharges in gas 15
    2.1. Townsend avalanche process 15
    2.2. Paschen's law 16
    2.3. Streamers 17
    2.4. Transition to breakdown 20
3. Creeping discharges on a dielectric surface 22
    3.1. Physical processes induced by the presence of an insulating solid 23
    3.2. Main features of pre-breakdown phenomena in the presence of solids 25
    3.3. Breakdown measurements with insulating surfaces 29
4. Conclusions and outline of the Ph.D. 33

Chapter 2: Insulating solids: selection and characterization **42**

1. Selection of the solids 43
    1.1. Material of reference for Schneider Electric 45
    1.2. New materials 46
    1.3. Materials with various relative permittivity 47
2. Dielectric characterization 51
    2.1. Determination of the relative permittivity of solids 51
    2.2. Surface charges on solids: Surface Potential Decay characterization 55
    2.3. Absorption current measurements 62
3. Conclusion 71

Chapter 3: Influence of solid's nature on breakdown voltage 75

1. Introduction 76
2. Experimental setup for breakdown measurements 78
   2.1. General presentation 78
   2.2. Test cells 81
   2.3. Electrode systems 82
   2.4. Field calculations 84
3. Experimental protocol used for breakdown measurements 87
   3.1. High voltage impulse shape 87
   3.2. Breakdown procedure 87
4. Preliminary breakdown measurements: choice of the adequate electrode system 92
   4.1. Point-plane electrode system 92
   4.2. Gap between electrodes 94
   4.3. Polarity of the impulse 95
   4.4. Influence of pressure, comparison with $SF6$ 95
5. Breakdown measurements 96
   5.1. Parallel field configurations 97
   5.2. Perpendicular field configuration 106
6. Conclusion 110

Chapter 4: Pre-breakdown streamers: study of initiation and sequence of events leading to breakdown 113

1. Experimental setup 114
   1.1. Transient current measurements 114
   1.2. Surface charge measurements 115
2. Characterization of pre-breakdown streamers 116
   2.1. Parallel field, positive polarity, and atmospheric pressure 116
   2.2. Parallel field, positive polarity, and pressure up to 0.3 MPa 121
   2.3. Perpendicular field, positive polarity, and atmospheric pressure 125
   2.4. Parallel field, negative polarity, and atmospheric pressure 126
   2.5. Influence of solid permittivity on the transition to breakdown 127
3. Investigations on streamer initiation in the presence of solids 128
   3.1. Measurement procedure 128
   3.2. Ambient air 128

3.3. Comments about streamer inception in ambient air 130
3.4. Epoxy/Silica 131
3.5. Discussion about streamer inception with Epoxy/Silica solid 131
3.6. Others materials: PPA, PC, Epoxy resin 133
3.7. Polypropylene (PP), polytetrafluoroethylene (PTFE) 136
3.8. Comments about measurements in PP 137
3.9. Influence of the contact between electrode and solid 138
3.10. Influence of pressure 139
3.11. Correlation with breakdown measurements 142
4. Evidence of charges remaining on the solid surface after discharges 143
4.1. Field probe 143
4.2. Surface potential probe 144
4.3. Discussion about influence of surface charges 147
5. Conclusion 148

Conclusions and Perspectives 152
List of publications during Ph. D. work 156
Annex 1 158
Drying procedure 158
Impregnation procedure 159
Differential Scanning Calorimetry (DSC) 160
Thermal Gravimetric Analysis (TGA) 162
Annex 2 166

Introduction

This work takes place within the problematics of SF_6 replacement in medium voltage devices. SF_6 is a gas showing excellent dielectric properties (its breakdown voltage is about three times higher compared to air), of very wide use in high voltage systems, either for the dielectric insulation, or for current interruption in circuit breakers. Unfortunately, SF_6 is the strongest greenhouse gas and it needs to be replaced in medium voltage apparatus in the coming years. Among the different gases which could be used as good substitutes for SF_6 , compressed air can be an acceptable alternative in several cases. Indeed, very different discharge phenomena occur when SF_6 is replaced by other gases, and consequently the design rules must be adapted and redefined accordingly.

The dielectric withstand of the apparatus is directly dependent on the gas nature and pressure used. The dielectric behavior of pure gases was established a long time ago. However, it is known that the weak points in practical systems are not related to the gas alone, but rather to its combination with insulating solids. At the interface between gas, dielectric solid, and metal (called “triple point”), the initiation of discharges is favored. It is also generally accepted that the propagation of discharges is favored along dielectric surfaces (“creeping discharges”). A number of studies were devoted to these problems, but several questions still remain without answers, such as the influence of the solid nature on these phenomena, or the sequence of pre-breakdown phenomena when conditions (e.g. field geometry, gas pressure) are changed. Such data are essential for the design of new medium voltage devices built with alternative gases. In addition, there exists also today a perspective to replace standard insulating materials (such as Epoxy/Silica composites) by new materials with enhanced properties. In addition to experimental studies, numerical simulations of discharge initiation and propagation along solids were developed. However, these models are still unable to predict breakdown over a wide range of conditions, since physical phenomena involved during the initiation and propagation of creeping discharges remain insufficiently characterized and understood. In a number of situations, the design of devices using new materials is still based on experimental investigations.

To this end, it remains necessary to work on the problematics of triple points, creeping discharges, and breakdown phenomena, especially by investigating a large range of insulating materials. This constitutes the main purpose of this thesis. This question will be addressed mainly experimentally, since no model is able today to predict the behavior of creeping discharges on a particular material. Experiments will include a detailed study of steps leading to breakdown under impulse voltage (“pre-breakdown” phenomena).

It will be also essential to properly characterize solid materials, in order to understand the influence of parameters such as permittivity, water content, or surface charges, on discharge and breakdown phenomena. Several materials properties will be investigated prior to the study of creeping discharges.

In *Chapter 1,* we will review several aspects related to creeping discharges: basic physics of discharges in air, previous observations about creeping discharges. Compared to the case of a discharge developing in air alone, the presence of an insulating solid induces several effects, that may influence both the initiation of the discharge (modification of the field geometry at the triple junction gas/metal/insulating solid), and its propagation when the discharge creeps on the solid.

In *Chapter 2*, several materials will be selected, described and characterized to highlight some properties supposed to have an influence on the creeping discharge process: permittivity, conductivity, presence of water, ability to store or dissipate surface charges.

In *Chapter 3*, the objective will be first to get a better knowledge of the influence of solid's nature on breakdown voltage, because it represents a key point for the design and reliability of medium voltage apparatus. We will mainly consider here the influence of solids on discharge propagation and transition to breakdown. Therefore, the experimental conditions will be first defined in order to get results relevant for this objective.

Finally, in *Chapter 4*, we will study pre-breakdown phenomena in more details, using transient current measurements and time-resolved visualization. Further investigations will be done in this chapter to better characterize the three different steps of the discharge process leading to breakdown: streamer initiation, propagation, and transition from streamer to breakdown spark. The measurement of transient currents will allow obtaining a better characterization about the influence of the solid nature on discharge initiation.

Chapter 1: State of the art for creeping discharge over solid insulator

In this chapter, we will first introduce the context of this work with the problematic of insulation defects due to triple points in medium voltage apparatus. We will focus on the discharge development in gas involving the presence of insulating solids. The creeping discharge phenomenon will be studied from its inception, propagation, and up to the transition to breakdown. From all these elements, we will finally be able to define the objectives of our work.

1. Context

1.1. Electrical network

1.1.1. Overall presentation

The electrical network is used to deliver electricity from a main producer (nuclear, hydro-electric, …) to consumers. The high voltage transmission lines are used to transport power to the subgenerators or substations (Fig. 1). The medium voltage distribution lines are then used to transport power to the consumers [1]. My work will focus on medium voltage distribution devices such as switchgears (up to 50 kV).

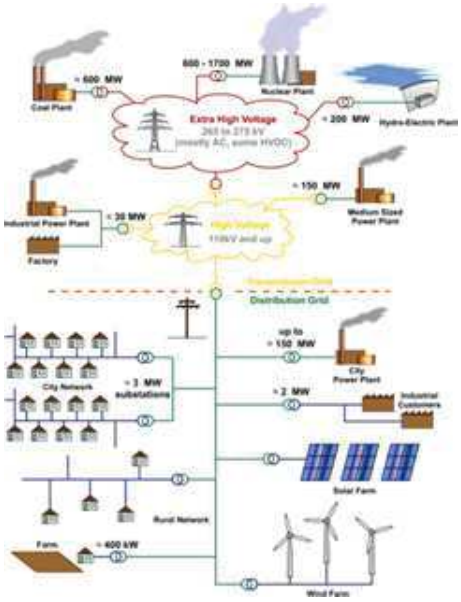

Fig. 1: Diagram of global electricity network [2].

1.1.2. Switchgears

This section will present different types of switchgears produced by Schneider Electric in medium voltage, and concerned by this study (Fig. 2). A switchgear has different functions: isolate the equipment, divide large networks into sections for repair purposes, reconfigure networks to restore power supplies and control other equipment.

Fig. 2: Schneider Electric product range [3].

A switchgear is composed of several parts (Fig. 3) described below. The basic components are [4]:

- Conductors, required to carrying electrical current. They generate heat due to their internal resistance, and will also be subjected to electromagnetic mechanical forces.
- Insulators, required to providing electrical insulation to earth in order to withstand both the system voltage, and any transient voltages which may be impressed upon the switchgear. The insulation within switchgears is constantly electrically stressed throughout the life of the equipment. The insulation also should withstand mechanical forces transmitted from the conductors.
- Moving contacts.

Fig. 3: Example of medium voltage switchboard [3].

1.2. Insulation test methods and device validation

Electric equipment should resist to normalized electrical shocks and should work for more than thirty years (at 24 kV). Several tests methods permit the validation of equipments. One of them concerns lightning impulse voltage [4].

A lightning impulse generates an over voltage in the system. The insulation of the apparatus must be designed to withstand a fixed minimum voltage without damage, defined as BIL (or Basic Insulation Level). Operating voltage level of surge protecting devices must be lower than the minimum withstanding of the equipment.

The IEEE standard (141/1992 ch. 6.3.2 “Insulation tests and ratings”) specifies that electrical power and distribution apparatus assigned to a given insulation class should be capable of withstanding, without flashover or apparent damage, a 1.2/50 µs full-wave impulse test of specified crest value (Fig. 4).

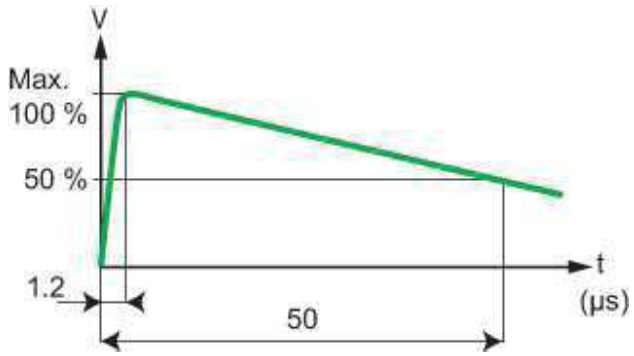

Fig. 4: Normalized lightning wave [5].

1.3. Insulating materials

Solid insulating materials are used to cover conductors, provide support to busbars and other conductors. Epoxy resin is one of the most popular electrical materials used in electrical equipment’s due to its excellent dielectric and mechanical properties. Gases are used to fill compartments in order to provide both insulation, and dry and clean environment.

1.3.1. Problem of the SF_6 replacement

One of the mostly used gases for insulation is SF_6. This gas is remarkably stable with a rapid recombination in case of dissociation by a discharge. The molecule consists of a large central sulphur atoms surrounded by six fluorine atoms. The excellent dielectric withstand of SF_6 gas (3 to 5 times better than air) justifies its wide use for the insulation of extra high-voltage and medium voltage equipment.

Unfortunately, SF_6 is the strongest greenhouse gas (Global Warming Potential: GWP = 22 800), and therefore has a strong contribution to global warming (Fig. 5).

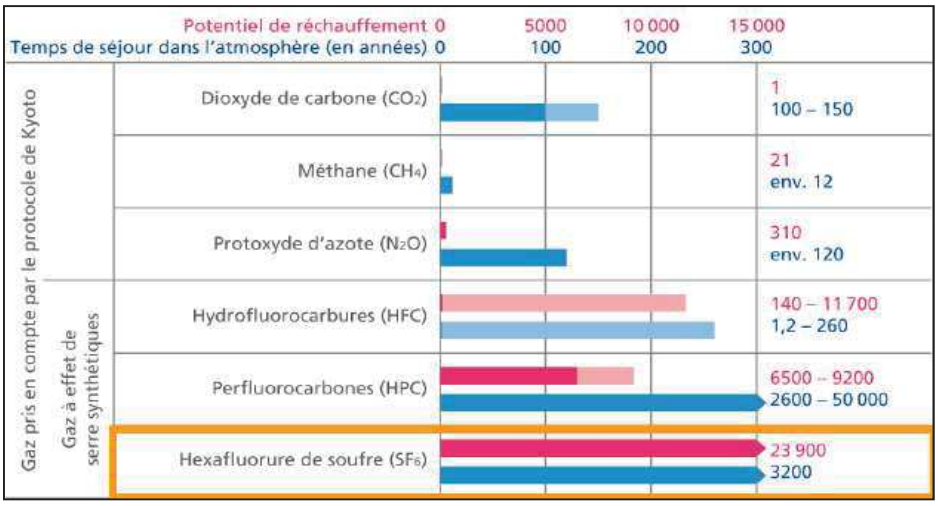

Fig. 5: List of greenhouse gases (Kyoto protocol) [6].

With the coming ban of SF_6 by the European commission because of the non-ecologic properties of the gas, replacement of SF_6 gas became a necessity. However, the substitution of SF_6 by another gas usually induces a reduction of the dielectric withstand.
This problematic constitutes a starting point of our study. Together with the research of new replacement gases (not considered in this study), the design procedures of insulation must be further developed, requiring a better understanding of discharge phenomena occurring at different places in the equipment under impulse voltage. One possible solution for the replacement of SF_6 in several cases is simply the use of compressed air.

1.3.2. Examples of Schneider Electric products concerned by the replacement of SF_6

Tab. 1. shows examples of Schneider Electric's switchgears for medium voltage applications, functions of the apparatus concerned by SF_6 replacement, and corresponding alternative insulation solutions. In several cases, the insulation could be achieved by dry air, which justifies the investigations carried out in this study, which will mainly concern this gas.

Product range	Function of the apparatus concerned by SF_6 replacement	Alternative
SM6 (AIS)	Switch + disconnector	Dry air insulation + vacuum interrupters
FBX, RM6, GMA, GHA and DVCAS (all our GIS/RMU range)	Insulation	Dry air or new gases
SF, LF	Current interruption	Vacuum interrupters

Tab. 1: Examples of Schneider Electric's products concerned by the replacement of SF_6 [3].

1.4. Problem associated with the use of solid insulators

1.4.1. Triple Points (TP)

Triple points (also frequently called “triple junction”) corresponds to the contact region of three materials: solid insulator, gas and conductor. This geometry induces a reinforcement of the local electric field due to the mismatch of permittivities between gas and insulating solid (Fig. 6).

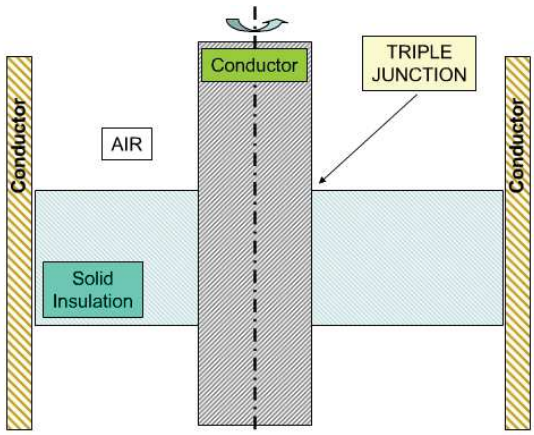

Fig. 6. Representation of the triple junction [7].

At the junction point, equipotential lines are compressed, and spread out to take up their normal positions far of it (Fig. 7). Triple points constitute the main reason for discharge initiation in high voltage systems. Several strategies can be used to minimize, or even suppress, their negative influence on the dielectric withstand of systems.

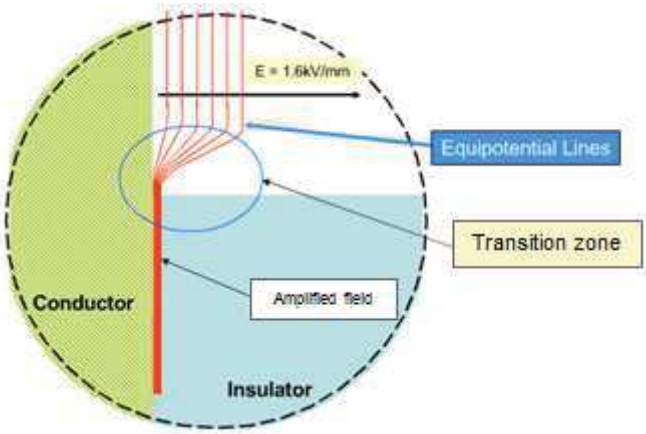

Fig. 7: Visualization of the equipotential lines at the triple junction [7].

1.4.2. Design rules

The design rules are adapted to minimize the electrical field value at treat triple point by optimizing the shape of electrodes and insulators. The optimum design will be the one with

an electrical field close to zero at the triple point. Fig. 8 shows a typical arrangement to "protect" a triple point.

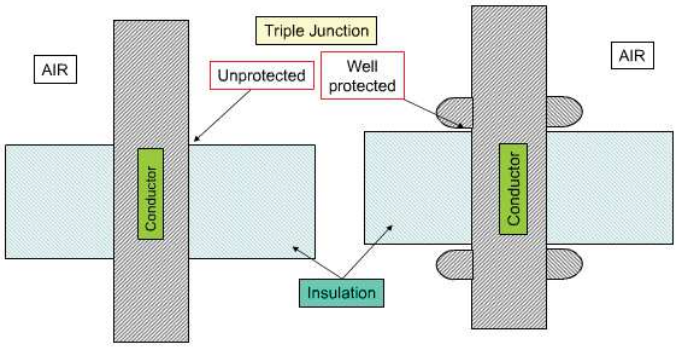

Fig. 8: Protection of the triple point [7].

To be effective the main design rules are described as follows:

- Conductive parts should be as close as possible to triple junctions (but must not touch them);
- The "conducting well" formed must be as deep as possible;
- The well must be as narrow as possible.

Simulations are done before prototyping to compare different design solutions, evaluate the value of the field, design field deflectors and insulator shapes, and detect critical zones. COMSOL™ and Flux 2D/3D™ are examples of softwares frequently used for this purpose.

1.4.3. Surface tracking

Phenomenon of surface tracking appears when discharges creep over insulating solids. A permanent carbonized conductive path is formed on the surface of the solid insulator (Fig. 9), which modifies the electric field distribution, and favors the triggering of subsequent discharges. This phenomenon constitutes one of the main technological issues to consider for the replacement of SF_6 gas. To solve it, the main goal is to work on the material of the solid insulator, gas, and design to avoid surface tracking.

Fig. 9: Photographs of surface tracking [3].

2. Discharges in gas

Before focusing on creeping discharges, it is necessary to describe discharges in gas without solid. The “breakdown” phenomenon in air, constituted by the appearance of an electric arc able to short-circuit the electrodes and dissipate a large amount of energy, can be the consequence of several different physical processes (frequently called “pre-breakdown” phenomena): electron avalanches, streamers, leaders. In the following, we will present the basic features of these processes.

2.1. Townsend avalanche process

According to the basic theory established by Townsend in 1910 [8], discharges start by the presence of free electrons. When electrons are accelerated by a high enough electric field, ionization of atoms and molecules take place, leading to the formation of “secondary” electrons. The result is an avalanche multiplication process, which permits electrical conduction through the gas (Fig. 10).

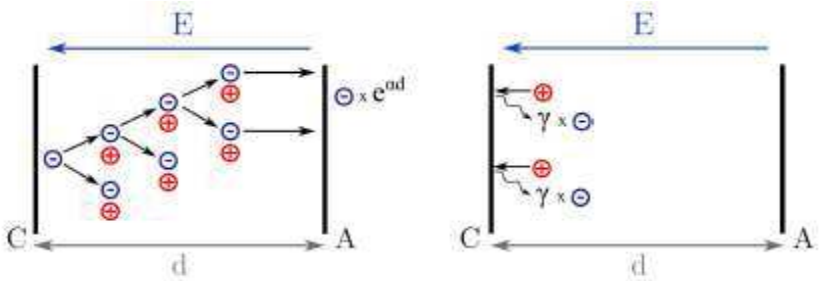

Fig. 10: Visualization of a Townsend avalanche.

The minimum critical field E_{cr} necessary to induce this process is such that ionization coefficient α and attachment coefficient η are equal. The net ionization coefficient is (1):

$$\overline{\alpha} = \alpha - \eta \qquad (1)$$

Other processes (called secondary effects) will also contribute to the ionization:

- The production of electrons at the cathode from the impact of positive ions produced during the primary avalanche. These secondary electrons produce new avalanches (γ secondary process);
- Action of metastable at the cathode (ε process);
- Photoemission at the cathode (δ process) due to photons created by the discharge;
- Photo-ionization of the gas (β process) under the action of photons.

A general ionization coefficient can be written (2):

$$\omega = \gamma\bar{\alpha} + \varepsilon + \delta + \beta \qquad (2)$$

P. Ségur [9] suggests the following equation for breakdown criterion:

$$1 - \frac{\omega(e^{\bar{\alpha}d}-1)}{\bar{\alpha}} = 0 \qquad (3)$$

If ε, δ and β are neglected:

$$\gamma(e^{\alpha d} - 1) = 1 \qquad (4)$$

This first breakdown criterion (Townsend breakdown mechanism) is based on a series of successive avalanches. In SF_6, the critical electrical field is around three times higher than for air (90 kV/cm.bar compared to 30 kV/cm.bar for air).

2.2. Paschen's law

The Paschen's law highlights that the breakdown voltage of a gas mainly depends of the product pd (p: gas pressure, d: gap distance). Increasing the pressure means that we increase the number of atoms per unit volume. Consequently, the average distance a free electron can travel before colliding with an atom (mean free path) is shorter. Its accumulated energy, and hence the probability of ionizing a molecule and producing a secondary electron will decrease, making more difficult to produce an electron avalanche.
From Paschen's curve (Fig. 11), three types of breakdown can be identified:

- Towsend's breakdown, due to avalanches, around the minimum of the Paschen's curve;
- Streamer's breakdown, for high pd product (right branch);
- Pseudo-spark's breakdown, for low pd product (left branch).

The Paschen curves are valid only for uniform electric field. The Townsend mechanism and the corresponding breakdown criterion were presented in the previous section 2.1. The streamer process, relevant for our study, will be presented in the next section.

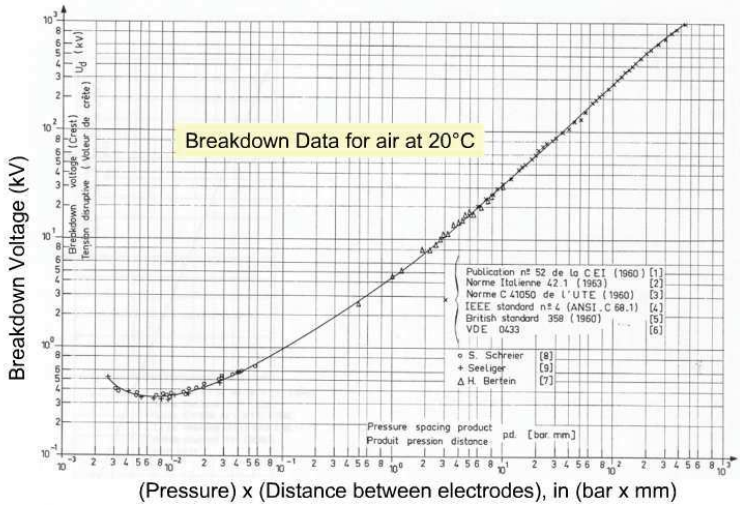

Fig. 11: Paschen curve for air at 20 °C [10].

2.3. Streamers

When the product "pd" is large enough (e.g. pd > 1 bar cm in air [11], or in the case of non-uniform fields, the development of the electronic avalanche is not simply controlled by the applied electric field. When the discharge initiates, electronic and ionic densities become such that a space charge field comparable to the applied field appears, which in turn strongly modifies the discharge process. The Loeb-Meek criterion [12] appears when the number of electrons created by the electronic avalanche exceeds the limit of 10^8. "Streamers" becomes the reason of breakdown, constituted by narrow filamentary plasmas driven by highly nonlinear space charge waves [13]. This process is much faster than the Townsend one, because it is not necessary to wait for the migration of ions up to the cathode to induce secondary electrons.

2.3.1. Negative streamers (propagating toward the anode)

When the Loeb-Meek criterion is reached around the cathode, a negative streamer is created. It is composed of a "negative head" (Fig. 12) which propagate in the same direction as electrons. The enhanced electric field at the streamer head accelerates electrons. In the channel, where the electric field is relatively weak, electrons contribute to neutralization of the conductive channel.

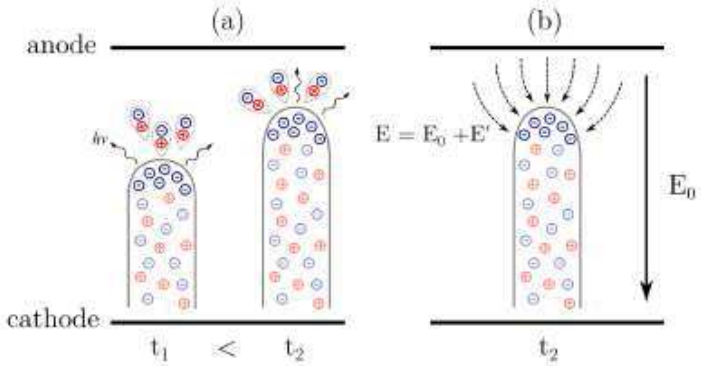

Fig. 12: Negative streamer [14].

2.3.2. Positive streamer (propagating toward the cathode)

The main mechanism of positive streamer propagation is photo-ionization, which principle is represented on Fig. 13. Species excited during the primary avalanche emit sufficiently energetic photons to ionize surrounding neutral molecules. In dry air, the dominant mechanism is the photonization of molecular oxygen (ionization potential: 12.06 eV) by photons emitted by excited states of N_2 [15, 16]. It is generally accepted that positive streamers develop in two stages. The initial phase called primary streamer is constituted by an ionization wave (Fig. 14). The ionization wave propagates in opposite direction of electrons. If the ionic space charge in front of the point is sufficiently intense, the resulting field (applied field + space charge field) will be maximum in front of the space charge. New electronic avalanches appear, establishing a new space charge downstream, inducing the propagation of a positive space charge from the point to the grounded plane. An ionized channel is formed upstream of the space charge, which contains the electrons from the space charge to the point. The space charge zone, with a very high electrical field (around 10^7 V/m), is very active (formation of ions, excited species and radicals) and very bright. Electrons created downstream the streamer head, maintain its propagation and supply the channel in electrons drifting until the point. By touching the plane, a second phenomenon starts in the channel already formed. It consists in the propagation of a secondary-streamer which re-illuminates the first third of the space between electrodes.

The characteristics of primary and secondary streamers are rather different. For example, the electron energy of the primary streamer is bout 5-10 times higher than with the secondary streamer. Secondary streamers propagate towards the cathode at a slower speed than primary streamers.

In SF_6, it was found that the electric field has to remain > E_{cr} (90 kV/cm) in the streamer column, in order to maintain its conductivity while it propagates [17]. This is not the case for air. The lower attachment coefficient in air makes that electrons are not rapidly lost if $E < E_{cr}$: the typical attachment time about 100 ns is long compared to typical propagation times. In

air at atmospheric pressure, the minimum field required for the propagation of positive streamers has been extensively documented experimentally, and remains close to E^{+}_{cr} = 4.4 kV/cm [18], in agreement with recent results of numerical simulations of positive streamers [19, 20]. The value of the similar field E^{-}_{cr} for negative streamers is a factor of 2-3 higher [13, 18]. It should be remembered that the fields E^{+}_{cr} and E^{-}_{cr} are the minimum fields needed for streamer propagation, but not for their initiation e.g. [21].

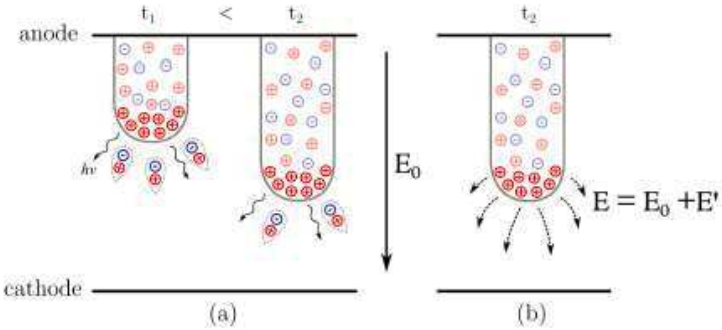

Fig. 13: Representation of a positive streamer between two plane electrodes. New electrons are accelerated by the electric field ($E_0 + E'$) to the head of the streamer, causing a secondary electronic avalanche. Once electrons reach the head of the streamer, the avalanche is neutralized and ions left at the front constitute the new head of the streamer, which in turn ionize its close vicinity by photo-ionization and create a new secondary avalanche, and so on [14].

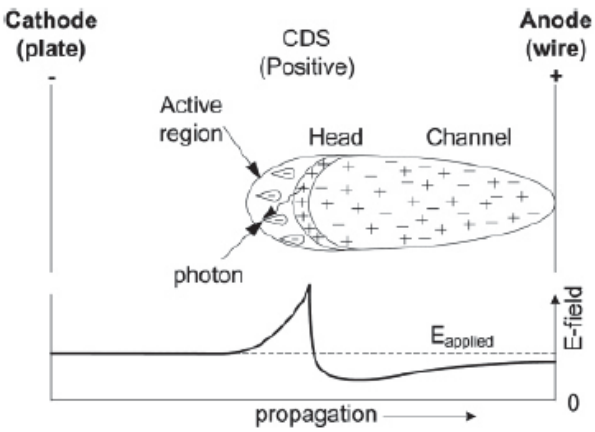

Fig. 14: Principle of the propagation of a primary positive streamer [23].

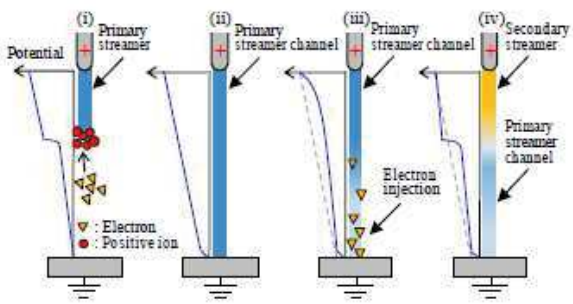

Fig. 15: Model of streamer propagation at needle-plane electrode [24].

2.4. Transition to breakdown

After secondary streamer development, the discharge is close to the breakdown phenomenon called “electric arc” or “spark” for transient arcs of short duration. Two main mechanisms of breakdown process are found in the literature.

2.4.1. Heating channel

The streamer forms a weakly conductive channel between electrodes. The arrival to the cathode is not associated with the immediate occurrence of the transient arc. The E/N reduced field (with N: gas density) is weak in the channel, and attachment is dominant in comparison with ionization, which causes a decrease in the current. If the voltage is further increased, the uncombined residual electrons gain energy and can ionize neutral molecules in the channel. Consequently, the density of electrons and the current increase. According to Marode et al. [18, 25], this process leads to a progressive increase in temperature which in turn causes a reduction of the density in the channel, and consequently an increase of the reduced E/N field. If the value of E/N exceeds the critical field, a new massive ionization phase can occur, leading to the transition to the arc (Fig 16).

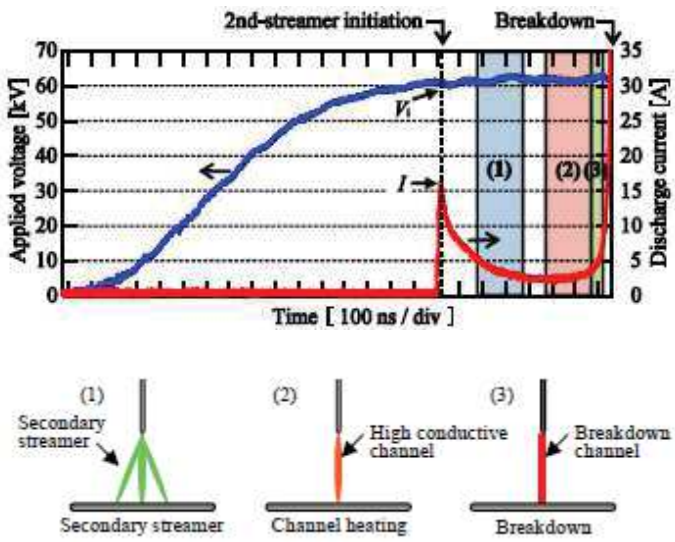

Fig. 16: Applied voltage and discharge current waveforms / model of breakdown mechanism [24].

2.4.2. Leader-type channel

Under conditions that still largely defy analytical formulation, a leader discharge might form at the stem of the streamer. Typically, the leader breakdown mechanism corresponds to values pd > 100 Bar.cm. At atmospheric pressure in uniform field, the leader mechanism is predominant in gaps ≥ 1 m [13]. The leader development in air has been extensively studied, notably by members of “Les Renardières group”. With respect to the streamer, the leader is

highly ionized, and constitutes a highly conductive plasma channel along the path prepared by the preceding streamers. Leader growth is accompanied by one or more “dark periods”. Immediately after a leader reaches the opposite electrode, a breakdown arc takes place. Gallimberti [26] assumes that the mechanism of streamer-to-leader transition in air is related to the thermal detachment of electrons from negative oxygen ions. The effective “destruction” of negative ions, inducing a compensation of electron attachment, becomes possible if the temperature exceeds 1500 K in dry air, and 2000 K in humid air. Such temperatures may exist in the plasma channel, and easily allow the formation of high conductivity leaders in electronegative gases.

During the propagation of a streamer in air, the Joule heat is first stored in the vibrational excitation of N_2 molecules. While the temperature of air increases, the VT-relaxation (VT: Vibrational Translational) grows exponentially, providing a fast thermal runaway of the plasma channel. The leader breakdown process in air has been observed at an average electric field of $\sim$ 1 KVcm $^{-1}$ in 10–30 m air gaps [27, 28, 29]. The exact details of the minimum field for leader formation (E_l) and scaling with density N are not known at present.

In non-uniform fields, leaders may form at much smaller voltage and distances. Experimental data in point-plane gaps show the formation and propagation of leaders in atmospheric air at distances down to 10 cm, and corresponding voltages about 70 kV [30].

A classification of the main breakdown mechanisms in air at atmospheric pressure in uniform field is given in Tab. 2.

10-4 < pd < 0.3 bar·cm	Townsend’s breakdown with a predominant secondary cathode emission. Typical discharge regime of glow discharges.
0.3 < pd < 5.0 bar·cm	Townsend and streamer breakdown can be observed depending on conditions (electrode geometry, applied voltage, etc.).
5 < pd < $\sim$100 bar·cm	The Townsend theory fails, streamer breakdown dominates. Faster breakdown process, at much lower fields than ones predicted by the Paschen’s curve. Secondary cathode emission can be ignored.
pd > $\sim$100 bar·cm	Leader breakdown mechanism. At atmospheric pressure, the leader mechanism becomes predominant in gaps ≥ 1 m.

Tab. 2: Classification of breakdown mechanisms in terms of *pd* values [13].

2.4.3. Breakdown "modes"

Different breakdown "modes" in air can be identified according to the conditions used. Fig. 17 is properly showing the evolution of breakdown voltage in a rod-plane geometry, together with the different pre-breakdown processes involved [30]. Several parameters of pre-breakdown processes (Paschen breakdown field in uniform field, streamer "stability field", leader gradient) allow explaining in a semi-empirical way the complex variation of breakdown voltage.

Several different zones can be identified:

- In short gaps, breakdown in quasi-uniform field occurs as soon as a discharge appears. The breakdown voltage is representative of the voltage required to initiating a discharge ("initiation controlled" breakdown mode);
- In larger gaps (more divergent fields), streamer appear and propagate. We will see in *Chapter 4* that breakdown results from the transition from streamer to spark ("streamer to spark" controlled breakdown mode);
- In even larger gaps (< 20 cm) leaders appears and it is necessary to further raise the voltage such as leaders reach the plane ("leader propagation" controlled breakdown mode).

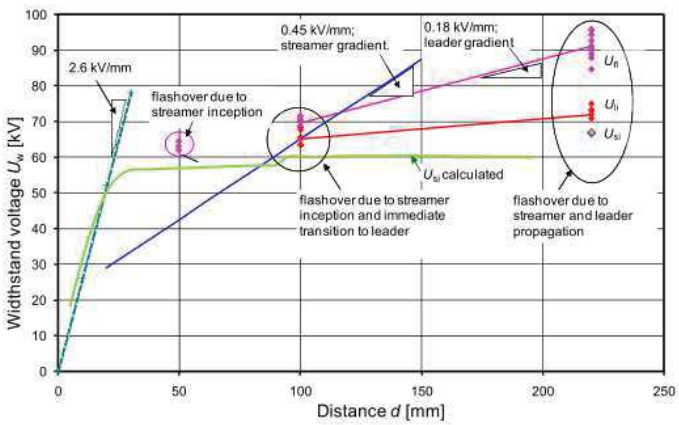

Fig. 17: Withstand voltage with respect to field inhomogeneity [30].

For the study of the influence of solids on breakdown, it will be very important to properly recognize these phenomena, since each process (initiation, propagation, transition to spark) can be influenced in a different way by the solid.

3. Creeping discharges on a dielectric surface

Dielectric surfaces exposed to tangential electric fields generally constitute the most sensitive part of high voltage insulations. Despite a large amount of experimental data collected on the subject [30-37], no acceptable physical interpretation of the development of a discharge in a gas/solid interface has been proposed yet. However, it is well known that

in the presence of these interfaces, several physical mechanisms can lead to the early establishment and propagation of a discharge. Among these mechanisms, we can note mainly the distortion of the electric field around triple points, the modification of the ionization and attachment coefficients, the accumulation of surface charges and the dynamic interaction between the surface and the discharge. These mechanisms can greatly affect the development of the discharge and thus participate largely in the reduction of the breakdown voltage.

3.1. Physical processes induced by the presence of an insulating solid

3.1.1. The distortion of the electric field: “triple point” effect

The Fig. 18 shows this first effect of a dielectric surface between two electrodes. Numerical simulations show that a solid dielectric parallel to the electrode axis deforms the field lines, by directing them towards its surface, and enhancing the field around the High Voltage (HV) electrode (“triple point” effect) [38, 39]. The distortion of the field is due to the higher permittivity of the solid compared to the air. In the presence of the solid, the critical volume (defined as the volume in which a free charge can trigger a discharge) is reduced [38]. With a solid, the faster drop of the field with distance from the HV electrode would "position" the critical ionization field E_{cr} closer to the HV electrode than in air. The reduction of the critical volume indicates that for a given voltage the probability of generating electrons under impulses of short durations would be lower [40].

The mechanisms leading to the formation of a discharge in a triple point geometry do not depend solely on the maximum intensity of the electric field. In a triple point geometry shown in Fig. 19, discharge initiation voltages were calculated using the Townsend Ionization integral model [41]. The calculated values of ionization integrals at various pressures (Fig. 19) indicate that discharges do not occur at the contact point between metal and insulating solid (where the field is maximum), but rather at some distance from that point where the ionization integral goes through a maximum. A fairly good agreement with measured inception voltages under AC or impulses was obtained.

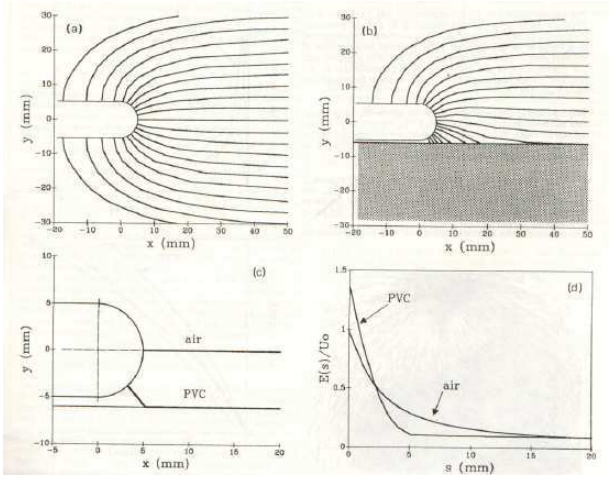

Fig. 18: Comparison of the electric field around the high-voltage electrode in air and in the presence of a dielectric surface [38].

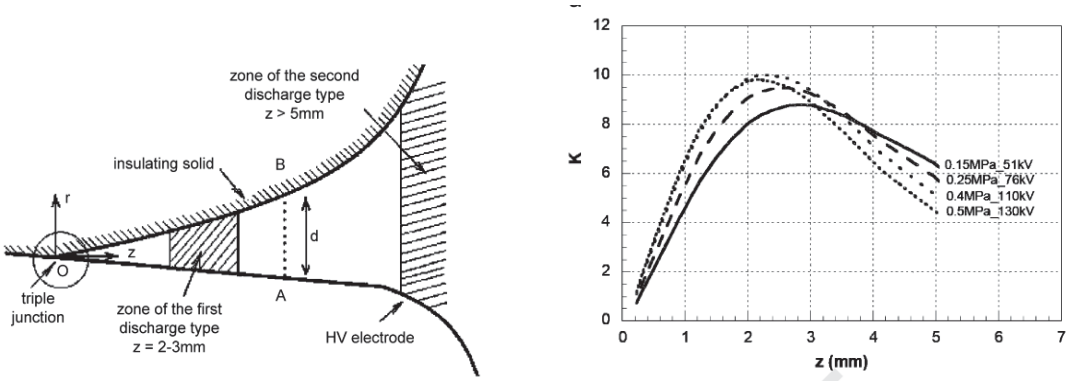

Fig. 19: Triple point geometry and calculation of the Townsend criterion integral K versus distance z and pressure for N2 [41].

3.1.2. A dielectric source or trap of free electrons

The structure of a discharge on a dielectric surface appears to be more complex than that in air. A dielectric can trap charges by attracting them, deprive a streamer of free charges, and in turn stop its propagation. When a charge is placed near a dielectric with ε larger than the surrounding media, it is electrostatically attracted to the dielectric. The higher the ε, the stronger the attraction.

Conversely, a dielectric surface can also emit electrons due to various processes:

- Photoemission (Photon induced secondary electron emission);
- Secondary electron emission due to electron or ion bombardment.

In this case, dielectric surfaces can contribute to favor secondary avalanches, and promote streamer propagation. Several experiments suggest that discharges in the presence of a dielectric surface are greater, with a more abundant branching [38]. Based on these mechanisms, [38], proposed to consider a modified ionization and attachment coefficients in

the presence of a dielectric surface. Consequently, the reduction of the dielectric strength of an air gap in the presence of a dielectric surface has often been attributed to both the distortion of the local electric field, and to the increase in the net ionization rate.

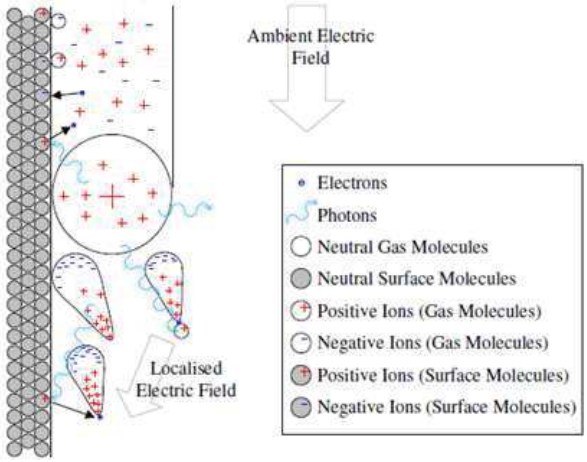

Fig. 20: Representation of the different processes involved in the propagation of streamers and the deposition of surface charge [39].

3.1.3. The accumulation of surface charges

Another phenomenon has been frequently invoked to explain the modification of breakdown conditions: the progressive accumulation of charges on the dielectric surface when series of voltage impulses are applied. These “surface charges” could also influence the initiation, propagation, and appearance of discharges [42-47].

Surface charges left by a preceding discharge can modify the spatial distribution of the electric field for the subsequent discharge. Some evidence of these surfaces charges was obtained by measurements of the surface potential after discharges [47, 48]. Rather large values of surface potentials (exceeding locally 10 kV) were recorded. In [48], the influence of accumulated surface charges on breakdown was evidenced by the degradation of breakdown voltage occurring when impulses of opposite polarity were applied. However, no clear evidence of the role of accumulated charges on pre-breakdown discharges (streamers, leaders) is available.

3.2. Main features of pre-breakdown phenomena in the presence of solids

3.2.1. Localization of streamers

Streamer discharges were observed to have a higher affinity to propagating along dielectric surfaces rather than through the gas alone Fig. 21 [49, 50].

This affinity for a dielectric surface was reported to depend on:

- Gas composition [51]
- Discharge gap geometry [49]
- Properties of the dielectric [52,53]
- Pressure [53]

In several experiments, for example in [50,53] two types of streamers in the presence of a solid were identified. A “surface” streamer along the solid surface, and a “volume” streamer in the surrounding air above the surface (Fig. 22). It was reported that the time for the streamer to reach the grounded plane is shorter and occur at lower voltage for the “surface” streamer [53]. Similar observations were done in pure Argon, in a pin-pin electrode geometry (Fig. 21) [49].

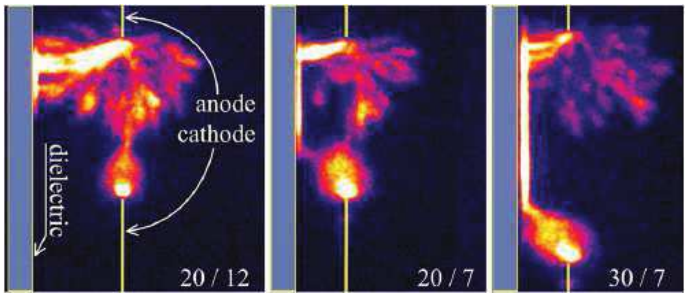

Fig. 21: Photographs of discharges for three different pin-pin electrode geometries in pure Argon. 20/12 denotes the geometry with 20 mm spacing between the electrodes and 12 mm between the electrodes and the dielectric [49].

Fig. 22: Photographs of streamers and breakdown on porcelain insulating surface at 77 kV [50].

Several parameters influence the development of streamers. It was observed that a higher relative permittivity, higher pressure, lower voltage, and asymmetrical sample placement increase the probability of the streamer following the dielectric surface [49,53].

The nature of the dielectric solid also influences the development of streamers. Ceramic induces less branching and more intense light emission compared to PMMA. This was attributed to the higher permittivity of ceramic compared to PMMA [54].

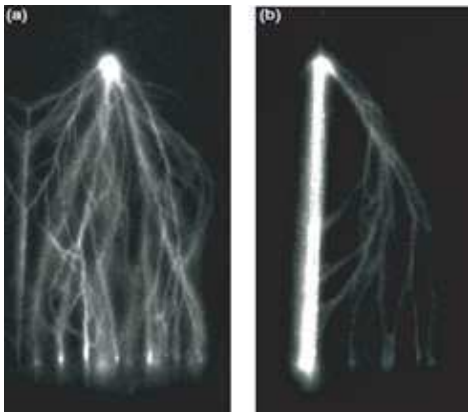

Fig. 23: Discharge images for a gap with PMMA solid. (a) B=9 mm and (b) B=0.3 mm, with B the distance between the needle electrode and the dielectric surface [54].

The position of the electrode relative to the dielectric also influences the propagation (Fig. 23). The number of "volume" streamers in surrounding air increases when the solid is shifted away from the electrode. The solid does not any more influences streamers above a certain distance from the barrier.

3.2.2. Streamer velocity

Many papers deal with the velocity of creeping streamers. Most studies converge on the fact that the velocity of streamers over insulating surface is higher than in air [55, 56]. This difference was attributed to the presence of residual charges on the surface, left from previous discharge. By increasing the applied voltage, and the voltage rate of rise, the streamer velocity is increasing.

Depending of the nature of the solid, the velocity of surface streamers also vary. On Fig. 24 velocities are up to 16 % higher along the BK7 (Borosilicate glass) surface than over Al_2O_3. However, this difference is small considering that their relative permittivity differ by roughly a factor of 2.

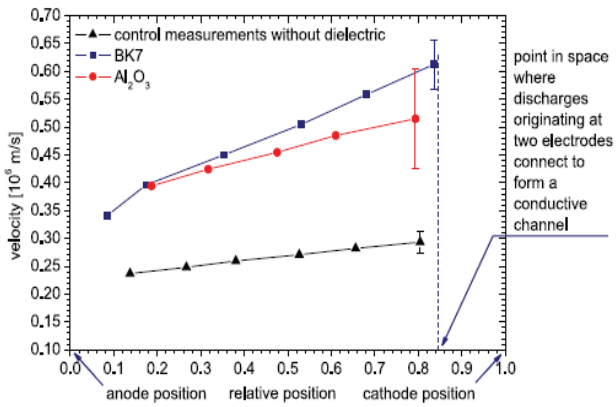

Fig. 24: Space resolved streamer velocities in air for to dielectric materials and without dielectric [49].

Streamers velocity is also dependent on pressure: it decreases at higher pressure (Fig. 25) [53].

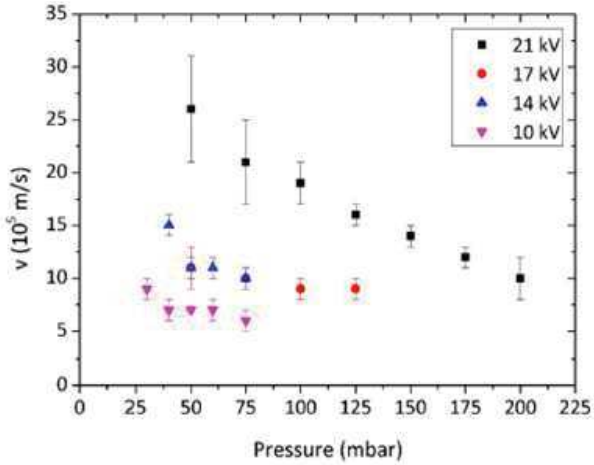

Fig. 25: Velocity of streamers in air propagating along a SiO_2-filled Epoxy resin sample as a function of pressure and pulse voltage [53].

As concerns the influence of streamer velocity on breakdown phenomena under impulse voltage, it can be concluded that this parameter is of secondary importance. With a velocity of 10^6 m/s, the crossing time of streamers in a 10 cm gap is 100 ns, i.e. small compared to the typical time scale of a 1.2/50 µs lightning impulse. Other parameters such as propagation length or voltage required for propagation are more relevant to explain breakdown phenomena.

3.2.3. Streamer length

The maximum length of the streamer depends on the applied voltage, the pressure, and the nature of gas [57]. Fig. 26 shows that by increasing the pressure, the length of surface streamers is reduced.

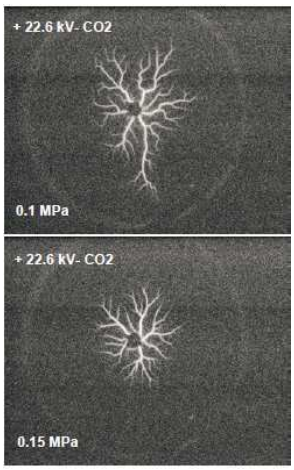

Fig. 26: Influence of the gas pressure on the discharge length at a glass/CO_2 interface [57].

3.3. Breakdown measurements with insulating surfaces

A number of papers deal with breakdown measurements in gases involving dielectric surfaces. We will summarize here some of the most important features recorded in these measurements.

3.3.1. . Time to breakdown

Time to breakdown characterize the time elapsed between voltage application and breakdown. Fig. 27 [50] shows an example of such measurements with breakdown occurring in a rod-plane gap under switching impulse (220/2100 µs) along cylindrical surfaces. Time to breakdown decrease when the voltage is increased, and slightly shorter times are recorded with solids compared to air. It is however very difficult to interpret such measurements. According to the breakdown "mode" (g.e. breakdown controlled by initiation, or propagation, or by transition to a spark), the total time to breakdown can include several different contributions: statistical inception time, propagation time, time for the transition to breakdown… Since breakdown measurements were carried out with widely changing conditions (electrode geometry, distance, voltage shape …), it is generally very difficult to interpret such measurements.

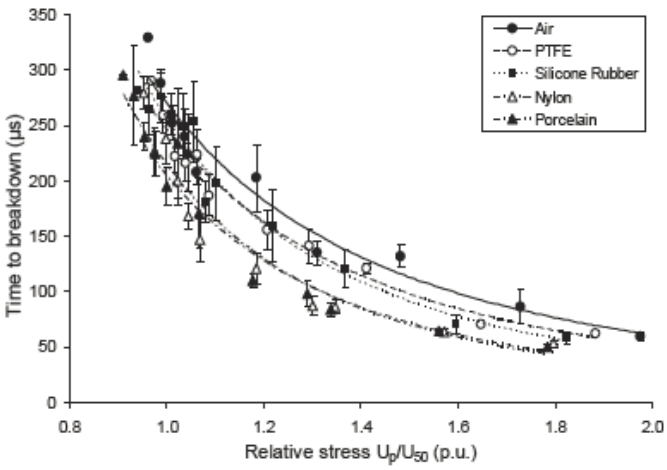

Fig. 27: Time to breakdown as a function of relative stress; fitting curves were drawn according to a power law; (d = 12 cm) [50].

3.3.2. Breakdown probability

The measurement of breakdown voltages cannot be considered as an "absolute" measurement since values are very dependent on the conditions used (gap geometry, voltage shape, etc.), and also on the protocol used to obtain measurements (number of shots at each voltage, rate of increase of voltage, number of measurements, etc.). Since breakdown phenomena include random processes (statistical initiation time, random

branching of streamers, etc.) the statistical treatment of data constitutes an important issue, which in turn may influence the conclusions obtained. Fig. 28 shows an example of breakdown probability measured in air and along insulating surfaces. In this example, an increase of breakdown voltage is recorded with insulating solids of different natures. These probability plots show that the influence of solids depends on the breakdown probability considered (e.g. 5 %, 50 %, 95 %): the influence of solids is lower at low breakdown probabilities. Breakdown measurements at low probabilities are more relevant in the context of applications.

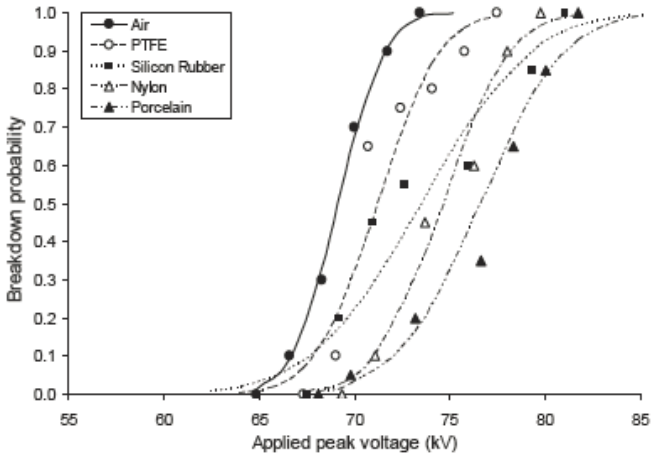

Fig. 28: Breakdown probability curves [50].

3.3.3. Influence of solid nature on breakdown voltage

Many papers dealing with pre-breakdown and breakdown along dielectric surfaces were carried out with a single solid nature. Several studies were carried out with different solid natures in the same experimental conditions in order to compare and classify solids. The flashover voltage along insulating surfaces can be lower or higher than the corresponding value without solid. Different types of insulating materials, either of polymeric or mineral natures, with a range of relative permittivities from 2.2 to 6.5 have been tested. From the available data in the literature this question is still under debate, since rather contradictory results were frequently obtained [58-62]. It is generally accepted that solid surfaces parallel to the field induce lower breakdown voltages, but several examples showing an opposite beneficial effect can be found in the literature.

Fig. 29 shows a first example of measurements showing a decrease of 50 % breakdown voltage under lightning impulse (LI) compared to air, with a slightly increase when permittivity is increased. For switching impulse (SI), same results are obtained with air (decrease of the breakdown voltage in the presence of solids). But in this case, breakdown voltage is slightly decreasing when permittivity is increased.

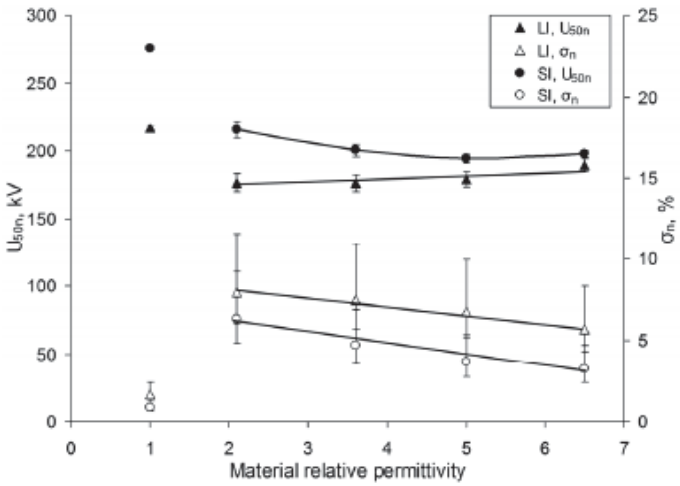

Fig. 29: 50 % breakdown voltage and corresponding standard deviation as a function of material relative permittivity. Rod-plane gap (12 cm) under lightning impulse (LI, 1.3/50 µs) and switching impulse (SI, 220/2100 µs) along cylindrical surfaces [59].

Another example on Fig. 30 shows an increase of the 50 % of breakdown voltage versus permittivity. In other studies such as [55], obtained with a few millimeter gap distance, no clear correlation (increase or decrease) between permittivity and breakdown voltage can be extracted. The presence of additives (fillers) in polymers also provided contradictory results [56]. The surface flashover voltage can either decrease or increase depending on the percentage of fillers.

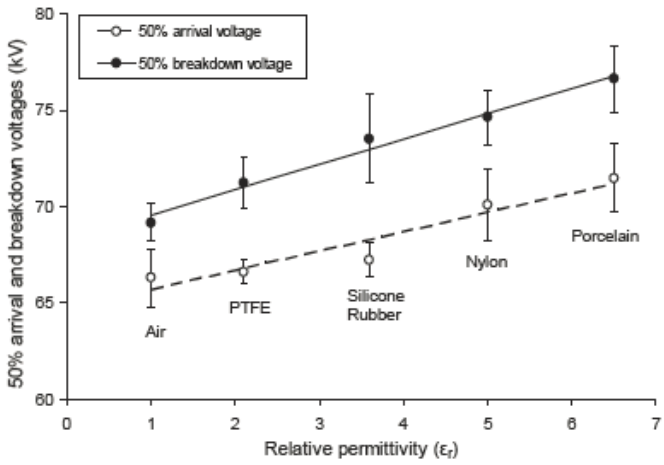

Fig. 30: Linear regression of the 50 % arrival and breakdown voltages over relative permittivity [50].

3.3.4. Comments about the influence of solid nature and permittivity

The examples shown above illustrate the large variability of breakdown measurements carried out with solids parallel to the gap axis. No clear tendency can be extracted from these measurements, concerning the influence of solid nature and/or permittivity. This large

discrepancy certainly results from the fact that experiments were done with different parameters (gap distance, electrode shapes, voltage shape, solid nature, presence of water, …). It was shown that different breakdown "modes" in air exist. Depending on the conditions used, measured breakdown voltages can be relevant of either initiation conditions, or propagation, or transition to spark. Since these processes are certainly influenced in different ways by the presence of solids, it is very difficult to properly compare experiments obtained in different conditions, unless the breakdown process is clearly identified.

3.3.5. Localization of the breakdown spark

With solid surfaces, parallel to the gap axis, previous studies showed that the breakdown spark may occur either on the solid surface or in the gas volume above the surface. Available data suggest that localization depends on parameters such as material's or gas' nature. Krile and al. show a spark in air following the surface profile while in nitrogen environment, breakdown occurs away from the surface in the gas (Figs. 31, 32) [63].

It was hypothesized that the electronegative oxygen in air scavenges electrons released from the surface, hence increasing the positive space charge of the surface. This positive surface charge causes the flashover to stay near the surface [63].

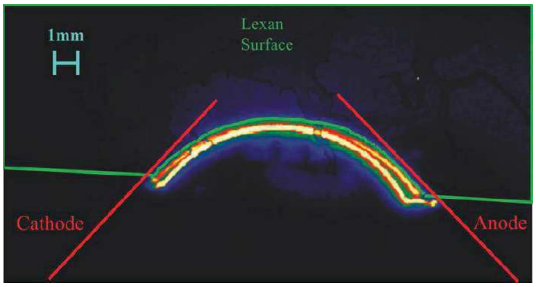

Fig. 31: Negative image of main breakdown in air, 12 mm Lexan gap. Breakdown voltage V_B=25 kV [63]

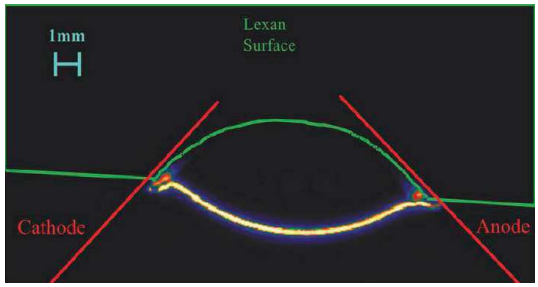

Fig. 32: Negative image of main breakdown in nitrogen, 12 mm Lexan gap. Breakdown voltage V_B=23.8 kV [63]

Solid's nature was also observed to influence the localization of breakdown, in a rod-plane gap (12 cm) under switching impulse (SI, 220/2100 µs) along cylindrical surfaces. For PTFE, Silicon rubber and Nylon, breakdown always occurred in the air over the solid insulator. Contrarily, with porcelain breakdown occurred on the surface (Fig. 33) [50]. Once again, these observations were obtained in quite different conditions, and it is very difficult to derive general conclusions from the available data.

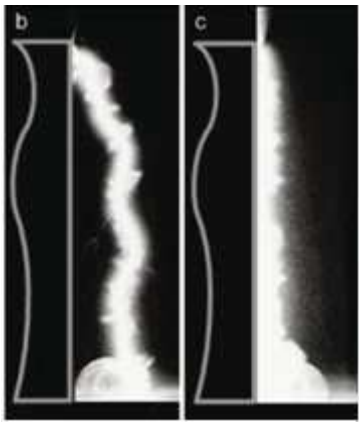

Fig. 33: Photos of breakdown on porcelain insulating surface: b) breakdown in free air (81 kV) and c) breakdown along the surface (102 kV) [50].

4. Conclusions and outline of the Ph.D.

In this chapter, we have reviewed several aspects related to creeping discharges: basic physics of discharges in air, and previous observations about creeping discharges. This topic was addressed since a very long time, but detailed studies remain however necessary to better characterize, understand and model the complex physical processes involved. Compared to the case of a discharge developing in the gas alone, the presence of an insulating solid induces several different effects, that may influence both the initiation of the discharge (modification of the field geometry at the triple junction gas/metal/insulating solid), and its propagation when the discharge creeps on the solid. It remains however difficult to provide a general interpretation based on published experiments, since the pre-breakdown phenomena involved, strongly depend on the conditions used (electrode geometry, high voltage wave shape, etc.). Many questions remain without clear responses:

- Influence of surface charging during breakdown experiments ?
- Influence of the solid respective to the different steps of the total breakdown process (initiation, propagation, transition to breakdown) ?
- Influence of field geometry? Most experiments were obtained with surface parallel to the field, but in real systems many other situations do occur.
- Influence of gas pressure? This question was addressed in very few papers.
- What are the relevant solid parameters ? Chemical nature ? Permittivity ? Water content ?

The primary objective of this work is to study the influence of the solid's nature on impulse breakdown voltage, and to try to establish a classification of solids. This question will be addressed experimentally, by paying special attention to several points:

- The study of the sequence of pre-breakdown events (initiation, propagation, transition to breakdown) in different conditions of field geometry and pressure.

Objective: to be able to selectively study the influence of solids on each of these phases.

- The control of remaining surface charges via the control of sample water content. Previous experiments with epoxy composites showed that the decay of surfaces charges can be dramatically modified by the presence of water [64].
- Selection and characterization of a large range of solids, involving both industrial grade composites, and pure materials.

This manuscript will be organized in the following way.

Chapter 2 :

- Selection of solid materials
- Conditioning (water content)
- Electrical characterization (measurements of permittivity, conductivity, Surface Potential Decay)

Chapter 3 :

- Experimental methods
- Selection of adequate test conditions (preliminary tests with different electrode geometries, field calculations, “parallel” and “perpendicular” electrode geometries, breakdown measurement procedure)
- Breakdown measurements with a wide range of materials, versus pressure

Chapter 4 :

- Experimental characterization of pre-breakdown streamers, versus pressure (time-resolved visualization and transient currents)
- Influence of solids on streamer initiation
- Study of charges remaining on the solid surface after discharges

Bibliography

[1] R. fan, S. Greiner, A. Jasim, W. Peng and C. Yang, “Energy flow in electrical grids”, March 25, 2014.
Link:
http://math.arizona.edu/~gabitov/teaching/141/math_485/Midterm_Reports/Energy_flow_midterm_report.pdf

[2] S. Riepl, “Grobes und prinzipielles Schema der Stromversorgung in Deutschland ».
Link: https://en.wikipedia.org/wiki/Electrical_grid

[3] Internal sources, Schneider Electric.

[4] Distributed switchgear IEEE Power.

[5] “Electrical Installation”, Collaborative platform helping to design electrical installations according to standard as IEC60364.
Link: http://www.electrical-installation.org/enwiki/Characterization_of_the_lightning_wave

[6] SF_6 certification, 2015, Internal sources, Siemens.

[7] S. W. Rowe, “Gas breakdown tutorial”, Internal sources, Schneider Electric.

[8] J. Townsend, « The Theory of Ionization of Gases by Collision », Constable & Company, London, 1910.

[9] P. Segur, "Gaz isolants", Techniques de l’Ingénieur, Traité Génie électrique, Dossier D2530, juin 1990.

[10] T. W. Dakin, G. Luxa, G. Oppermann, J. Vigreux, G. Wind, H. Windelnkemper, “Breakdown of gases in uniform fields Paschen curves for nitrogen, air, and sulfur hexafluoride”, Electra 32 61, 1974.

[11] E. M. Bazelyan and Yu. P. Raizer, “Spark Discharge”, Boca Raton, FL: CRC Press, 1997.

[12] L. B. Loeb, “Electrical Coronas: Their Basic Physical Mechanisms”, University of California Press, United States, 1965.

[13] Yu. P. Raizer, “Gas Discharges”, Springer, Berlin, 1991.

[14] C. Douat, “Etude d’un micro-jet de plasma à pression atmosphérique », Thèse de doctorat Université Paris Sud, 17 février 2014.

[15] S. Pancheshnyi, S. Starikovskaia and A. Starikovskii, “Role of photoionization processes in propagation of cathode-directed streamer”, *J. Phys. D: Appl. Phys.* **34** 105, 2001.

[16] Y.L.M. Creyghton, "Pulsed Positive Corona Discharges. Fundamental Study and Application to Flue Gas Treatment ", Doctoral Thesis, Technische Universiteit Eindhoven, 1994.

[17] A. A. Kulikovsky, “The role of photoionization in positive streamer dynamics”, J. Phys. D. Appl. Phys., Vol. 33, pp. 1514-1524, 2000.

[18] E. Marode, “The mechanism of spark breakdown in air at atmospheric pressure between a positive point and a plane. I. Experimental: Nature of the streamer track”, Journal of Applied Physics 46, 2005 (1975); doi: 10.1063/1. 321882.

[19] N. L. Allen and A. Ghaffar, “The conditions required for the propagation of a cathode-directed positive streamer in air”, J. Phys. D: Appl. Phys. 28 331, 1995.

[20] N. Y. Babaeva and G. V. Naidis, “Dynamics of positive and negative streamers in air in weak uniform electric fields”, IEEE Trans. Plasma Sci. 25 375-9, 1997.

[21] R. Morrow and J. R. Lowke, “Streamer propagation in air”, J. Phys. D 30, 614, 1997.

[22] N. I. Petrov and G. N. Petrova, “Physical mechanisms for the development of lightning discharges between a thundercloud and the ionosphere”, Tech. Phys.44, 472± 475, 1999.

[23] J. M. Plewa, "La simulation 3D des streamers utilisant le calcul haute performance", Thèse de doctorat Université de Toulouse, 13 octobre 2017.

[24] H. Kojima, K. Hotta, T. Kitamura, N. Hayakawa, A. Otake, K. Kobayashi, T. Kato and T. Rokunohe, “Classification of impulse breakdown mechanisms under non-uniform electric field in air”, IEEE Transactions on Dielectrics and Electrical Insulation, Vol. 23, No. 1, February 2016.

[25] E. Marode, "The mechanism of spark breakdown in air at atmospheric pressure between a positive point and a plane”, Theoretical: Computer simulation of the streamer track”, Journal of Applied Physics, Vol. 46, No. 5, p 2016-2020, (1975).

[26] I. Gallimberti, G. Bacchiega, A. Bondiou-Clergerie, P. Lalande, “Fundamental processes in long air gap discharges, C. R. Physique 3, pp.1335-1359 I, 2002.

[27] Les Renardières Group, « Results and conclusions », Electra 53 31, 1977.

[28] H. C. Barnes and D. E. Winter, “UHV Transmission design requirements-switching surge flashover characteristics of extra-long air gaps”, IEEE Transactions on Power Apparatus and Systems PAS-90 ; 4 1579-89, 1971.

[29] A. Bondiou, I. Gallimberti, “Theoretical modelling of the development of the positive spark in long gaps”, J. Phys. D 27 1252–1266, 1994.

[30] A. Pedersen, T. Christen, A. Blaszczyk and H. Boehme, “Streamer inception and propagation models for designing air insulated power devices”, Proc. of the Conference on Electrical Insulation and Dielectric Phenomena, 2009.

[31] F. Mauseth, J. S. Jorstad and A. Pedersen, “Streamer inception and propagation for air insulated rod-plane gaps with barriers”, IEEE, 2012.

[32] T. S. Sudarsham and R. Dougal, "Mechanisms of surface flashover along solid dielectrics in compressed gases", Review, IEEE Trans. Electr. Insul., No. 21, pp. 727-746, 1986.

[33] H. Craig Miller, "Surface flashover on insulators", IEEE Trans. Electr. Insul., Vol. 24, No. 5, pp. 765-786, 1989.

[34] L. S. Pritchard and N. L. Allen, "Streamer propagation along profiled insulator surfaces", IEEE Trans. Dielectr. Electr. Insul. Vol. 9, No. 3, pp. 371-380, 2002.

[35] N. L. Allen and P. N. Mikropoulos, "Surface profile effect on streamer propagation and breakdown in air", IEEE Trans. Dielectr. Electr. Insul., Vol. 8, No. 5, pp. 812-817, 2001.

[36] Y. Murooka, T. Takada, and K. Hidaka, “Nanosecond surface discharge and charge density evaluation part I: Review and experiments”, IEEE Electr. Insul. Mag., vol. 17, No. 2, pp. 6-16, 2001.

[37] A. Kumada, S. Okabe, and K. Hidaka, “Residual charge distribution of positive surface streamer”, J. Phys. D. Appl. Phys., Vol. 42,095209, 2009.

[38] I. Gallimbertti, I. Marchesi and L. Niemeyer, "Streamer corona at an insulating surface". Proc. of 7th Int. Symp. on HV Eng., Dresden (Germany), pp. 1-4, 1991.

[39] M. Akyuz, L. Gao, V. Cooray, T. G. Gustavsson, S. M. Gubanski, and A. Larsson, “Positive streamer discharges along insulating surfaces,” *IEEE Transactions on Dielectrics and Electrical Insulation*, vol. 8, no. 6, pp. 902–910, 2001.

[40] N. L. Allen and B. H. Tan, "Initiation of positive corona on insulator surface". Proc. of the 12th Int. Symp. on HV Eng., Bangalore (India) Vol. 3, pp. 5-8, 2001.

[41] C. Tran Duy, N. Bonifaci, A. Denat, O. Lesaint, A. Girodet, B. Gelloz, P. Ponchon, “Partial discharges at a triple metal/solid insulator/gas interface, and simulation of inception voltage”, J. Electrost, 66 319-27, 2008.

[42] D. C. Faircloth, « Surface charge density and its influence on insulator flashover”, University of Manchester Institute of Science and Technology, 2000.

[43] R. A. Fouracre, F. A. Twema, S. J. MacGregor and M. J. Given, "The influence of charge on surface flashover", 11th Int. Symp. on HV Eng., Conf. Publ. No. 467, Vol. 3, pp. 329-332, 1999.

[44] R. A. Fouracre, E. Santos, I. Timoshkin, M.J. Given and S. J. Macgregor, “Surface discharge propagation: The influence of surface charge”, 27th Intern. Power Modulator Sympos. and 2006 High Voltage Workshops, pp. 39-42, 2006.

[45] N. L. Allen and D. C. Faircloth, "Corona propagation and charge deposition on a PTFE surface", IEEE Trans. Dielectr. Electr. Insul., Vol. 10, No. 2, pp. 295-304, 2003.

[46] X. Jun and I. D. Chalmers, “The influence of surface charge upon flash-over of particlecontaminated insulators in under impulse-voltage conditions,” *J. Phys. D: Appl. Phys.*,vol. 30, no. 7, p. 1055, Apr. 1997.

[47] J. Deng, S. Matsuoka, A. Kumada and K. Hidaka, “The influence of residual charge on surface discharge propagation”, J. Phys. D: Appl. Phys. 43 (2010) 495203 (8pp).

[48] L. Caliap, « Etude de l’optimisation des isolants d’un point de vue diélectrique pour les contraintes du GIS », Thèse de doctorat (Institut polytechnique de Grenoble), Septembre 2010.

[49] A. Sobota, A. Lebouvier, N. J. Kramer, E. M. van Veldhuizen, W. W. Stoffels, F. Manders and M. Heverlag, “Speed of streamers in argon over a flat surface of a dielectric”, J. Phys. D: Appl. Phys. 42 (2009) 015211 (8pp).

[50] L. A. Lazaridis and P. N. Mikropoulos, “Flashover along cylindrical insulating surfaces in a non-uniform field under positive switching impulse voltages”, IEEE Transactions on Dielectrics and Electrical Insulation, Vol. 15, No. 3, June 2008.

[51] R. E. Jorgenson and al., “Effect of Dielectric Photoemission on Surface Breakdown: An LDRD Report”, Sandia Rep. SAND2000-3044, 2003.

[52] X. B. Meng, H. W. Mei, C. L. Chen, L. M. Wang, Z. C. Guan, and J. Zhou, "Characteristics of streamer propagation along the insulation surface: influence of dielectric material," IEEE Transactions on Dielectrics and Electrical Insulation, vol. 22, pp. 1193-1203, 2015.

[53] D. J. M. Trienekens, S. Nijdam, G. Akkermans, I. Plompen, T. Christen and U. Ebert, “Experimental investigation of streamer affinity for dielectric surfaces”, 32nd ICPIG, July 26-31, 2015, Iasi, Romania.

[54] V. V. Timatkov, G. J. Pietsch, A. B. Saveliev, M. V. Sokolova and A. G. Temnikov, “Influence of solid dielectric on the impulse discharge behavior in a needle-to-plane air gap”, J. Phys. D: Appl. Phys. 38 (2005) 877-886.

[55] J. M. Trienekens, S. Nijdam, U. Ebert, “Stroboscopic Images of Streamers Through Air and Over Dielectric Surfaces”, IEEE Transactions on Plasma Science, Vol. 42, No. 10, October 2014.

[56] N. L. Allen and M. Mikropoulos, “Streamer propagation along insulating surfaces”, IEEE Transactions on Dielectrics and Electrical Insulation, 6 (3), 357–362, 1999.

[57] M. Coulibaly, A. Beroual, « Caractérisation Optique et Electrique des Décharges se Propageant sur des Interfaces Solide/Gaz et Mélanges de Gaz sous Tension de Foudre », MGE’2008, May 2008, Toulouse, France. pp.on CD – 108-111/215.

[58] M. El-A. Slama, A. Beroual, A. Girodet and P. Vinson, “Creeping discharge and flashover of solid dielectric in air at atmospheric pressure: experiment and modelling”, IEEE Transactions on Dielectrics and Electrical Insulation, Volume: 23, Issue: 5, 2949 – 2956, October 2016.

[59] L. A. Lazaridis and P. N. Mikropoulos, “Negative impulse flashover along cylindrical insulating surfaces bridging a short rod-plane gap under variable humidity”, IEEE Transactions on Dielectrics and Electrical Insulation, Vol. 17, No. 5, October 2010.

[60] L. A. Lazaridis and P. N. Mikropoulos, “Positive impulse flashover along smooth cylindrical insulating surfaces under variable humidity”, IEEE Transactions on Dielectrics and Electrical Insulation, Vol.18, No. 3, June 2011.

[61] A. S. Pillai and R. Hackam, “Surface flashover of solid insulators in atmospheric air and in vacuum”, Appl. Phys., vol.58, pp.146-153, 1985.

[62] Q. Wu, Z. Peng, Y. Jiang, J. Tang and Y. Yang, “Surface flashover of the ATH/Epoxy under the nanosecond voltage pulse”, IEEE 10th International Conference on the Properties and Applications of Dielectric Materials, July 24-28, 2012.

[63] J. T. Krile, A. A. Neuber, J. C. Dickens and H. G. Krompholz, “DC flashover of a dielectric surface in atmospheric conditions”, IEEE Transactions on plasma science, Vol. 32, No. 5, October 2004.

[64] L. Zavattoni, « Conduction phenomena through gas and insulating solids in HVDC Gas Insulated Substations, and consequences on electric field distribution », Thèse de doctorat (Université de Grenoble), Octobre 2014.

Chapter 2: Insulating solids: selection and characterization

Several materials will be selected, described and characterized to highlight several properties of these materials, supposed to have an influence on the creeping discharge process: permittivity, conductivity, presence of water, ability to store or dissipate surface charges. The latter property will be investigated by a Surface Potential Decay (SPD) experiment.

1. Selection of the solids

This section present all materials used in this work. It was decided to not limit our study to the classical epoxy thermoset matrix filled with silica (60 % of silica), used by Schneider Electric in medium voltage apparatus

A large range of materials will be investigated, with mainly two underlying objectives (Fig. 1):

- Characterization of several "new" materials which could be integrated in future medium voltage applications (such as PA6T/66).
- Characterization of several standard materials mainly chosen as experimental probes to get a better understanding of creeping discharges, for example by extending the range of permittivity toward low permittivity (PTFE, PP) and large permittivity (glass, alumina ceramic).

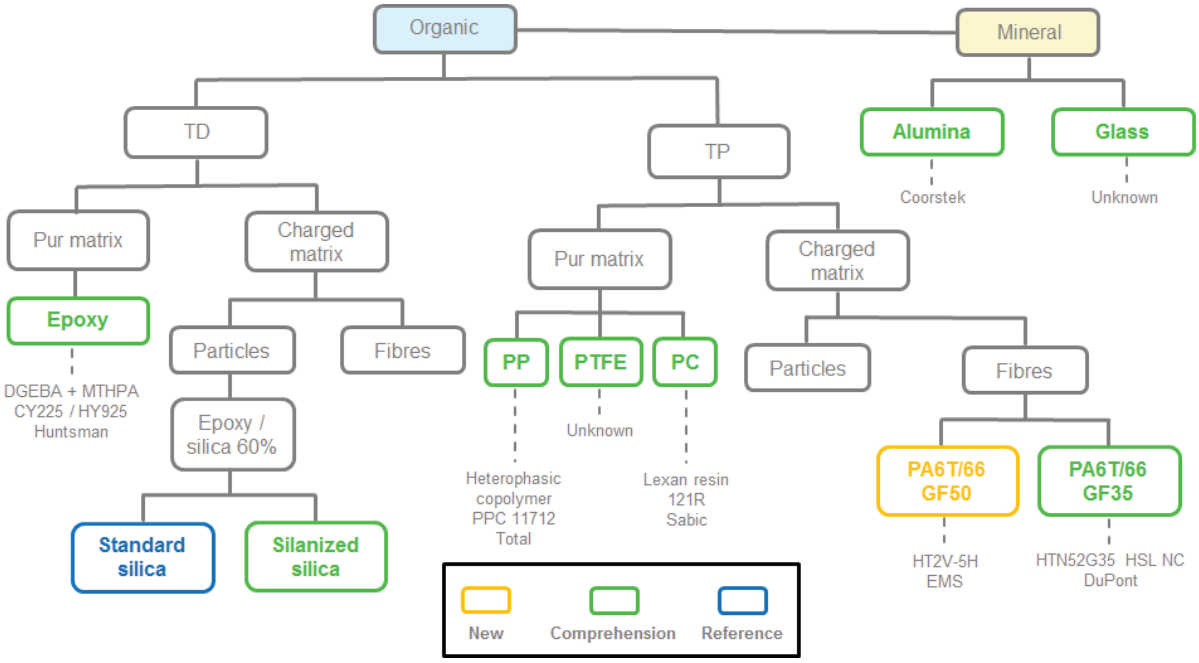

Fig. 1: Chart of the materials studied.

The initial shape of all samples was a square (10 x 10 cm), 3 mm in thickness. Due to the variety of experimental set-up used, we frequently had to cut materials to other shapes (8 cm diameter disks, reduced squares). Such a thickness is necessary to test thermoset samples without artefact du to molding process.

To evaluate the effect of water present in the material bulk on breakdown voltages, two extreme conditions were used: either thoroughly dried or fully impregnated with water. As we will see later, the presence of water has a large influence on the material conductivity, and hence on its ability to either store or quickly dissipate surface charges. The presence of water will be later used to check the influence of accumulated surface charges on the creeping discharge process.

The drying and impregnation procedures are described in details in *Annex 1*. Fig. 2 shows the mass uptake for five types of material. PA6T/66.GF50 can absorb up to 1.4 % (in mass) of water in these conditions. Compared with other materials, PA6T/66.GF50 absorbed the largest amount of water. It was required to wait up to forty days to obtaining saturation in these conditions. Epoxy/Silica and polycarbonate uptaked a smaller quantity of water (0.25 % in mass both). Epoxy resin uptaked an intermediate value of 0.6 % in mass. For all materials excepted PA6T/66.GF50, a typical time to saturation corresponded to about five days. The amount of water absorbed will affect the dielectric properties, and constitutes a key factor for the suitability of a material for electrical/electronic applications, when it is in contact with ambient air which temperature and relative humidity may show large variations.

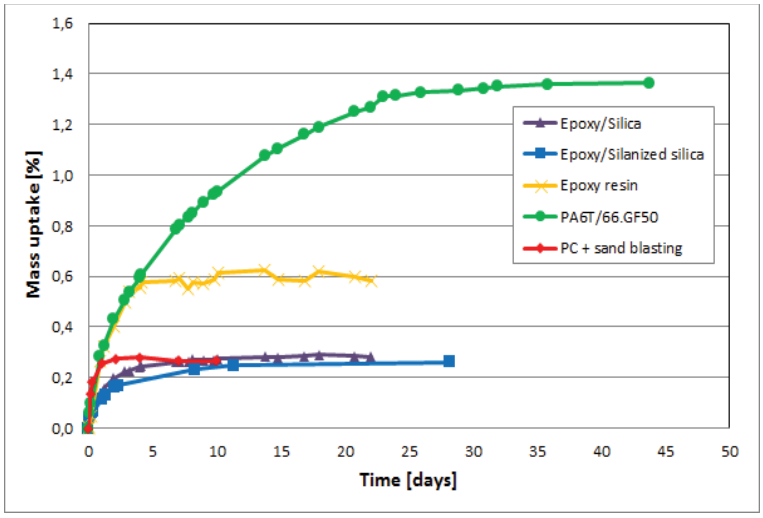

Fig. 2: Moisture uptake procedure according to solids' nature.

The Tab.1 summarizes the water content in the bulk of the material for 70 °C and 62 %RH (relative humidity conditions), according to the ISO-1110 standard (*Annex 1*).

Material	Water content [%]
Epoxy resin	0.60
Epoxy/Silica	0.25
Epoxy/Silanized Silica	0.24
PC	0.25
PA6T/66.GF50	1.38

Tab. 1: Summary of water content of solids at 70 °C and 62 %RH.

1.1. Material of reference for Schneider Electric

Epoxy/Silica is the material of reference for medium voltage apparatus in Schneider Electric (Tab. 2 and Tab. 3). In this work, it will serve as a reference. Epoxies in many forms are among the most widely used dielectrics. Parts molded from electrical grade epoxy compounds exhibit outstanding dimensional stability and retention of electrical properties with virtually no outgassing at temperature up to 260 °C. Epoxies are widely used for embedment of components for transformers, motors, generators, switchgear, coils, capacitors, resistors and electronic modules [1]. In our study, epoxy is processed with a DGEBA (di glycidyl ether of bisphenol A) pre-polymer and an anhydride hardener based on MTHPA (methyl tetra hydrophtalic anhydride). As noted earlier, epoxy serves as a reference compared to other materials for medium voltage applications.

Thermosetting resins, by themselves, can be brittle and of little practical value, but are made useful by compounding with reinforcements and fillers, which may constitute 50 % or more of compound weight. In this work, an epoxy thermoset matrix reinforced with silica filler was molded. Two types of reinforcements were used: standard silica and silanized silica. Samples were molded at the research center of Schneider Electric.
For all the materials studied, a description of the properties will be done. Figures wrote in blue correspond to values found in the literature, in red for the supplier data sheets and in green from our experimental studies.

Acronym	Epoxy/Silica
Supplier / Commercial reference	Huntsman® / DGEBA CY225 – MTHPA HY925 – 60 % silica E6
Chemical family	Organic Epoxy charged with mineral material
Temperature behavior	T_g > 105 °C
	$T_{Max\ of\ use}$ = 120 °C
Matrix type	Reticulated
Macromolecule and properties of chemical bonds (for organic material)	Benzene bonds and double bonds (Fig. 6)

Tab. 2: Material properties of Epoxy/Silica.

Dielectric constant	3.73
Tangent of the loss angle	0.02
Resistivity [Ω.cm]	10^{15}

Tab. 3: Dielectric properties of Epoxy/Silica (according to Huntsman® technical data sheet).

1.2. New materials

New materials are investigated in this study, to replace Epoxy/Silica on longer terms for health reasons and regulation risk. Two fiber reinforced thermoplastic compounds were selected from the family of high temperature plastic (Fig. 4). As many other thermoplastics, high performance are often improved significantly by compounding materials with reinforcements and fillers. Glass is the most common reinforcing fiber. It contributes to improve mechanical strength and electrical insulation properties with reduced flammability [1].

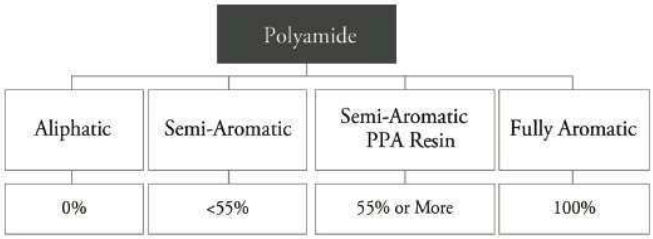

Fig. 3: Presentation of polyamides [2].

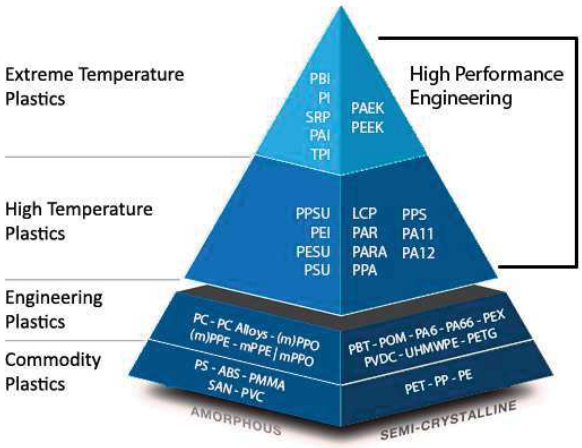

Fig. 4: Performance category of thermoplastics [3].

Among Polyamides, the selected polymer is belonging to Polyphthalamide (PPA) range (Fig. 3). It has very good mechanical and thermal properties. Few detailed data on electrical properties are available on PPA, in addition to the data sheets provided by manufacturers. Therefore, it is necessary to carry out additional electrical characterization on this material, to use it in electrical applications. Among several possible PPA, the selected grade is based on PA6T/66 matrix. Two different compounds were evaluated:

- EMS® supplied PPA reinforced with 50 % of glass fibers (PA6T/66.GF50):

Acronym	PA6T/66.GF50
Supplier / Commercial reference	EMS® / HT2V-5H
Chemical family	Organic Polyphthalamide / Glass fibers
Temperature behavior	$T_{Max\ of\ use}$ = 165 °C
Matrix type	½ crystalline
Macromolecule and properties of chemical bonds (for organic material)	Benzene bonds and double bonds (Fig. 6)

Tab. 4: Material properties of PA6T/66.GF50.

Dielectric constant	4.09
Tangent of the loss angle	0.05
Resistivity [Ω.cm]	10^{10}

Tab. 5: Dielectric properties of PA6T/66.GF50.

- DuPont® supplied PPA reinforced with 35 % of glass fibers (PA6T/66.GF35):

Acronym	PA6T/66.GF35
Supplier / Commercial reference	DuPont® / HTN52G35HSL NC
Chemical family	Organic Polyphthalamide / Glass fibers
Temperature behavior	$T_{Max\ of\ use}$ = 165 °C
Matrix type	½ crystalline
Macromolecule and properties of chemical bonds (for organic material)	Benzene bonds and double bonds (Fig. 6)

Tab. 6: Material properties of PA6T/66.GF35.

Dielectric constant	3.80
Tangent of the loss angle	0.010
Resistivity [Ω.cm]	10^{15}

Tab. 7: Dielectric properties of PA6T/66.GF35.

1.3. Materials with various relative permittivity

Some materials were selected to study the effect of relative permittivity. They have for characteristic a high or a low relative permittivity. Fig. 5 presents a relative permittivity scale with all the materials used in our study.

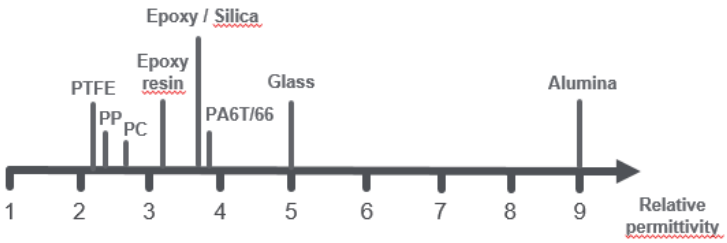

Fig. 5: Large range of permittivity of the solids used in this work.

1.3.1. Alumina

Alumina is a sintered ceramic material with a high relative permittivity of 9. This material will be used for comprehension of the influence of relative permittivity on breakdown voltage.

Acronym	-
Supplier / Commercial reference	Coorstek® / Alumina 96 %
Chemical family	Mineral
Temperature behavior	$T_{Max\ of\ use}$ = 2072 °C
Matrix type	-
Macromolecule and properties of chemical bonds (for organic material)	-

Tab. 8: Material properties of alumina [4].

Dielectric constant	8.5
Tangent of the loss angle	0.002
Resistivity [Ω.cm]	10^9 - 10^{12}

Tab. 9: Dielectric properties of alumina [4].

1.3.2. Glass

Glass is a non-crystalline amorphous solid. Its relative permittivity is rather high: 5 at room temperature under 1 KHz.

Acronym	-
Supplier / Commercial reference	Unknown supplier
Chemical family	Mineral
Temperature behavior	$T_{Max\ of\ use}$ = 600 °C
Matrix type	-
Macromolecule and properties of chemical bonds (for organic material)	-

Tab. 10: Material properties of glass [5].

Dielectric constant	5.3
Tangent of the loss angle	0.0050
Resistivity [Ω.cm]	10^9 - 10^{11}

Tab. 11: Dielectric properties of glass [5].

1.3.3. Polycarbonate

Polycarbonate (noted PC), is used for a variety of electrical/electronic applications. It has a good flexibility, heat resistance and dimensional stability [1]. In our work, the roughness of the PC sample has been adjusted by sand blasting technique. With two sand grain having different diameters, it was possible to obtain two different surface roughness. Nevertheless, final surface roughness was not characterized after sand blasting. These surface modifications will be used in *Chapter 3* and *4* (study of creeping discharge). A smooth surface is required for dielectric characterization to have a good contact with electrodes.

Acronym	PC
Supplier / Commercial reference	SABIC / LEXAN™ - Resin 121R
Chemical family	Organic Polycarbonate
Temperature behavior	$T_{Max\ of\ use}$ = 120 °C
Matrix type	Amorphous
Macromolecule and properties of chemical bonds (for organic material)	Benzene bonds and double bonds (Fig. 6)

Tab. 12: Material properties of PC [6].

Dielectric constant	2.60 – 3.20
Tangent of the loss angle	0.0010 – 0.0100 0.01
Resistivity [Ω.cm]	10^{15}

Tab. 13 Dielectric properties of PC [7].

1.3.4. Polypropylene

Polypropylene (noted PP), is a highly versatile resin suitable for processing into molded insulation parts, extruded wire or cable insulation, and dielectric films. PP may be processed with all conventional injection molding methods. It's the most rigid polyolefin and one of the lightest plastics. The principal electrical uses of PP is for extruded primary insulation on wire and cables, and capacitors. It's also used extensively for injection-molded battery cases [1]. In this work, PP was chosen for its low permittivity in breakdown experiments (*Chapter 3*). It was also chosen from the hypothesis that PP implies dielectric relaxations. PP used in our

case is coming from Total® supplier with the reference: PPC 11712 Polypropylene, Heterophasic Copolymer.

Acronym	PP
Supplier / Commercial reference	Total® / PPC 11712 Polypropylene, Heterophasic Copolymer
Chemical family	Organic Polypropylene
Temperature behavior	$T_{Max\ of\ use}$ = 110 °C
Matrix type	½ crystalline
Macromolecule and properties of chemical bonds (for organic material)	Single bonds (Fig. 6)

Tab. 14: Material properties of PP [6].

Dielectric constant	2.2
Tangent of the loss angle	0.0005
Resistivity [Ω.cm]	10^{13}- 10^{15}

Tab. 15: Dielectric properties of PP [7].

1.3.5. Polytetrafluoroethylene

Polytetrafluoroethylene (noted PTFE), is a hydrophobic material. It has many applications such as hookup wire and coaxial cables. PTFE has also excellent dielectric properties, making it suitable for use as an excellent insulator in connector assemblies and cables.
In this work, PTFE was chosen for its low permittivity in breakdown experiments and for its electronegativity property with the presence of fluorine (*Chapter 3*).

Acronym	PTFE
Supplier / Commercial reference	Unknown supplier
Chemical family	Organic Polytetrafluoroethylene
Temperature behavior	$T_{Max\ of\ use}$ = 250 °C
Matrix type	Amorphous
Macromolecule and properties of chemical bonds (for organic material)	Single bonds (Fig. 6)

Tab. 16: Material properties of PTFE [6].

Dielectric constant	2.10
Tangent of the loss angle	0.0002
Resistivity [Ω.cm]	10^{18} - 10^{19}

Tab. 17: Dielectric properties of PTFE [7].

Comments on the chemical structures of the solids studied

Fig. 6 shows two groups of materials: with double bond or/and aromatic ring and with only single bond. A single bond is a chemical bond between two atoms involving two valence electrons while with a double bond four electrons are involving instead of two. From this classification, two materials stand out: PTFE and PP.

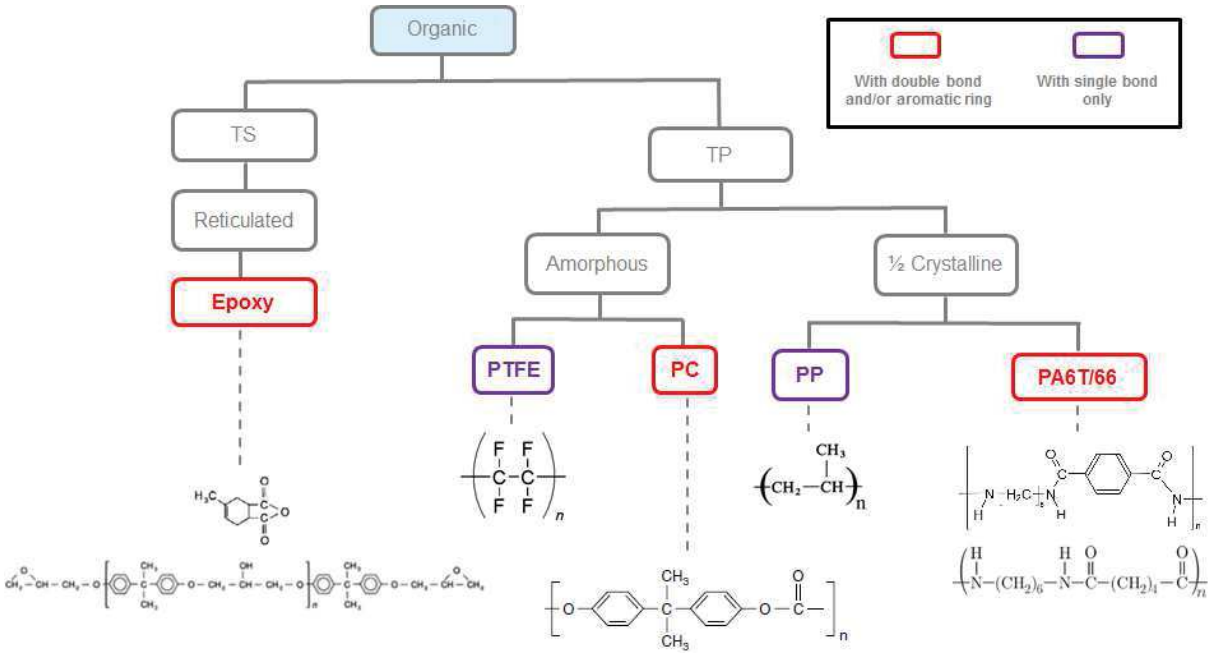

Fig. 6: Chemical structure of the materials studied. PTFE [8], PA6T/66 [9], PP [10], PC [11], Epoxy [12].

2. Dielectric characterization

2.1. Determination of the relative permittivity of solids

Dielectric spectroscopy allows obtaining dielectric properties of a material as a function of frequency and temperature. It is based on the measurement of the current induced by an AC applied electrical field, interacting with electric dipoles and charges within the material. From the frequency spectrum, information about the dynamics of molecules can be deduced. The detailed analysis of the data obtained was outside the scope of this work. The goal of this measurement was mainly to obtain values of relative permittivity of the material (ε_r) at 50 Hz and 1 MHz.

2.1.1. Experimental system

To perform our measurements, we used an electrode system with an identical configuration than that used for measurements of absorption currents. The sample is placed between two conductive electrodes forming a capacitance. The set-up presented in Fig. 7B is placed in a climatic chamber.

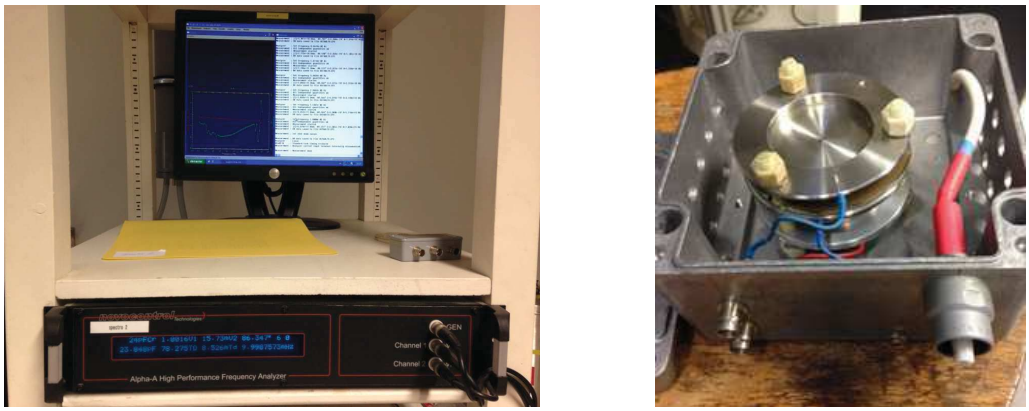

A) B)

Fig. 7: Photographs of: A) Novocontrol dielectric spectroscopy set-up; B) Electrodes system.

Once the sample temperature is stabilized, a voltage with fixed frequency is applied. Values and phase of current as well as voltage are measured (Fig. 8). A range of temperatures from 10 °C to 80 °C and frequency from 10^{-2} to 10^{6} Hz were investigated.

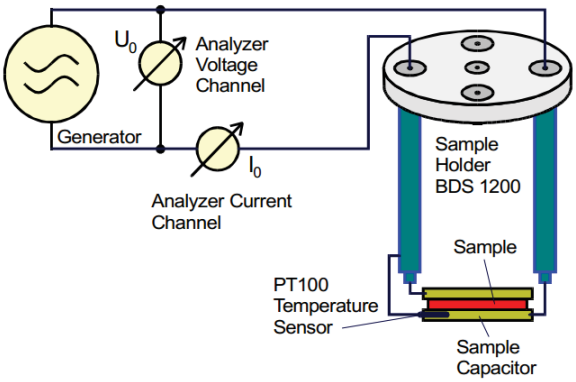

Fig. 8: Diagram of principle for dielectric spectroscopy measurements [13].

A large range of materials was investigated with this system with dry and wet conditioning. Unfilled and composite materials were tested such as those based on organic matrix made of Epoxy, PC and PA6T/66. The measurement of ε', ε'', tan delta, versus temperature created a database which extensive presentation and detailed physical analysis is outside the initial scope of this thesis.

In this manuscript, only the permittivity measurements for dry and wet PA6T/66 and Epoxy/Silica are presented. Two main values of permittivities are of interest for this work:

- 50 Hz: working frequency of power equipment;
- 1 MHz: maximum frequency of measurements.

1 MHz corresponds to a 1 µs period, i.e. the typical time scale of creeping discharge experiments. This value of permittivity will be considered to characterize materials in these experiments.

2.1.2. Results

Relative permittivity depends on frequency and temperature. Starting from low frequencies, the real part of relative permittivity decreases. The increase of permittivity at very low frequencies in composite materials is probably related to the interfacial polarization occurring at the matrix/filler interfaces. At higher frequencies, the motion of ions and dipoles "freezes" out because the molecules cannot catch up with the oscillating external field [14].

Fig. 9 describes a moderate variation of relative permittivity with temperature: from 3.8 to 4.6 at 0.01 Hz, between 10 °C and 80 °C. This variation becomes negligible at 50 Hz and 1 MHz. At 1 MHz, the value of relative permittivity of dry Epoxy/Silica is of 3.6.

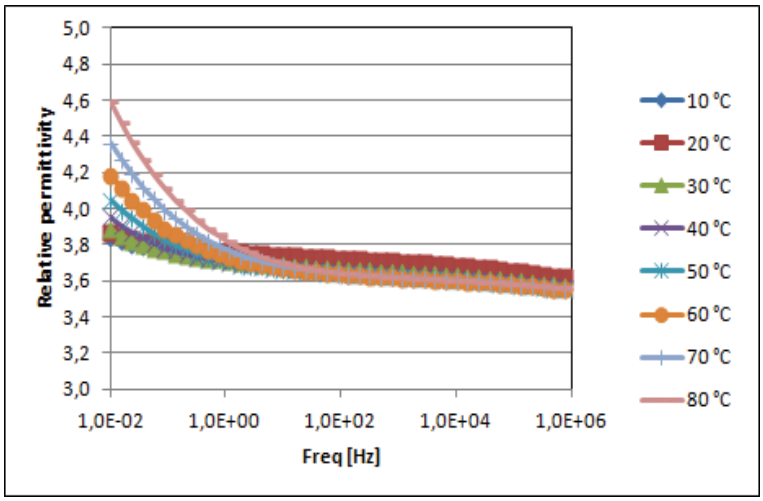

Fig. 9: Example of relative permittivity measurements of dry Epoxy/Silica.

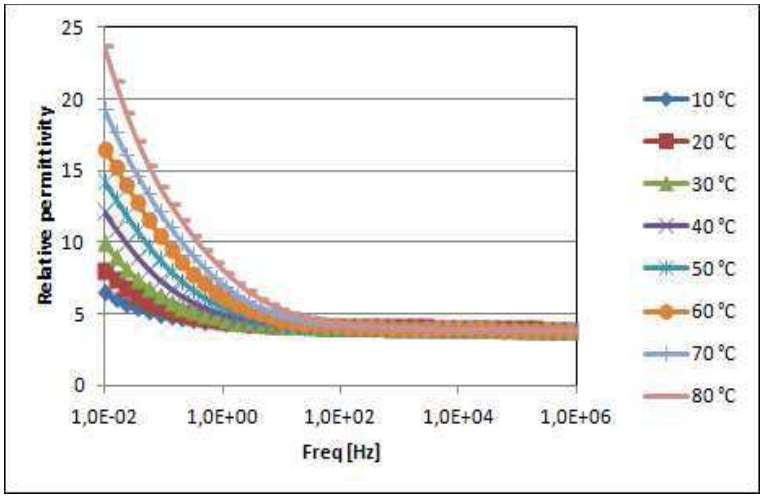

Fig. 10: Example of relative permittivity measurements of wet Epoxy/Silica.

On Fig. 10, we can observe an increase of relative permittivity due to the presence of water in the bulk of the material, especially at low frequencies, with a larger variation with

temperature (from 7 to 24 at 0.01 Hz, between 10 °C and 80 °C). At 1 MHz, a small increase of permittivity (3.8 instead of 3.6) is recorded.

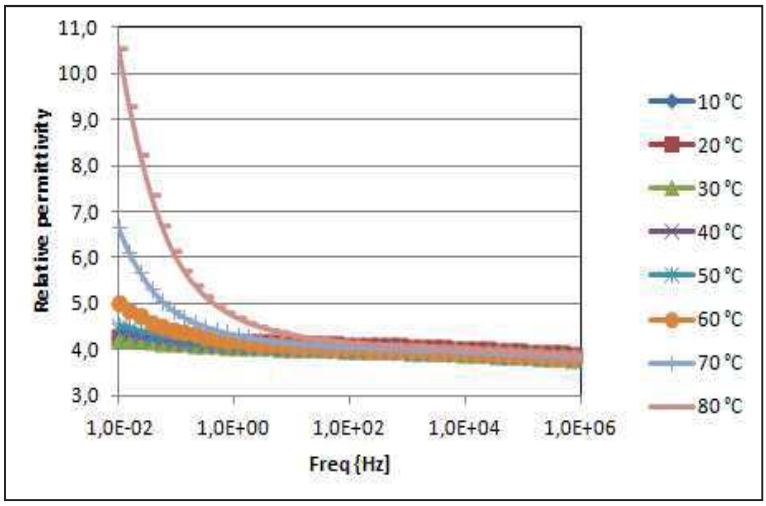

Fig. 11: Example of relative permittivity measurements of dry PA6T/66.GF50.

Fig. 11 shows a larger variation of relative permittivity with temperature in dry PA6T/66.GF50: from 4.0 to 10.5 at 0.01 Hz, between 10 °C and 80 °C. Compared to dry Epoxy/Silica (Fig. 9) the variation is larger.

Fig. 12 describes a huge variation of relative permittivity with temperature in wet PA6T/66.GF50. At low frequency, relative permittivity is reaching very high values, probably due to the combined influences of the presence of water and of interfacial polarization. From a practical point of view, this measurement points to the much higher sensitivity to the presence of water of PA6T/66.GF50 compared to Epoxy/Silica (Fig. 10). In PA6T/66.GF50, even the permittivity at 50 Hz shows large variations when water is present, whereas it remains stable in Epoxy/Silica. At 1 MHz the relative permittivity recorded is 4.1 at 20 °C.

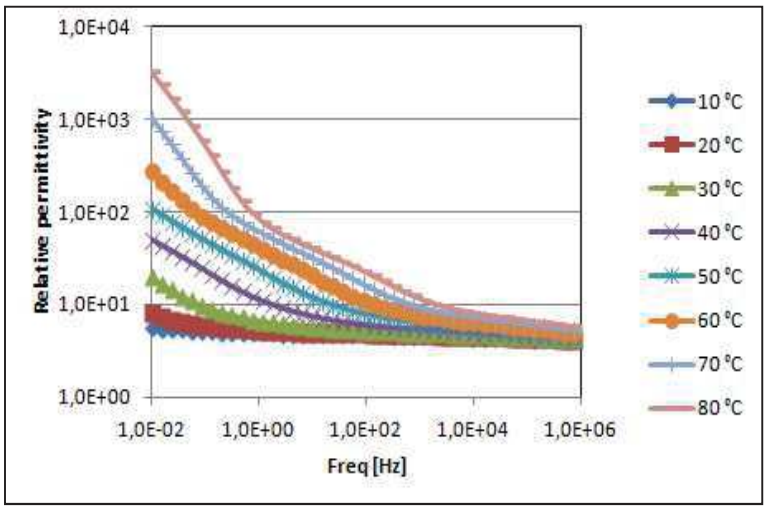

Fig. 12: Example of relative permittivity measurements of wet PA6T/66.GF50 (1.38 % of water).

In Tab. 18 an overview of dry and wet materials investigated are presented. A range of relative permittivity from 4.1 to 2.6 were measured by dielectric spectroscopy. For most materials, relative permittivity at 1 MHz increases slightly with the presence of water. Indeed, some materials uptake much smaller amount of water (filled Epoxy and PC) compared to Epoxy resin and PA6T/66.GF50.

Material	ε_r – 50 Hz / 20 °C	ε_r– 1 MHz / 20 °C
Epoxy resin – dry	3.2	3.1
Epoxy resin – wet (0.60% of water)	3.5	3.3
Epoxy/Silica – dry	3.7	3.6
Epoxy/Silica – wet (0.25% of water)	4.1	3.8
Epoxy/Silanized silica – dry	3.7	3.6
Epoxy/Silanized silica – wet (0.24% of water)	3.7	3.5
PC – dry	2.6	2.6
PC – wet (0.25% of water)	2.6	2.6
PA6T/66.GF50 – dry	4.1	3.9
PA6T/66.GF50 – wet (1.38% of water)	4.8	4.1
PA6T/66.GF35 – dry	4.1	3.8

Tab. 18: Summary of relative permittivity's measured at 50 Hz and 1 MHz at 20 °C.

In addition to these technical materials, a range of well-known standard materials was also used in creeping discharge experiments, mainly with the objective to increase the range of permittivities. Their characteristics are listed in Tab. 19.

Material	ε_r – 1kHz / 20 °C
PTFE	2.1
PP	2.2 – 2.4
Alumina	9
Glass	5

Tab. 19: Summary of relative permittivities for standard materials.

2.2. Surface charges on solids: Surface Potential Decay characterization

In the view of the study of creeping discharges, it is important to know how and how long charges can be eliminated from the solid insulator surface. Indeed, during breakdown measurements, series of high voltage impulses are applied to the material. When partial discharges not leading to breakdown occur, charges can be deposited and accumulate on the material surface. In turn, this may influence the breakdown process. One way to quantify this process is to perform Surface Potential Decay (SPD) experiments.

The Surface Potential Decay experiment allowed measuring the time required to evacuate surface charges in a controlled atmosphere (temperature and relative humidity). The decay can occur due to three main mechanisms, namely: bulk neutralization, surface conduction and neutralization by ions present in the gas.

- Bulk neutralization: represents the charge decay through the bulk of the solid material and be due to intrinsic conduction, charge injection and polarization processes.
- Surface conduction: refers to the charge leakage along the sample surface due to the tangential electric field, which appears when surface charge is distributed unevenly.
- Gas neutralization: indicate a compensation or neutralization of surface charges by free ions attracted to the charged surface from the surrounding gaseous environment.

Many previous works have been achieved on this subject with the study of the influence of many factors. In [15] the presence of water in the material favors the surface voltage decay during the first seconds of the measurement. This behavior is related to an increase in surface trap density as well as structural disorder due to the presence of water. The influence of relative humidity also influence the SPD by increasing it when humidity is high [16, 17]. By increasing temperature, SPD is strongly increasing. [18] shows that the temperature has a predominant role in the potential decay. The higher the temperature, the faster the surface potential decreases. There is also an influence of solid's nature on SPD.

In this study, the aim is to characterize the influence of solid nature, temperature, relative humidity and material water content on surface potential decay.

2.2.1. Experimental system

The surface potential decay experiment includes two successive steps:

- 1: corona charging of the surface (Fig. 14);
- 2: measurement of the surface potential versus time with an electrostatic non-contact probe (Trek model 347, Fig. 15).

The rotating sample support allows the transition between the two steps (Fig. 13). To fix the sample, a grounded ring is used with a conductive interlayer to provide a good electrical contact with the ground. All measurements were carried out in a climatic chamber to obtain stable temperature and relative humidity (RH) of the surrounding air.
A negative DC high voltage (- 8 kV) is first applied to a needle electrode to generate a corona discharge. A grid electrode tied at -1 kV is placed between the needle and the sample surface. In this way, a uniform field is generated between the grid and the solid surface. The charging process (transport of negative ions to the surface) stops when this field becomes zero, i.e. when the surface potential becomes identical to the grid potential. The charging

process was performed for five seconds. The sample was then rapidly moved under the electrostatic probe, and the measurement of potential decay started two seconds after the end of the charging process. The distance between the probe and the solid surface is 2 mm.

Similar experiments were also done by placing a conducting layer (copper sheet) on the sample surface, under the corona discharge. In this case, a similar electric field is induced in the material, but no more ions are present on the material surface. The recorded potential decay then represents the self-discharge of a capacitor with a floating electrode.

Fig. 13: Overview of the experimental setup [18].

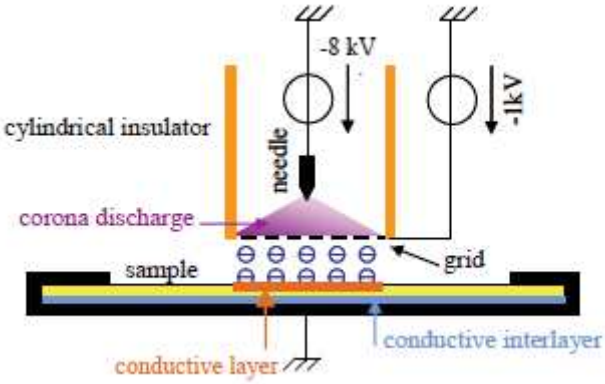

Fig. 14: Corona charging during the first step of surface potential decay experiment.

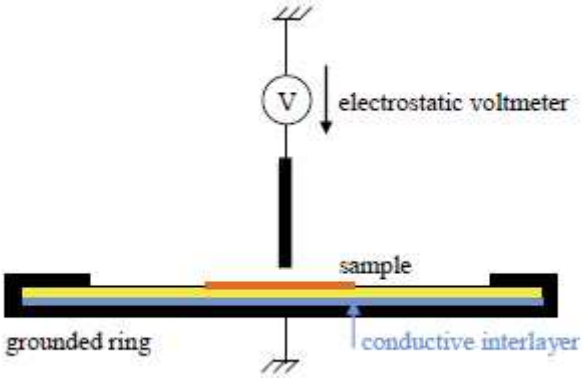

Fig. 15: Surface potential decay measurement with an electrostatic non-contact voltmeter.

2.2.2. Experimental protocol

To achieve this study samples were first dried or impregnated. Samples are then placed in the experimental set-up, and parameters are adjusted to regulate surrounding temperature and relative humidity. The time to reach stabilization can last up to one hour. Then the electrostatic probed is positioned above the solid surface to measure the initial surface potential before the measurement. This initial potential (due to static charges already present on the sample) should be < 100 V to properly compare results between materials. In several cases, the start of measurements was delayed by several hours until the defined minimum value (< 100 V) is reached. Several materials such as Epoxy/Silica showed high initial surface potentials due to manipulation of samples and other surrounding factors.

2.2.3. Results

To evaluate the measurement reproducibility, experiments were repeated up to six times. In each table (presented in sections below), the maximum, minimum and average values are indicated.

2.2.3.1. Influence of the solid

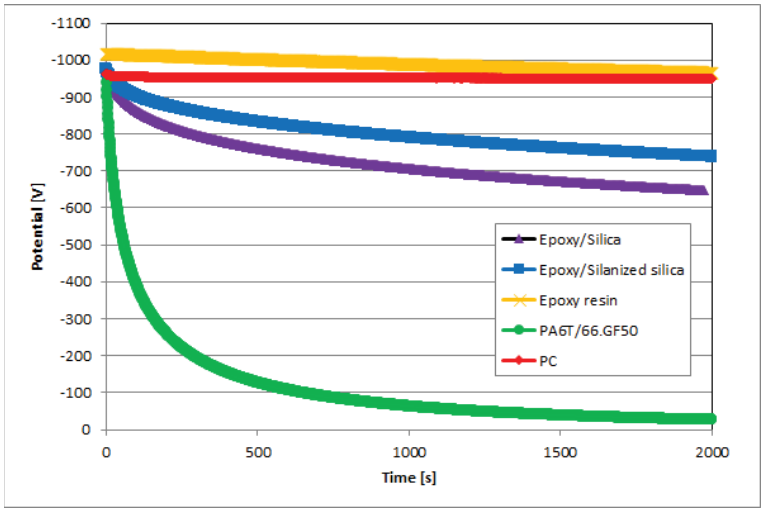

Fig. 16: Comparison of SPD for several dry materials with surrounding conditions of 60 °C / 20 %RH.

Fig. 16 shows the influence of the solid on surface potential decay in identical conditions (dried samples, 60 °C and 20 %RH). Surface potential is decaying faster on PA6T/66.GF50 than with others materials. It takes only few seconds for PA6T/66.GF50 to reach 50 % of the initial charging potential (- 1000 V). This time is much larger with Epoxy/Silica: to reach the same value it takes about twenty hours. The highest time required for charges to evacuate the surface is obtained with PC and Epoxy resin. For these materials, more than three days are needed to reach the 50 % value. Despite a fixed initial potential (- 1 kV) was applied, the

measured potential at the start of the measurement shows some variation (up to - 1020 kV) for Epoxy resin. This is due to the initial presence of charges on resin Epoxy samples, very difficult to eliminate.

2.2.3.2. Influence of sample water content on SPD

Fig. 17 shows typical results obtained at 60 °C and 20 %RH, with either a dry or water-saturated PA6T/66.GF50. A very large influence of the sample water content on potential decay can be observed. In the case of the wet sample, the potential decay occurred very quickly (a few seconds), i.e. very close to the limits of the measurement system (the delay between charging and starting of SPD measurement is 2 seconds, and one measurement of surface potential was taken every second). Therefore, a rather large uncertainty of measurements exists in this case.

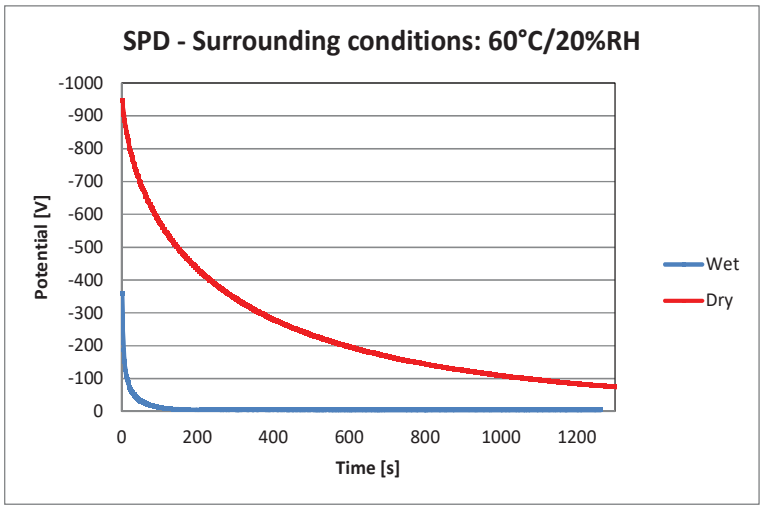

Fig. 17: Comparison of SPD for dry and wet PA6T/66.GF50.

Similar measurements were performed on Epoxy/Silica (Tab. 20), and similar tendencies were obtained than with PA6T/66.GF50.

Epoxy/Silica	SPD time (50%)
Dry	17 h
Wet	10 min

Tab. 20: SPD time to reach 50 % of charging voltage, with 20 %RH and 40 °C for dry and wet Epoxy/Silica.

Wet materials logically evacuate surfaces charges much faster than dry material.

2.2.3.3. Influence of temperature on SPD

Tab. 21 and 22 summarize measurement results obtained in a variety of conditions. The values quoted in these tables correspond to the time required to reach 50 % of the initial charging potential (i.e. - 500 V), for different values of temperature at a fixed relative humidity of 20 % and 30 % for dry and wet materials. Tab. 21 also shows the results obtained in identical conditions with a conducting layer on the material surface. Although SPD was a little bit faster in the presence of the layer, the values and the tendency at different temperatures are in line with those obtained without layer.

Dry PA6T/66.GF50	40 °C	60 °C	70 °C
Maximum	19 min	4 min	50 s
Minimum	7 min	1 min	38 s
Average	**13 min**	**2.5 min**	**44 s**

Dry PA6T/66.GF50 + conductive layer	40 °C	60 °C
Maximum	9 min	1 min
Minimum	7 min	1 min
Average	**8 min**	**1 min**

Tab. 21: SPD at different temperatures with 20 %RH for dry PA6T/66.GF50.

Wet PA6T/66.GF50	40 °C	60 °C
Maximum	3 s	< 1 s
Minimum	2 s	< 1 s
Average	**2.5 s**	**< 1 s**

Tab. 22: SPD at different temperatures with 30 %RH for wet PA6T/66.GF50.

Tab. 21 shows the large influence of temperature on SPD. Tab. 22 suggests a lower influence of temperature for the wet sample, but these measurements are characterized by a large uncertainty.

Similar measurements were performed on Epoxy resin but only with temperatures of 40 °C and 60 °C. Similar observations were done: by raising the temperature, surface potential decay is getting faster (Tab. 23).

Wet Epoxy resin	SPD
40 °C	10 min
60 °C	1 min

Tab. 23: SPD at different temperatures with 20 %RH for wet Epoxy resin.

2.2.3.4. Influence of surrounding air relative humidity

Tab. 24 and 25 show the influence of relative humidity RH of the surrounding air, at a fixed temperature of 40 °C for both dry and wet samples.

Dry PA6T/66.GF50	20 %RH	50 %RH
Maximum	19 min	7 min
Minimum	7 min	5 min
Average	**13 min**	**6 min**

Dry PA6T/66.GF50 + conductive layer	20 %RH	50 %RH
Maximum	9 min	6 min
Minimum	7 min	5 min
Average	**8 min**	**5.5 min**

Tab. 24: SPD at different relative humidity at 40 °C for dry PA6T/66.GF50.

Wet PA6T/66.GF50	30 %RH	50 %RH
Maximum	3 s	2 s
Minimum	2 s	1 s
Average	**2.5 s**	**1.5 s**

Tab. 25: SPD at different relative humidity at 40 °C for wet PA6T/66.GF50.

For dry PA6T/66.GF50, the surface potential decreases slightly faster with increasing RH from 20 %RH to 50 %RH. For wet PA6T/66.GF50, increasing the relative humidity has a low effect on SPD, but these measurements show a large uncertainty.

2.2.4. Discussion of results

A review of the physical processes involved in SPD experiments was proposed in [19]. These processes include the influence of currents flowing in the solid volume (conduction and polarization), at the surface (surface conduction), and also the possibility of charge neutralization at the sample surface by charges drained from the surrounding gas by the electric field existing above the sample. In [20], the authors carried out experimental and theoretical investigations to assess the influence of volume absorption currents on the potential decay. According to the materials and experimental parameters used, the measured potential decrease may result from a combination of these mechanisms, or may be dominated by a particular mechanism.

The results obtained here with PA6T/66 and epoxy are in agreement with those obtained in [21] with epoxy/alumina composites. The relative humidity of surrounding gas is playing a secondary role in SPD compared to the sample water content and temperature.

These results tend to show that surface conduction, which is considerably enhanced at high relative humidity, probably has a secondary influence on surface voltage decay. On the other hand, conduction processes occurring in the material volume, strongly influenced by temperature and water content, appear to constitute the dominant process involved in SPD.

The fact that the presence of a conducting layer has a moderate influence on SPD validates the comparison of SPD experiments with the self-discharge of a capacitor with one electrode floating. This basic representation contains several shortcomings, but it can be helpful to better understand the process by building a simplified equivalent electrical circuit.
In the following, we try to evaluate this hypothesis by measuring absorption currents in uniform fields under constant applied voltage.

2.3. Absorption current measurements

Current measurements can provide information on the solid reaction when a constant voltage is applied. This set-up measures the current versus time depending on solid nature, temperature and water content of solid.

2.3.1. Experimental system

The sample is placed between two electrodes plus a guard ring. Electrodes are made of conductive silicone. This electrode set-up is housed in an enclosure under controlled gas (nitrogen at 0.4 MPa), and fixed temperature (Fig. 18).

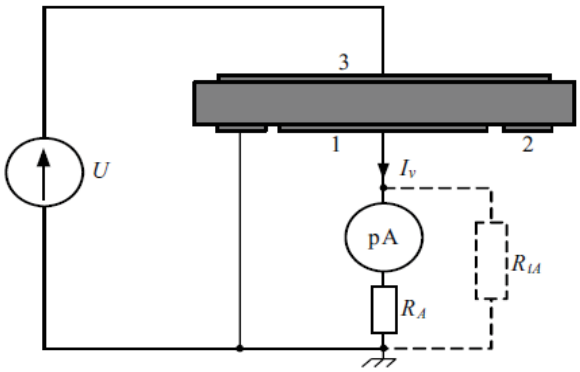

Fig. 18: Volume current measurement under application of a constant dc voltage (1 kV) [20].

A)

B)

Fig. 19: Set-up for current measurement.
A) Metal enclosure for measurements under pressure.
B) Electrodes arrangement.

Current down to 10^{-13} A are measured with a high sensitivity electrometer (Keithley 657). Connections are done with a low noise triaxial cable.

2.3.2. Experimental protocol

The sample is placed between electrodes and the set-up is installed in the metal enclosure (Fig. 19A). Vacuum is done and pressure of 0.4 MPa of dry nitrogen is applied. The metal enclosure is placed in a climatic chamber to control the temperature. A thermocouple gives the sample temperature during the measurements. After stabilization of temperature, DC voltage (1 kV) is applied across the sample, and the volume current is recorded versus time (Fig. 20). The recorded current includes both contributions of polarization and conduction processes due to the applied field. Current correlated to polarization decrease versus time. At long times, when this current becomes much lower than the conduction current, the recorded current may stabilize to a value Ic corresponding to a steady conduction process. Volume resistivity can then be calculated from Ic. Unfortunately, in many cases this stabilization was not reached even after several days, i.e. a situation frequently observed with very high resistivity polymers.

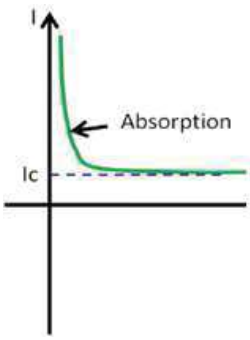

Fig. 20: Diagram for explanation of current measurements.

To investigate the influence of temperature, a temperature cycle is applied with the climatic chamber. The cycle comprises five steps: 20 °C / 40 °C / 60 °C / 40 °C / 20 °C (Fig. 21). Each temperature step lasted five hours. The relative humidity remained below 2 % for all temperatures.

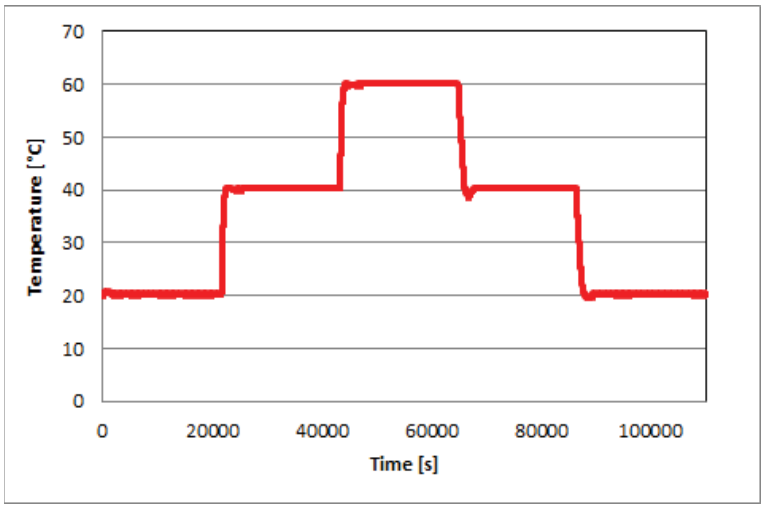

Fig. 21: Temperature cycle for current measurements.

2.3.3. Results

2.3.3.1. Absorption current

Fig. 22, 23, 24 and 25 show typical recorded currents induced by the application of a DC voltage of 1000 V. Currents show the classical behavior of absorption currents, decaying versus time according to a power law (equation 1):

$$i_a = A\, t^{-n} \qquad (1)$$

(n varies between 0.40 and 0.56 on Fig. 24). These absorption currents are due to the contributions of various physical processes occurring when a DC field is applied to the material, including polarization and conduction mechanisms. In such polymer/glass composite material, many interfaces are present, inducing also large interfacial polarization phenomena.

On Fig. 22 dealing with dry Epoxy/Silica material, we can observe that there is no obvious stabilization of the current at 20 °C, even if the current was recorded for long durations (above 10 hours). Thus, a stabilized DC conduction current cannot be obtained from these measurements. At very low currents (< 0.1 pA), the noise of measurement led to stop the experiment.

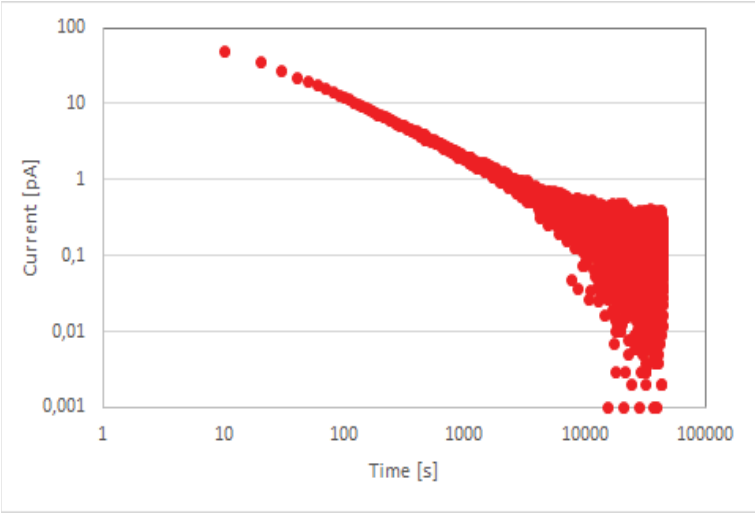

Fig. 22: Absorption current measurements in dry Epoxy/Silica, under the application of a constant DC voltage (1000 V) at 20 °C.

The same observation was done with wet Epoxy/Silica (Fig. 23). Water uptake didn't induce a measurable higher stabilized current. However, recorded absorption currents were about four times higher than for dry materials.

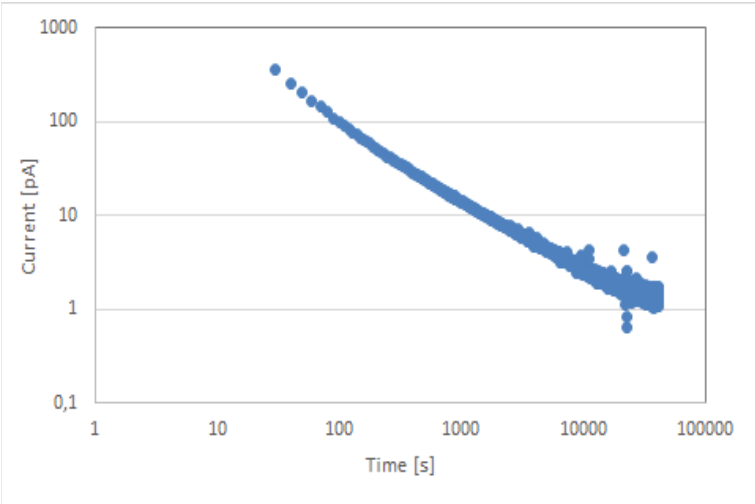

Fig. 23: Absorption current measurements in wet Epoxy/Silica, under the application of a constant DC voltage (1000 V) at 20 °C.

On Fig. 24 dealing with dry PA6T/66.GF50 composite, we can observe that there is also no observable stabilization of the current for the three temperatures investigated. It's interesting to note that the current gets a similar value as in dry Epoxy/Silica at 20 °C.

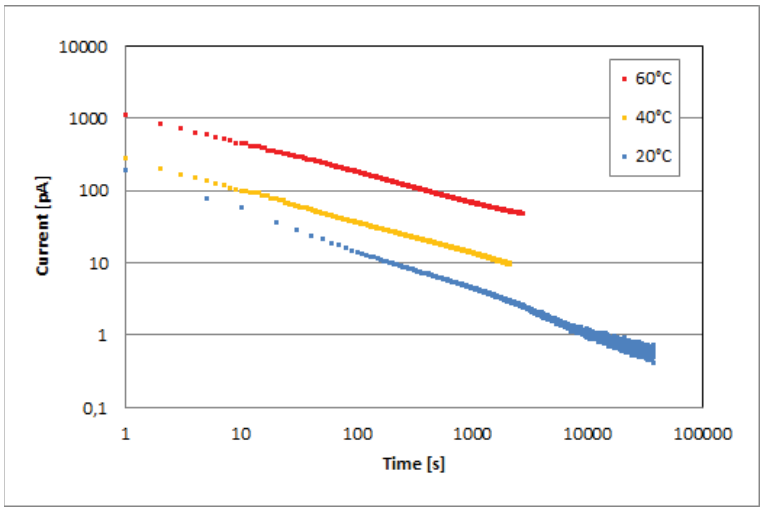

Fig. 24: Absorption current measurements in dry PA6T/66.GF50, under the application of a constant DC voltage (1000 V) at different temperatures.

Conversely, in the wet PA6T/66.GF50 composite, stabilization occurred after 1000 s on Fig. 25. This is due to the large increase of DC conductivity when water is present, such as previously reported with other materials. Compared to the dry PA6T/66.GF50 material, the absorption current before stabilization also increased by a factor about five.

Compared to wet Epoxy/Silica, the current at 10000 seconds is eighty time larger with wet PA6T/66.GF50. This increase can be explained by the much larger quantity of water uptake in PA6T/66.GF50 (1.38 % in mass) compared to Epoxy/Silica (0.25 % in mass).

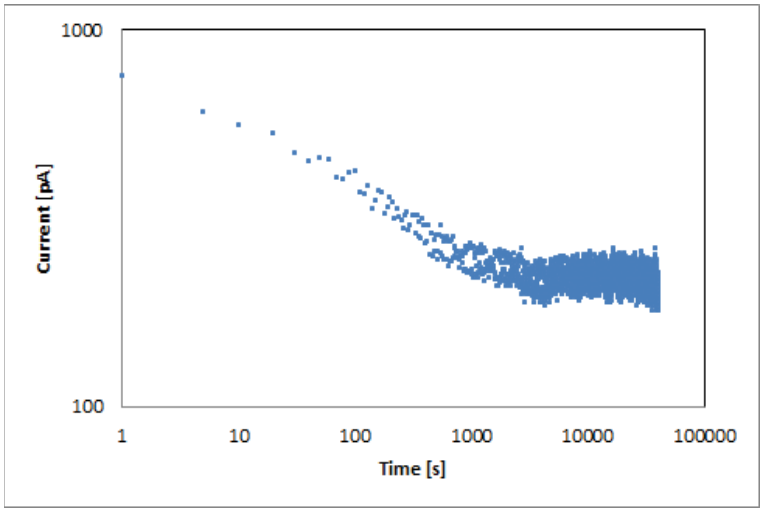

Fig. 25: Current measurements in wet PA6T/66.GF50, under the application of a constant DC voltage.

In most of measurements, it was not possible to observe a stabilization of the current even after one day. In order to classify materials, a “pseudo conductivity” was calculated from currents measured at an arbitrary time of 5 hours.

2.3.3.2. Resistivity calculations

With the electrode system presented in Fig. 26, a volume resistivity is calculated from the IEC 60093 standard [20] (equation 2):

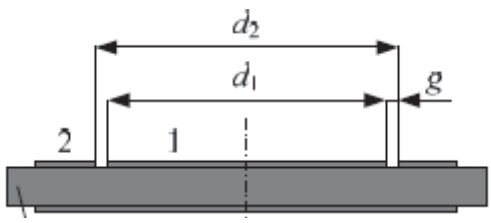

Fig. 26: Electrode system.

$$\rho_V = R_V \frac{A}{h} \qquad A = \pi \frac{(d_1+g)^2}{4} \qquad (2)$$

With R_V : volume resistivity, h : sample thickness, A : effective surface area of the measuring electrode (guarded electrode).

2.3.3.3. Influence of temperature on dried materials

Fig. 27 shows the variation of volume resistivity calculated from currents recorded at 5 hours with temperature. By increasing temperature from 20 °C to 60 °C, the value of volume resistivity decreases by two decades.

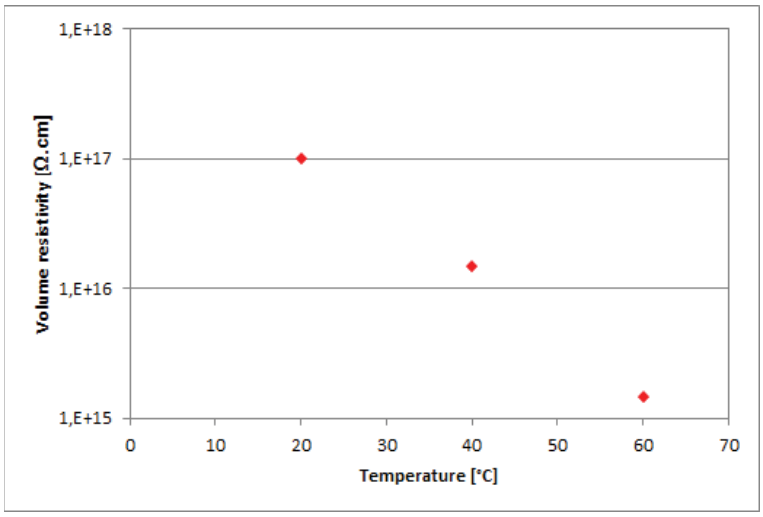

Fig. 27: Evolution of volume resistivity at 5 hours versus temperature for dry PA6T/66.GF50.

With an Arrhenius plot (Fig. 28), an activation energy of $E_a = 0.9\ eV$ can be obtained for PA6T/66.GF50.

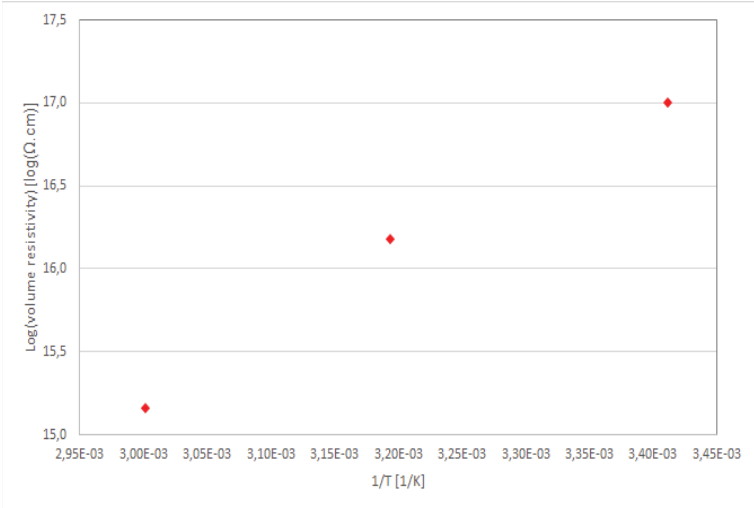

Fig. 28: Arrhenius plot of volume resistivity for dry PA6T/66.GF50.

For Epoxy/Silica, the noise on measurements of low values of current was rather high (Fig. 29). Measured currents are lower in Epoxy/Silica than in PA6T/66.GF50. From these results, we can estimate a volume resistivity of 10^{17} Ω.cm for dry Epoxy/Silica at 20 °C, 40 °C and 60 °C. This value is close to volume resistivity of PA6T/66.GF50 at 20 °C.

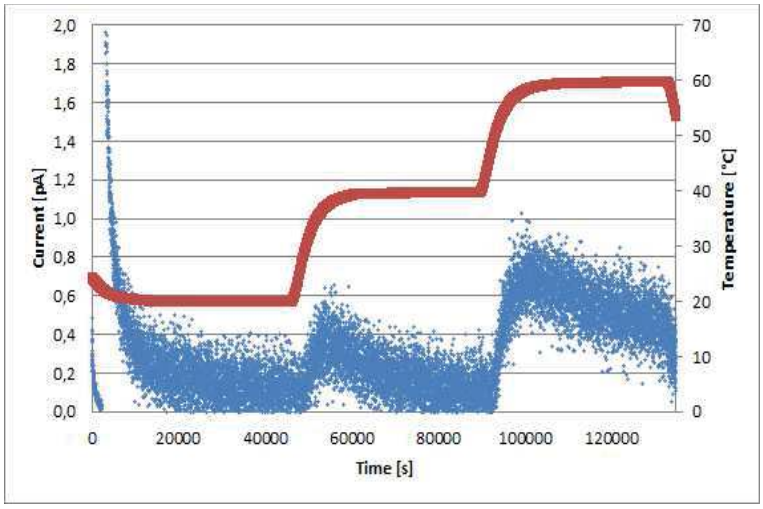

Fig. 29: Example of current measurements with temperature variations for dry Epoxy/Silica.

2.3.3.4. Influence of water content

Compared to dry Epoxy/Silica, it was easier to calculate volume resistivity for wet Epoxy/Silica (0.25 % water in mass) due to the increase of current. Volume resistivity decreases strongly with temperature (from 20 °C to 60 °C) (Fig. 30). From the Arrhenius plot (Fig. 31) an activation energy of $E_a = 0.6\ eV$ was calculated.

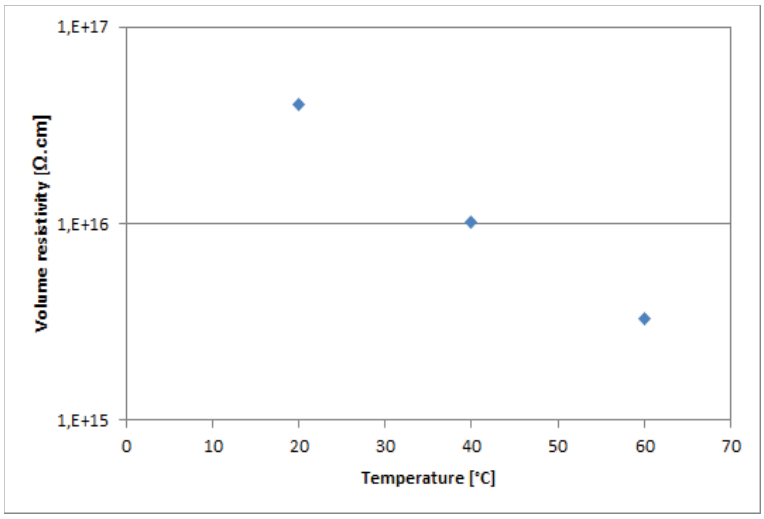

Fig. 30: Evolution of volume resistivity versus temperature for wet Epoxy/Silica (0.25% of water).

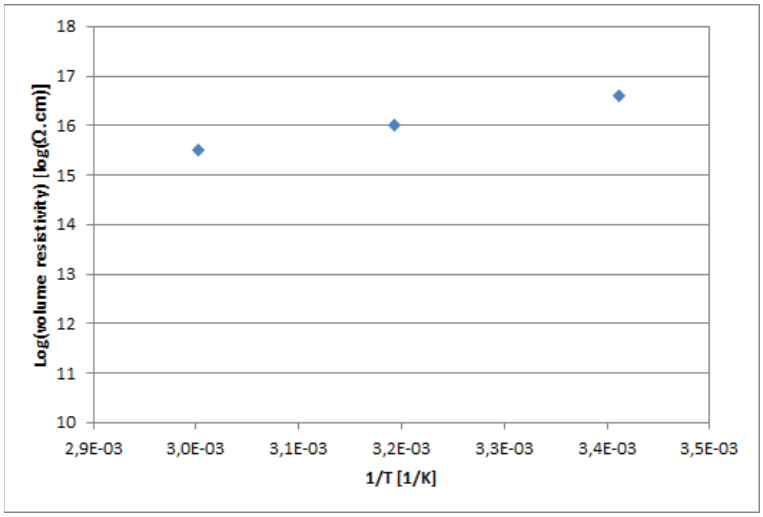

Fig. 31: Arrhenius plot of volume resistivity for wet Epoxy/Silica (0.25% of water).

Fig. 32 shows a strong decrease of volume resistivity in presence of water (1.38 % in mass). The largest decrease can be observed at 60 °C with three decades difference. With Fig. 33 an activation energy of $E_a = 0.9\ eV$ is obtained for the dry sample, while $E_a = 1.8\ eV$ for wet PA6T/66.GF50.

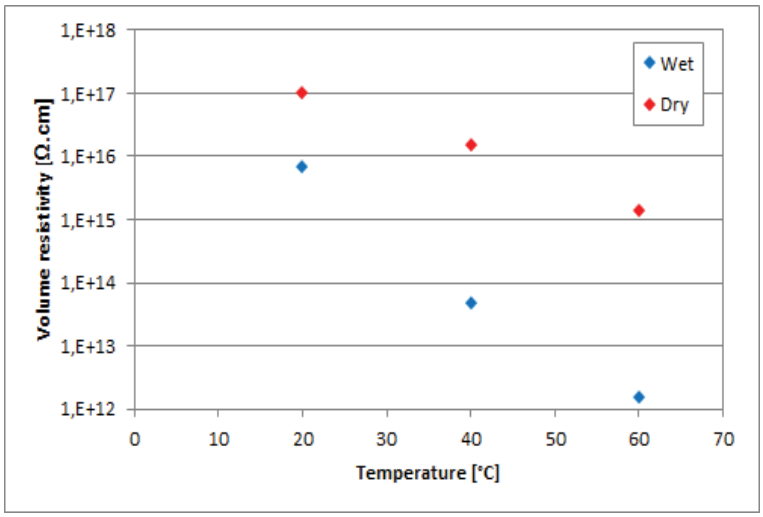

Fig. 32: Evolution of volume resistivity versus temperature for wet (0.25 % of water) and dry Epoxy/Silica.

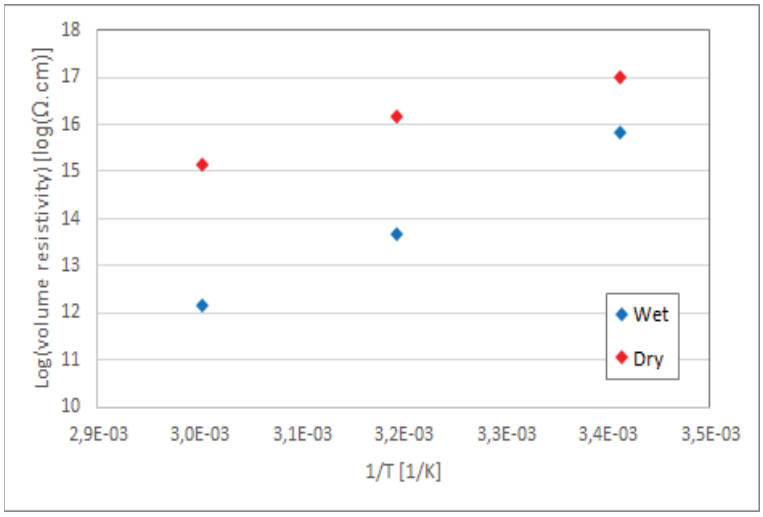

Fig. 33: Arrhenius plot of volume resistivity for wet (1.38 % of water) and dry PA6T/66.GF50.

2.3.3.5. Correlation between SPD and current measurements

The quantitative correlation between absorption currents measured under constant DC voltage and SPD experiments involving a decreasing voltage is a complex question, that cannot be solved simply [19]. A first-order approximation can be done at the initial instants of SPD, when the voltage decrease remains small compared to the initial charging voltage. Considering the experiments carried out with a conducting layer, the voltage decay can be basically compared to the self-discharge of a capacitor due to absorption currents (equation 3).

$$C = \varepsilon_0 \varepsilon_r \times \frac{A}{d} \qquad (3)$$

With d the distance between the two electrodes and A the area of the electrode.

Fig. 34 shows the comparison between SPD measurements at short times with a conducting layer, and the calculated voltage decay of the sample capacitance due to absorption currents measured. Although this simple model contains a number of shortcomings, we can observe a good agreement between these plots obtained at different temperatures. This validates the fact that surface potential decay measured in our conditions mainly results from absorption currents flowing through the sample volume, at least at the initial instants of SPD.

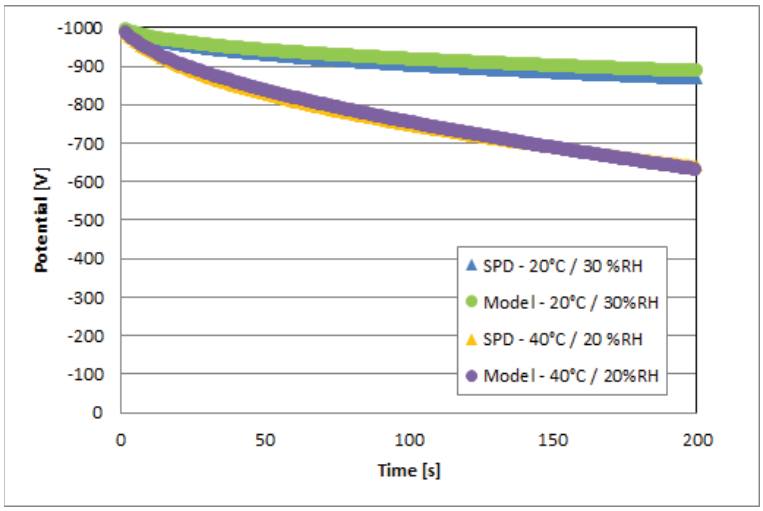

Fig. 34: Comparison between SPD with a conductive layer, and calculated voltage decay of the equivalent capacitor due to absorption currents for dry PA6T/66.GF50.

3. Conclusion

In this chapter, several materials were selected to study several of their properties supposed to have an influence on the creeping discharge process: permittivity, conductivity, presence of water, ability to store or dissipate surface charges. From these results, we will be able to correlate breakdown and pre-breakdown measurements of *Chapter 3* and *4*.

Surface Potential Decay highlights differences between materials regarding the behavior of surface charges versus time. To some extent, these results can be correlated to absorption current measurements. SPD is the fastest on PA6T/66.GF50 because it has also the lowest resistivity. These data will be used later to evaluate the influence of surface charges during creeping discharge experiments with these materials. In the “perpendicular field” breakdown experiments described later, the field geometry will be identical to that existing during SPD experiments (i.e. main field perpendicular to the surface). Consequently, the SPD behavior observed here can be properly used to analyse results. In the second configuration (“parallel field” breakdown experiments) the field direction will be different, but we will suppose that the classification of solids regarding their ability to store or dissipate surface charges will remain the same.
Values of permittivity’s at 1MHz will be used to study the influence of permittivity on breakdown voltage.

Bibliography

[1] W. Tillar Shugg, “Handbook of electrical and electronic insulating materials”, Second edition, Chap. 3 p. 37, September 1992.

[2] DUPONT™ ZYTEL® HTN High Performance Polyamide Resin, Product Reference Guide.

[3] Polymers International, Australia.
Link: http://polymers.com.au/thermoplastics/

[4] R. C. Rowe, P. J. Sheskey, M. E. Quinn, “Handbook of Pharmaceutical Excipients”, Pharmaceutical Press. pp. 11-12, 2009.

[5] Saint-Gobain Main Website.
Link: http://www.saint-gobain-sekurit.com/glossary/glass-properties

[6] Maurice Reynes, « Technologie des plastiques » 3° édition revue et augmentée, Hermes, 1998.

[7] Kaye & Laby, Tables of Physical & Chemical Constants, National Physical Laboratory.
Link: http://www.kayelaby.npl.co.uk/general_physics/2_6/2_6_5.html
Link: http://www.kayelaby.npl.co.uk/general_physics/2_6/2_6_3.html

[8] Encyclopedia Britannica.
Link: https://www.britannica.com/science/polytetrafluoroethylene

[9] PolymerProcessing.com, Information, education, resources and expertise in the field of polymer processing.
Link: http://www.polymerprocessing.com/polymers/PP.html

[10] Van der Burgt, F. P. T. J. “Crystallization of isotactic polypropylene : the influence of stereo-defects”, Eindhoven: Technische Universiteit Eindhoven DOI: 10.6100/IR559498, 2002.

[11] C. L. Beyler and M. M. Hirschler , “Thermal Decomposition of Polymers”, Chapter 7, Section one, p.111-131, 2002.

[12] P. Bardonnet, “Résines époxydes (EP) – Composants et propriétés”, Techniques de l’Ingénieur, traité Plastiques et Composites A 3 465, 1992.

[13] Institut für Festkörperphysik, Technische Universität Wien.
Link: https://www.ifp.tuwien.ac.at/spectroscopy/research/

[14] Laboratory for soft matter and biophysics, Katholieke Universiteit Leuven (KU Leuven).
Link: http://fys.kuleuven.be/zmb/Research_themes/rt_dielectric/rt_dielectric

[15] A. Aragoneses, I. Tamayo, A. Lebrato, J. C. Canadas, J. A. Diego, D. Arencon and J. Belana, "Effect of humidity in charge formation and transport in LDPE", Journal of Electrostatics 71 611-617, 2013.

[16] T. Augusto de Lima Burgo, C. A. Rezende, S. Bertazzo, A. Galembeck and F. Galembeck, "Electrical potential decay on polyethylene: role of atmospheric water on electric charge build-up and dissipation", Journal of Electrostatics 69 401-409, 2011.

[17] B. Lutz, J. Kindersberger, "Influence of relative humidity on surface charge decay on epoxy resin insulators", Proceedings of the 9th International Conference on Properties and Applications of Dielectrics Materials, July 19-23, 2009, Harbin, China.

[18] L. Zavattoni and O. Lesaint, "Surface potential decay of an epoxy resin : influence of material's water content , air's relative humidity and temperature," 8th SFE conf., Cherbourg-Octeville (France), 3-5 july, 2012.

[19] P. Molinié, "A review of mechanisms and models accounting for surface potential decay," *IEEE Trans. Plasma Sci.*, vol. 40, no. 2 Part 1, pp. 167–176, 2012.

[20] M. Lisowski and R. Kacprzyk, "Changes proposed for the IEC 60093 standard concerning measurements of the volume and surface resistivities of electrical insulating materials", IEEE Transactions on Dielectrics and Electrical Insulation, vol. 13, No. 1, February 2006.

[21] L. Zavattoni, O. Gallot-Lavallée and O. Lesaint, "Surface potential decay of an epoxy resin: influence of material's water content, air's relative humidity and temperature", SFE 2012, Cherbourg, France, pp. 155-160, 2012.

Chapter 3: Influence of solid's nature on breakdown voltage

1. Introduction

As shown in *Chapter 1*, many studies were carried out about the influence of solid's insulator on the breakdown voltage. However, the question is still under debate since contradictory results are frequently obtained regarding the influence of solids. In *Chapter 2*, a large range of materials was selected and characterized to study the influence of their properties on the breakdown voltage.

The objective of this chapter is first to get a better knowledge of the influence of solid's nature on breakdown voltage, because it represents a key point for the design and reliability of medium voltage apparatus. As explained above, we will mainly consider here the influence of solids on **discharge propagation and breakdown**, and not on discharge initiation that will be studied in *Chapter 4*. Therefore, the experimental conditions will be first defined in order to get results relevant for this objective.
Another objective will be to check whether or not if the charge of insulators constitutes an important issue during breakdown tests, by changing their conductivity via the impregnation with water.
The influence of field geometry will be investigated by using two main electrode systems using a point to initiate discharges ("parallel field" and "perpendicular field"), and also another one using a sphere electrode in order to reproduce the case of discharges initiated by a less divergent field.

The starting point of this study was the electrode system (Fig. 1) previously used by Schneider Electric to perform breakdown measurements along insulating solids. This mock-up is more representative of optimized design in real apparatus.

Fig. 1: Photograph of Schneider Electric electrodes for breakdown measurements with solids.

This electrode system has been set up to minimize the effect of the "triple point", as in optimised applications (Fig. 2). The "triple point" effect relates to the local field enhancement existing in gases at contact points between electrode/gas/insulating solid, due to the mismatch of permittivity between gas and solid. Such triple points constitute well-known sources of discharges in gas-insulated systems [1]. Compared to a point-plane gap, the field along the solid is more uniform with this electrode system (Fig. 3), and with a low electric field at the triple point. A small protuberance of 1 mm radius induces a local field enhancement, representing a surface defect able to trigger breakdown in the gas in the

vicinity of the insulating solid surface. In real systems, such defect may arise due to e.g. the presence of a particle on one electrode.

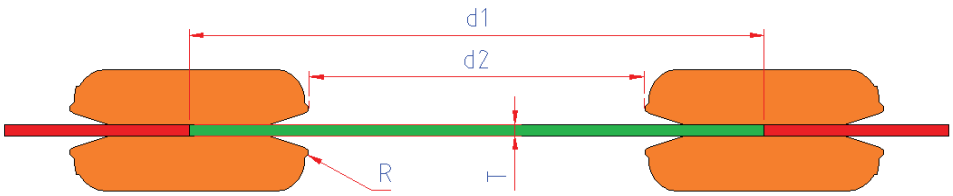

Fig. 2: Schematic drawing of Schneider Electric electrodes configuration, with R = 1 mm, d1 = 80 mm, d2 = 38 mm and T = 3 mm.

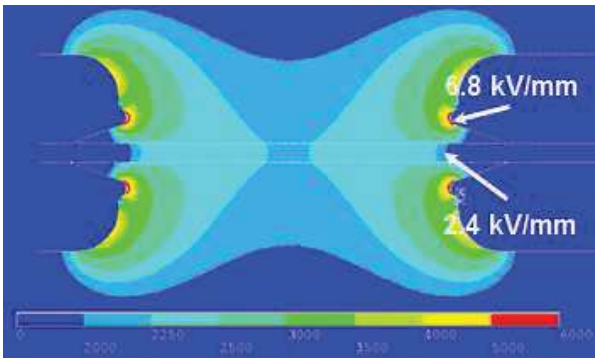

Fig. 3: Numerical simulation of field with Schneider electrodes (Flux2D ® software).

Preliminary breakdown measurements were performed with this system, using a 1.2/50 µs standard lightning impulse. Fig. 4 shows typical results for dry and wet materials (*Chapter 2*). Considering error bars, no clear influence of the solid's nature on breakdown voltage was observed in these measurements.

Only breakdown voltage was recorded, and it was not possible to carry out more refined investigations such as transient current measurements and discharge visualizations. In these breakdown measurements, it could not be determined if partial discharges occurred at voltages lower than the breakdown voltage, and if they first propagated on the solid surface before going to breakdown. This system also represented the case of a main field essentially parallel to the surface, whereas in practical systems the field at different locations may also be perpendicular to the surface.

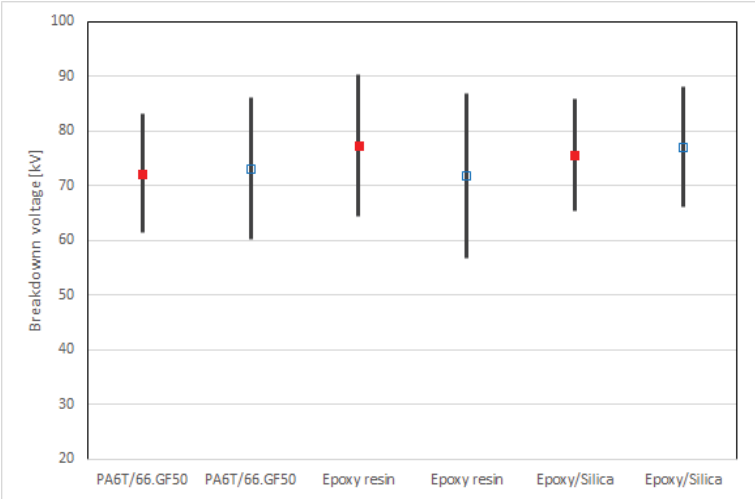

Fig. 4: Breakdown voltages measured with the Schneider Electric electrode system (parallel field) for dry (full dots) and wet (open dots) materials.

In the following, we will first select appropriate setup to get breakdown voltage measurements representative of discharge propagation (i.e. characterized by a discharge initiation voltage significantly lower than the breakdown voltage). To this end, the appropriate electrodes (radius of curvature and gap distance) need to be selected. In the second phase, we will perform breakdown measurements with these electrodes.

2. Experimental setup for breakdown measurements

A measurement bench has been set up to measure breakdown voltage in different electric field configurations. Two test cells were used to perform measurements either in atmospheric air, or under gas pressure.

2.1. General presentation

Fig. 5, Fig. 6 and Fig. 7 show an overview of the setup used in this chapter. It includes a Marx impulse generator, a voltage divider, a series resistance, a test cell, an oscilloscope, an image intensifier, a photomultiplier and a computer. This test bench is placed in a Faraday cage and controlled by a control desk outside the cage.

Fig. 5: Control desk of Marx generator.

Fig. 6: Marx generator, test cell, and optical bench within the Faraday cage.

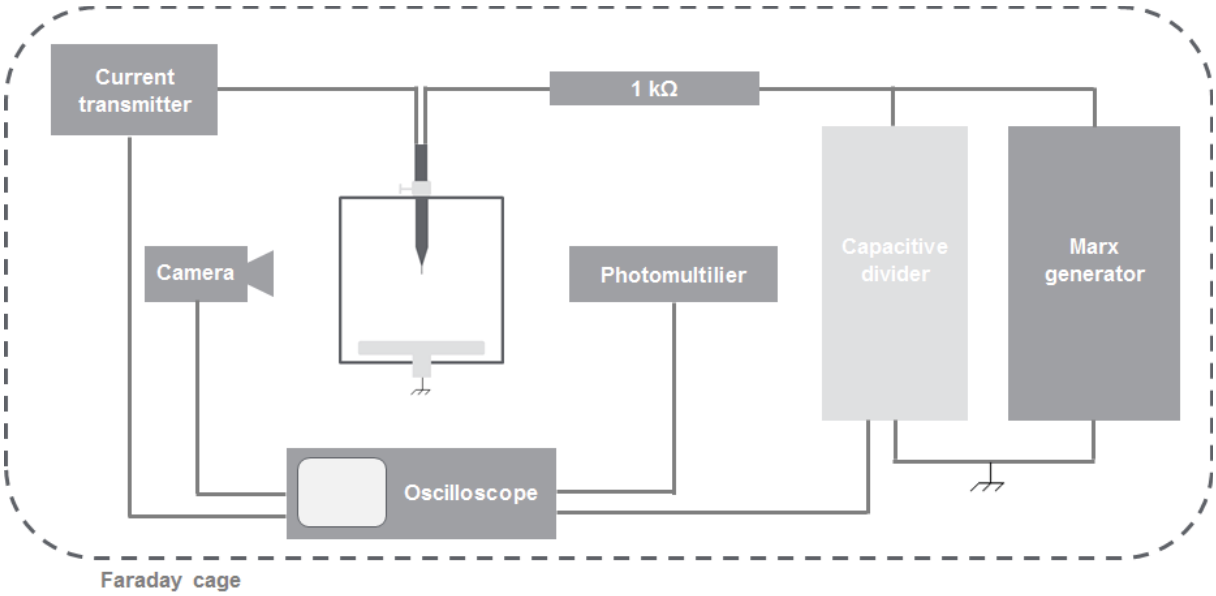

Fig. 7: Schematic representation of the set-up used for breakdown measurements.

2.1.1. The Marx generator

The Marx generator produces a high voltage pulse by first charging several capacitors in parallel with a high voltage DC power supply. To create the output pulse, the first spark gap of the generator is triggered, and the subsequent closing of all spark gaps connects all capacitors in series via resistors [2]. The Marx generator used in our study has a low energy (maximum 400 J at 500 kV), inducing a low degradation of materials, and allowing to obtain more results with a single sample. Positive and negative polarity measurements were carried out in this study. The shape of the high voltage pulse is recorded with a capacitive divider.

2.1.2. Signal recordings

Electrical signals are recorded with a digital oscilloscope Tektronix MDO 3054 with 500 MHz bandwidth and high-speed sampling rate of 2.5 G/s.

2.1.3. Photocurrent measurements

Some measurements of the light emitted by discharge precursors (streamers, leaders) were taken by a photomultiplier (RTC 56AVP) connected to the oscilloscope. This photomultiplier detects the light with a wavelength between 300 nm and 600 nm. An adjustable diaphragm regulates the quantity of light to avoid saturation.

2.1.4. Visualization

To visualize discharges, a high-speed gated image intensifier (Hamamatsu V3063U) was used to capture an “instantaneous image” of high-speed phenomena occurring within extremely short time durations, by means of a fast gate operation (down to 50 ns). Fig. 8 shows the corresponding spectral response of the intensifier (200 nm to 860 nm). The objective used (achromatic triplet of 45 mm focal length) was made of quartz in order to keep the UV sensitivity down to 200 nm, favorable for visualization of discharges in air.

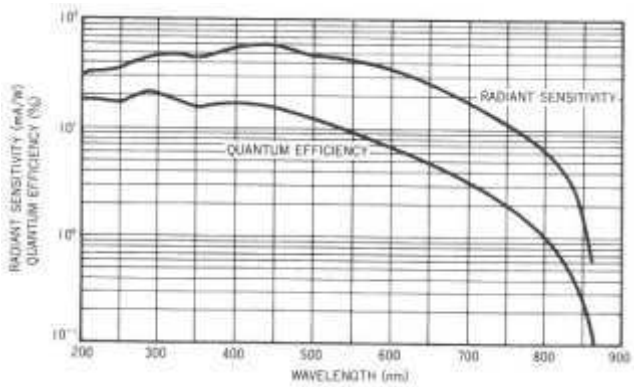

Fig. 8: Spectral Response of the Hamamatsu V3063U intensifier [3].

2.2. Test cells

Two test cells were used for breakdown measurements: one for atmospheric air measurements and one for measurements under pressure.

2.2.1. First test cell

The test cell for atmospheric air measurements is composed of a transparent box (33 x 30 x 30 cm) made in PMMA (Fig. 9). High voltage from Marx generator is applied to the electrode holder. Another similar test cell with open sides (in order to avoid UV absorption by PMMA) was also used for visualization.

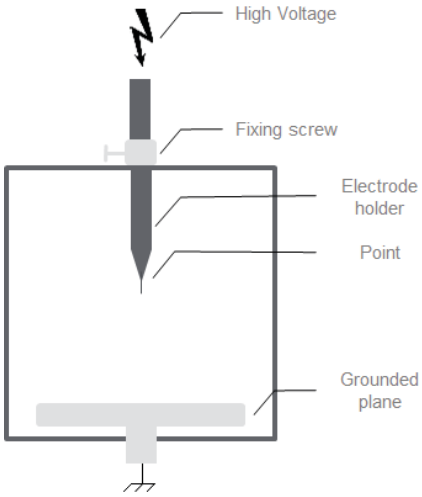

Fig. 9: Atmospheric air test cell.

2.2.2. Second test cell

The second test cell was designed and manufactured for pressure measurement up to 0.3 MPa. Fig. 10 shows the overview of the cell made of a cylindrical structure in PVC, with two quartz windows to permit visualization of discharges occurring between electrodes. The electrodes setup is the same as used in the first cell.

Fig. 10: Second test cell for pressure measurements.

2.3. Electrode systems

2.3.1. Point – plane geometry

This electrode system induces a highly non-uniform electrical field. The point connected to high voltage (Fig. 11 and Fig. 12 A and B) had a 0.5 mm tip radius of curvature (see next sections). The point extremity was bent with a 45° angle, in order to get in contact with the insulating solid, placed parallel to the point-plane gap axis. Most of the tests were performed with a d = 5 cm gap.

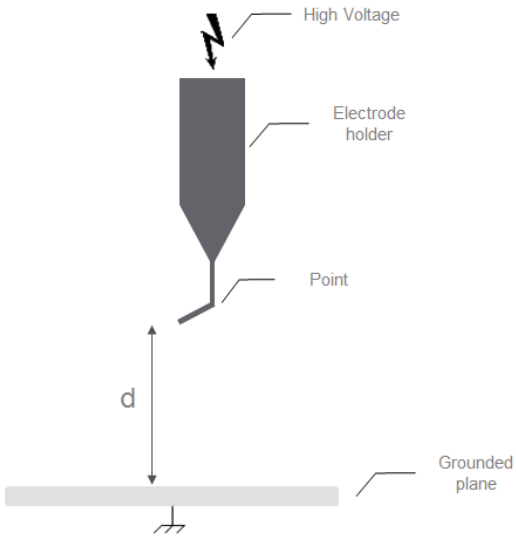

Fig. 11: Schematic drawing of point-plane electrodes configuration without solid.

Fig. 12 presents two electrodes configurations used in the presence of a solid insulator:

- Fig. 12 A: “parallel field” configuration. In this case, the main direction of the field (showed in red line) is parallel to the solid surface;

- Fig. 12 B: “perpendicular field” configuration. With the presence of an additional grounded electrode behind the solid (made of adhesive aluminium tape), the electric field direction becomes mostly perpendicular to the solid surface.

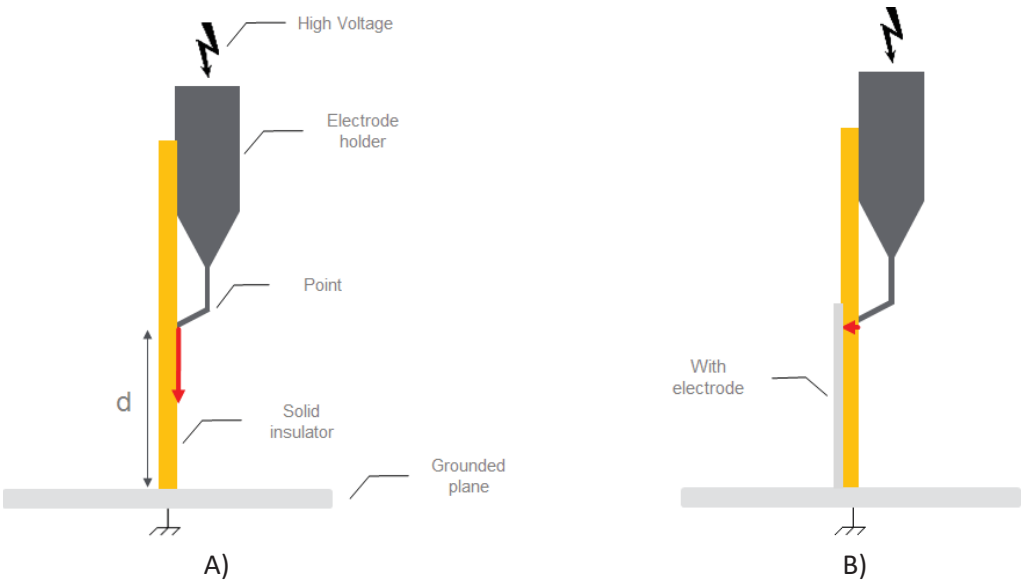

Fig. 12: Schematic drawing of A) “parallel” and B) “perpendicular” field configurations.

Contrarily to the Schneider Electric electrode setup presented in the introduction, these setups are not directly representative of real apparatus configurations. The point extremity is in contact with the solid surface. Around the contact point, a small “triple junction” between gas, solid and electrode is formed. In this region, the electric field in the gas is enhanced due to the mismatch of permittivities, hence facilitating discharge inception and resulting in an inception voltage significantly lower than breakdown voltage.
The “parallel” and “perpendicular” field geometries constitute two extreme cases, considering that in real systems, actual field distributions along dielectric surfaces will be intermediate between these limits.

2.3.2. Sphere-plane Geometry

This electrode setup (Fig. 13) has a close configuration to the point-plane but with a ten times larger electrode radius (5 mm), and hence lower maximum field. The electrode is in contact with the solid, surface. A local field enhancement arises in the region of contact with the solid. It will be used as an alternative to the point-plane geometry (Fig. 12A), with a much lower difference between inception and breakdown voltage.

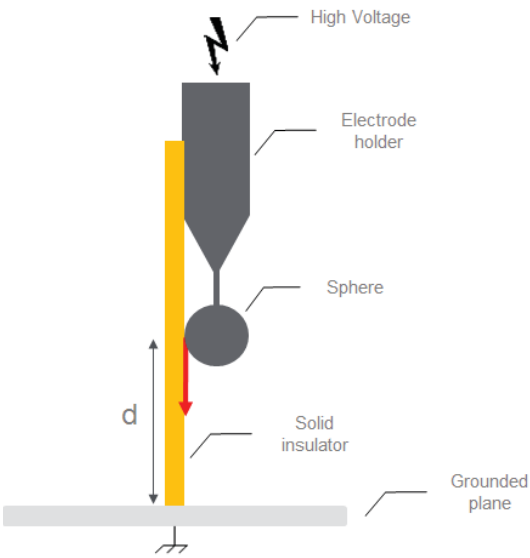

Fig. 13: Sphere – plane configuration

2.4. Field calculations

A 3D simulation model was developed with COMSOL™ to quantify the electric field for the different configurations of electrodes presented above (Fig. 14).

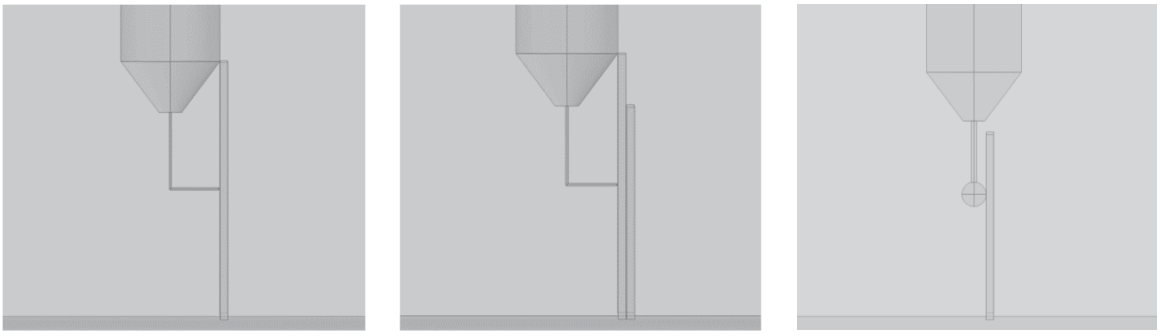

A) B) C)

Fig. 14: Representation of electrodes geometries with a gap of 5 cm

A) Point of 0.5 mm radius, parallel field configuration.

B) Point of 0.5 mm radius, perpendicular field configuration.

C) Sphere of 5 mm radius, parallel field configuration.

Fig. 15, 16 and 17 show the electric field distribution for the three setups of electrodes (zoom on the extremity of the point and sphere). Electric field was calculated for three relative permittivities: PP ($\varepsilon_r = 2.3$), glass (ε_r = 5.0) and alumina (ε_r = 9.0). In all cases, there is an enhancement of the electric field at the triple point with the increase of the relative permittivity of the solid. The maximum electric field is located in the gas at the triple point, where the electrode is in contact with the solid insulator.

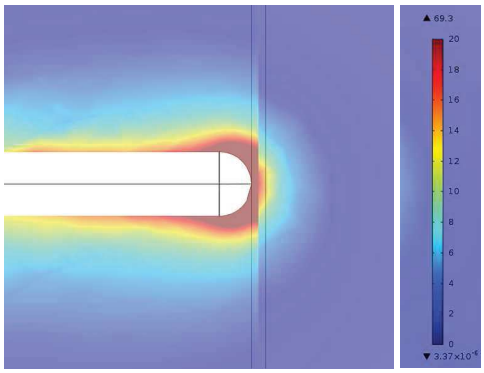

$\varepsilon_r = 2.3$

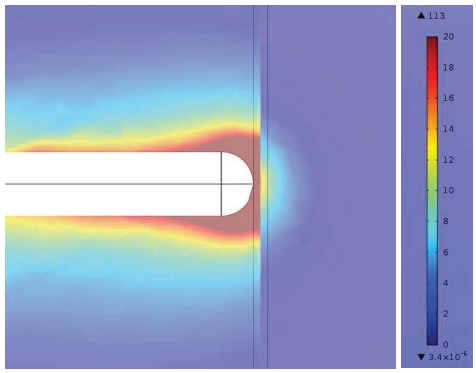

ε_r = 5.0

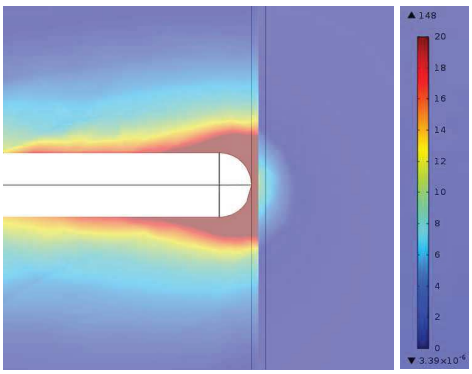

ε_r = 9.0

Fig. 15: Electric field [kV/mm] of the point-plane geometry in parallel field with a point of 0.5 mm of radius and a gap of 5 cm (V = 50 kV).

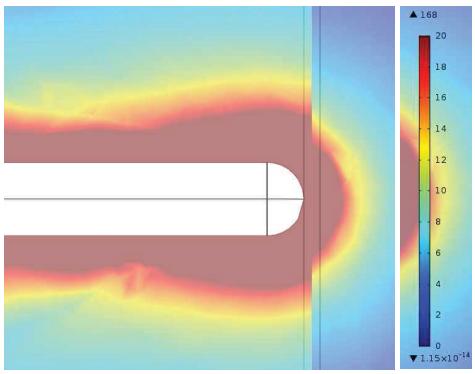

$\varepsilon_r = 2.3$

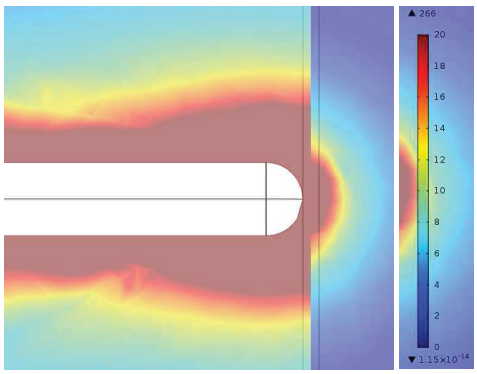

ε_r = 5.0

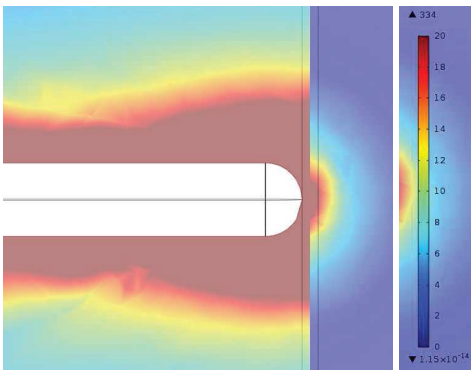

ε_r = 9.0

Fig. 16: Electric field [kV/mm] of the point-plane geometry in perpendicular field with a point of 0.5 mm of radius and a gap of 5 cm (V = 50 kV).

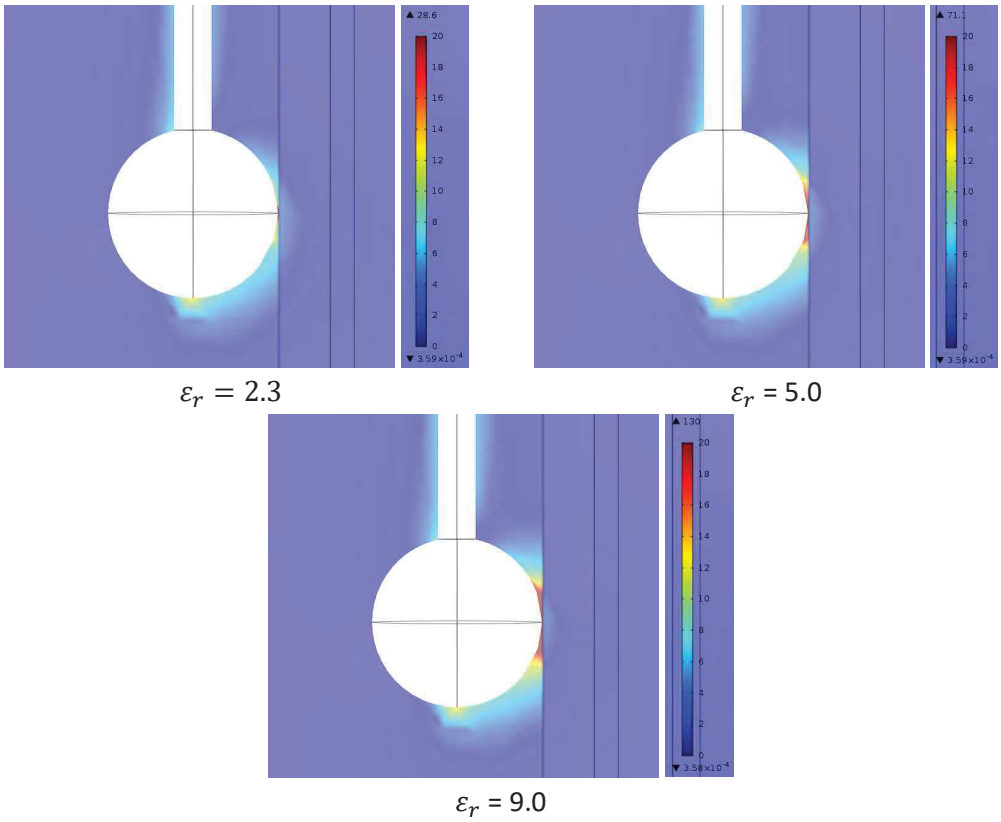

Fig. 17: Electric field [kV/mm] of the sphere-plane geometry in parallel field with a point of 5 mm of radius and a gap of 5 cm (V = 50 kV).

Figs. 18 and 19 show the value of the electric field versus relative permittivity in parallel and perpendicular field, calculated with 50 kV (value close to measured breakdown voltages). Values correspond to the maximal electric field calculated. In Fig. 18, the perpendicular field configuration enhances the electric field at the extremity of the point compared to parallel configuration. For Epoxy/Silica (the reference material) in perpendicular field, the electric field is 28 % higher than in parallel field.

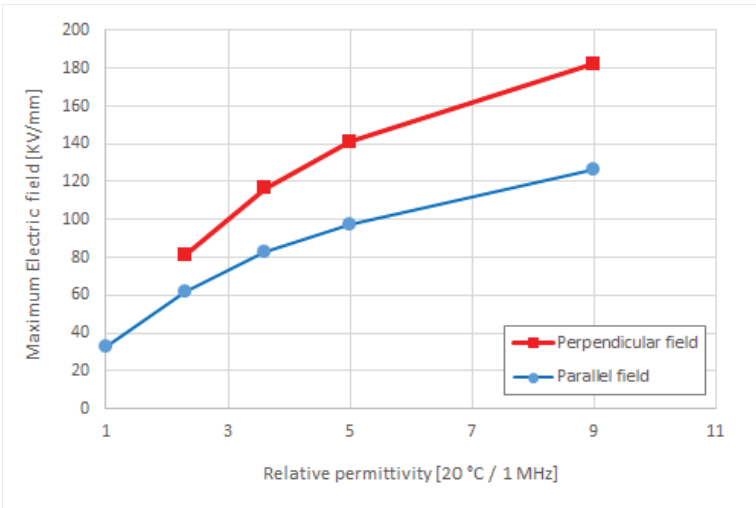

Fig. 18: Electric field for point (0.5 mm) – plane geometry.

In sphere – plane configuration (Fig. 19), the electric field is lower due to the larger radius of the electrode. Without solid, the electric field is 86 % higher for the point (0.5 mm radius) than for the sphere (5 mm radius). In the presence of alumina, the maximum electric field can reach 126 KV/mm with the point instead of 45 kV/mm with the sphere.

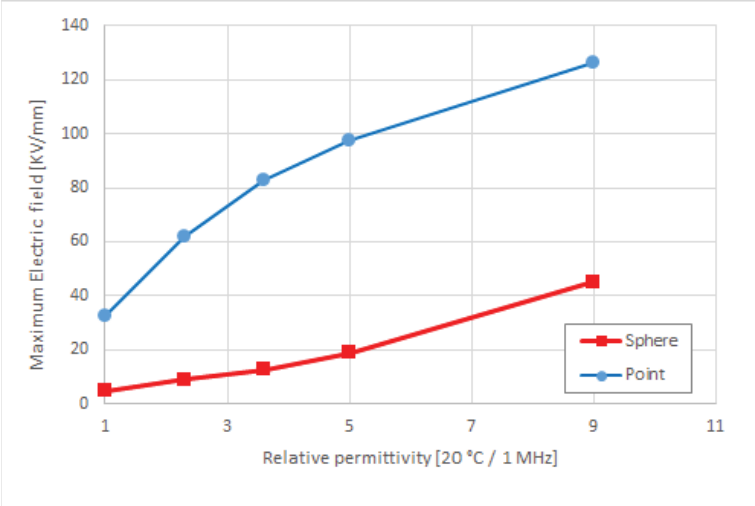

Fig. 19: Electric field for point (0.5 mm) – plane and sphere (5 mm) – plane (parallel field).

3. Experimental protocol used for breakdown measurements

3.1. High voltage impulse shape

Measurements were done with a non-standard 0.4/1400 µs impulse of positive polarity, instead of the classical 1.2/50 µs lightning impulse used in many studies. The main reason for this is as follows. With lightning impulse, the voltage drops rapidly after the maximum value, and this strongly complicates the interpretation of results, when phenomena last more than about 10 µs. For a comprehensive and simpler characterization of the initiation and propagation of the discharge, it is much more favourable to use a wave with a long tail (1.4 ms in our case), such that the voltage remains fairly constant when phenomena occur. This will be more clearly illustrated with measurements of inception delay times presented in the next chapter. For instance, plotting inception delays (up to 100 µs in some measurements thereafter) versus voltage would have no understandable meaning with a lightning impulse.
On the other hand, some precautions should be done when comparing our breakdown results with those obtained with the standard lightning impulse.

3.2. Breakdown procedure

The purpose of these measurements is to obtain comparative breakdown voltage values for a large range of materials. Breakdown voltage varies as a function of several parameters such as voltage polarity, geometry of electrodes, distance between electrode, etc. The

measurements usually show some scatter, and it was necessary to perform several measurements (15 in our experiments) for each type of material, in order to appreciate the statistical scatter.

Several different procedures can be used to measure breakdown voltages. In our investigations, the procedure described below is derived from that used at Schneider Electric. It provides a good repeatability of measurements, and it's close to the industrial procedure used for validation of apparatus.

The measurement starts from 15 kV (i.e. the minimum value which can be applied with our Marx generator). The applied voltage is raised by 2 kV steps until breakdown (Fig. 20). The time between each shot is fixed to 30 s. After breakdown, the voltage is lowered by 10 kV and raised again up to breakdown. This process was repeated three times for each sample.

For each material, five samples were tested, leading to a total of 15 measurements per material. On average, about 130 shots were necessary to fully characterize one material. Since a large variety of materials was investigated (more than 20) in different geometries, several thousand shots were necessary to obtain the breakdown results presented thereafter. For this reason, most of measurements were obtained in ambient air. Measurements in the pressure test cell required a significantly longer procedure, since it was necessary at each sample to open the cell, evacuate it, and flush it with new gas before starting measurements.

Fig. 20: Protocol for breakdown measurements with a single sample (Epoxy/Silanized Silica in ambient air, d = 5 cm, r = 0.5 mm).

With 3 breakdowns per sample and with the low breakdown energy induced by the test setup, breakdown was not destructive for the materials. A rapid recovery of dielectric strength after breakdown was observed: after 3 breakdowns with a new sample, no

appreciable decrease of breakdown voltage occurred in measurements (values of breakdown voltages 2 and 3 were sometimes higher than the first measured).

Our breakdown procedure is slightly different and simpler compared to other “standard” methods frequently used. Standard procedures were not selected mainly for a matter of time. For example, a procedure frequently used for dielectric breakdown measurements is the “Up-and-down” [4]. This procedure consists of an increase of the voltage level by an amount ΔU if no disruptive discharge occurs in a group of n voltage applications, otherwise the voltage level is decreased by the same amount. When n = 1, it corresponds to a 50 % disruptive -discharge voltage test.

An alternative statistical method was also applied to several materials in parallel field configuration at atmospheric pressure. These measurements provide further information on the significance of breakdown measurements. The procedure is detailed below, together with partial discharge recordings.

The first partial discharge (PD) is a luminous phenomenon that characterizes the inception of the discharge (Fig. 21). By raising the applied voltage, the probability to observe a PD increases.

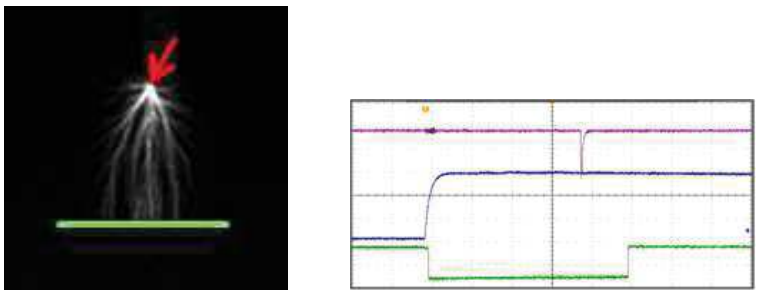

A) B)

Fig. 21: A) Time-resolved photograph of PD at 28 kV. The arrow represents the point and the horizontal line the grounded plane.

A) Oscilloscope recording from photomultiplier

B). Upper trace: photomultiplier current (200 mA/div.). Middle: voltage (10 kV/div.). Lower: intensifier’s gate. Horizontal scale: 2 µs/div.

From Fig. 21 B), we can observe that the PD corresponds to a peak (of negative sign) on the photomultiplier recording. With the procedure described on Fig. 22, it is possible to determine PD and breakdown probability versus applied voltage. Series of impulses at fixed voltage were applied starting from 15 kV, and raised by 2 kV steps until breakdown. At each step, ten measurements were done, and the occurrence of partial discharge or breakdown was noted.

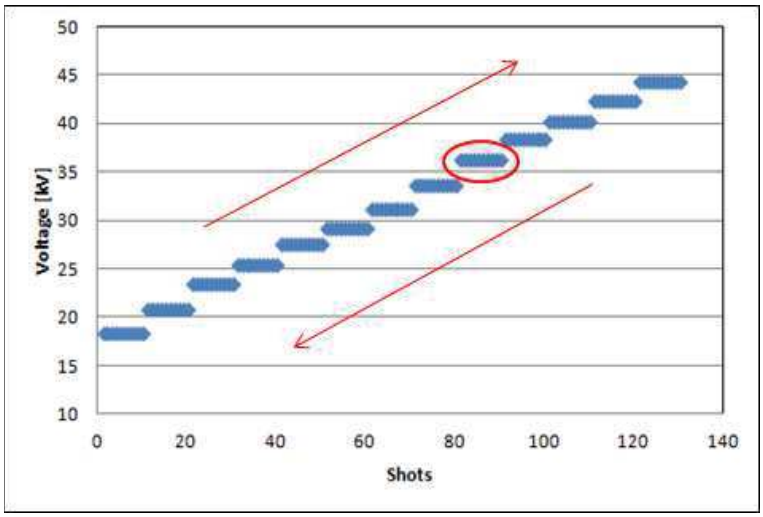

Fig. 22: Experimental procedure to determine the probability of occurrence of PD and breakdown.

Fig. 23 shows the breakdown probability for several materials. We can observe that the transition to breakdown occurs at slightly higher voltage for materials of low permittivity (PP and PTFE).

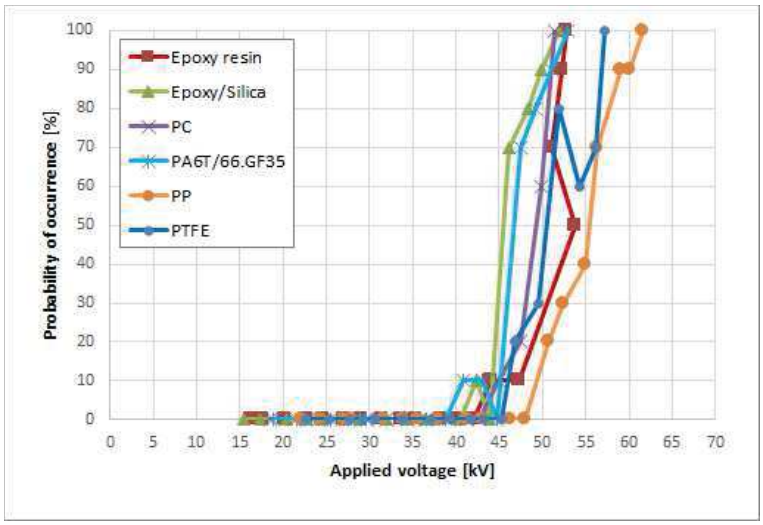

Fig. 23: Breakdown probability for several materials (ambient air, parallel field, d = 5 cm, r = 0.5 mm).

In contrast with breakdown measurements with the Schneider Electric electrodes, it is possible to observe an influence of the solid's nature. Indeed, further measurements (section below) are necessary to fully assess statistically these results, by investigating several samples of each nature. The examples below illustrate the variation occurring when several samples of one material are investigated.

Fig. 24 shows that the probability in air without solid can vary from a measurement to another (in the same condition, at different moments). The transition to breakdown can be shifted by up to 6 kV. This rather large instability in air alone will be further characterized in *Chapter 4*.

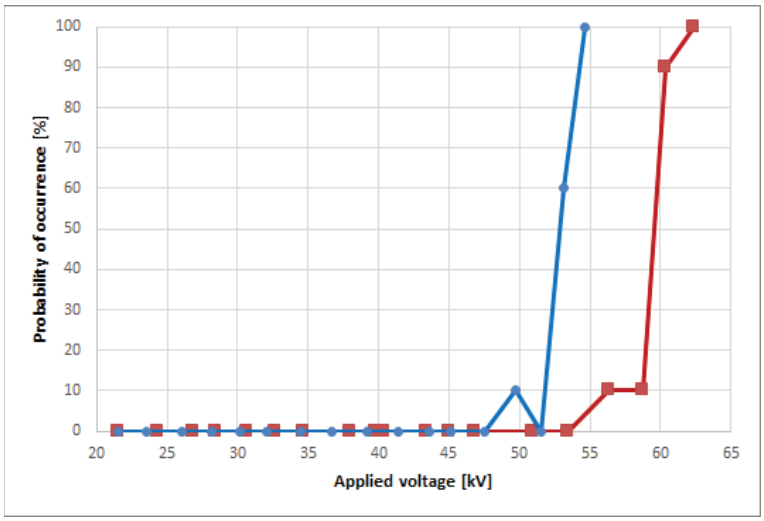

Fig. 24: Breakdown probability in air without solid (ambient air, d = 5 cm, r = 0.5 mm).

Similar measurements were repeated on three different samples of Epoxy/Silica and PP (Fig. 25 and 26). Fig. 25 shows that for PP the lowest voltage at which transition to breakdown occurs (48 kV) remained constant for the three samples.

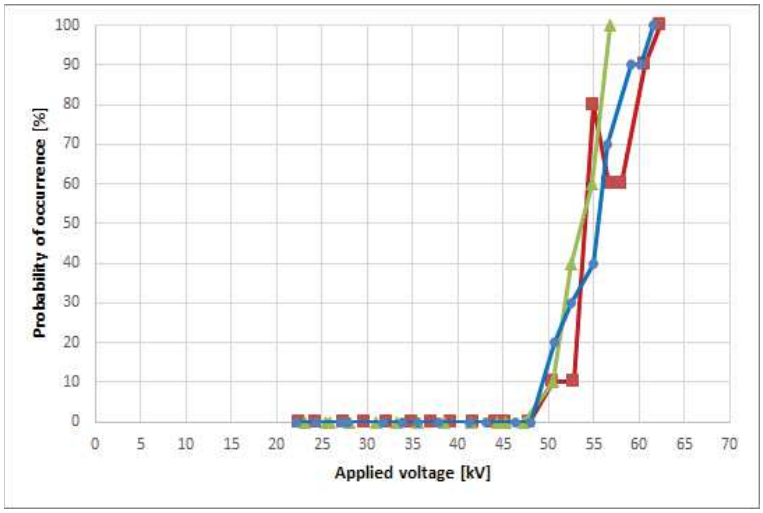

Fig. 25: Breakdown probability for PP (ambient air, parallel field, d = 5 cm, r = 0.5 mm).

Fig. 26 shows that with Epoxy/Silica differents results are obtained. For the three identical samples, three different probability plots were obtained. As in air without solid, the lowest voltage at which transition to breakdown occurs shows some variation, as well as voltages corresponding to 50 % or 100 % voltage probabilities.

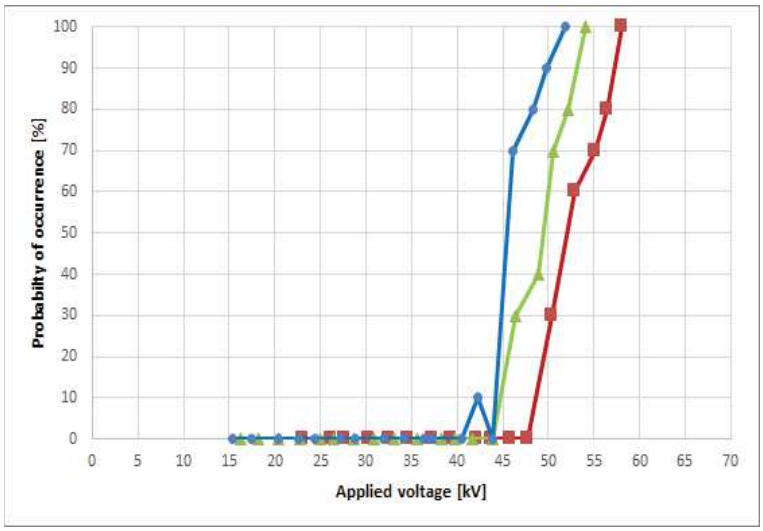

Fig. 26: Breakdown probability for Epoxy/Silica (ambient air, parallel field, d = 5 cm, r = 0.5 mm).

Although it provides complementary results, this procedure was not adapted to our study because it is very time-consuming (about 130 shots are required to characterize a single sample). Therefore, the procedure described in Fig. 20 was used to characterize a large variety of materials. With 5 samples and a total of 15 measurements per material, the average value with error bars showing minimum and maximum values adequately illustrate the scatter of measurements due to the different samples.

A comparison of the two methods of Fig. 20 and 22 shows that the method of Fig. 20 provides data corresponding to a low breakdown probability, more relevant to the practical design of apparatus.

4. Preliminary breakdown measurements: choice of the adequate electrode system

Several configurations were evaluated and selected depending on the purpose of our study.

4.1. Point-plane electrode system

The configuration presented in *section 2.3.1*. (Fig. 11), enhances the electric field near the triple point. Three different point radius were tested: 0.5 mm, 1.2 mm and 2.0 mm.

Fig. 27, 28 and 29 show probability of occurrence of PD and breakdown versus applied voltage for the three different points. PDs were detected with photomultiplier recordings.

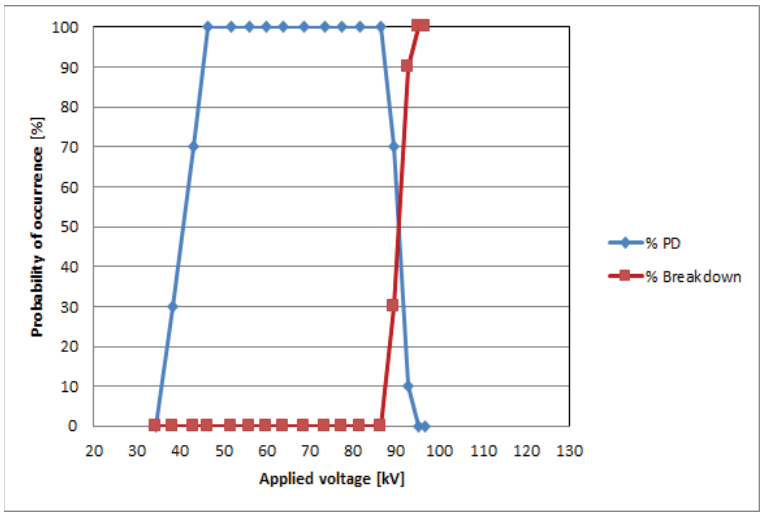

Fig. 27: Probability of occurrence with a tip radius r = 0.5 mm and a gap d = 10 cm.

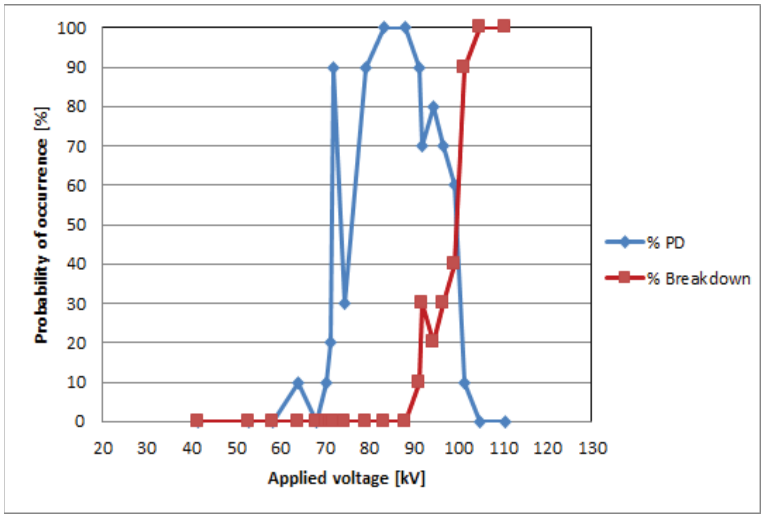

Fig. 28: Probability of occurrence with a tip radius r = 1.2 mm and a gap d = 10 cm.

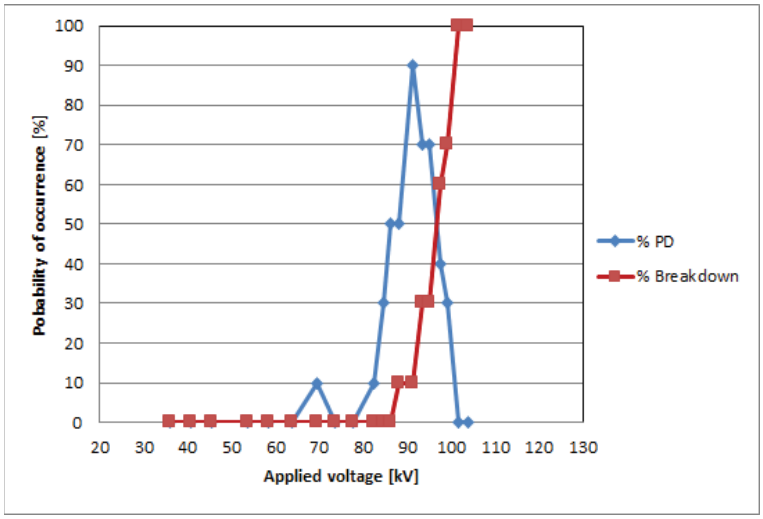

Fig. 29: Probability of occurrence with a tip radius r = 2.0 mm and a gap d = 10 cm.

In all cases, PD's were recorded before breakdown occurs. Logically, with a tip of r = 0.5 mm, PDs occur at lower voltage, about 50 kV below the breakdown voltage. By increasing r to 1.2 mm, the gap between PD and breakdown is reduced (30 kV). Finally, for a tip radius r = 2.0 mm, the difference between the two voltages becomes very small. In this latter case, breakdown occurs as soon as discharges appear. The measured breakdown voltage then reflects the voltage level required to initiating discharges, and not any more the voltage required for PDs to transform into a breakdown spark. A similar transition to an "initiation-controlled" breakdown regime can be obtained by reducing the gap distance with a fixed radius of curvature [5].

Electric fields on the point needed to initiate discharges for different electrode radius are presented in Tab. 1. When the radius of the electrode increases, the electric field required to initiate the first PD decreases. In [5], a coherent value was obtained, with a value of 2.6 kV/mm with an electrode radius of 3.5 mm. The decrease of inception field is logical, considering that in divergent field, the discharge criterion does not correspond to a fixed field value, but to the integral of ionisation coefficient over some distance (*Chapter 1*). With a highly divergent field (small radius r), the rapid decrease of field versus distance leads to a lower ionisation integral. A higher maximum field at the point is thus needed to initiate discharges.

Point radius [mm]	Maximum electric field [kV/mm]
0.5	20
1.2	15
2.0	11

Tab. 1: PD initiation field for a 10 cm gap electrodes.

From these measurements, we can conclude that for our study, the electrode with r = 0.5 mm is the most appropriate to obtain breakdown voltage measurements representative of discharge propagation and transition to breakdown, and not of discharge initiation. With this radius, stable breakdown measurements were obtained, whereas a larger scatter and instability occurred with larger points, and even more with the sphere electrode.

4.2. Gap between electrodes

The choice of d = 5 cm mainly resulted from the size of the samples (10 cm squares). With a 10 cm gap, the point was too close to the edge of the sample. In both case (5 and 10 cm), PD were observed before breakdown.

4.3. Polarity of the impulse

Some comparative breakdown measurements were investigated in positive and negative polarity. Fig. 30 shows the results obtained in negative polarity for three different types of materials. As expected, breakdown voltage values are much higher than in positive polarity (- 90 kV instead of + 55 kV). Without solid quite large error bars are obtained. The presence of solids did not lower the breakdown voltage (an opposite tendency is even observed on Fig. 30). Further measurements should be achieved to get a better understanding of these phenomena.
For our study dedicated to optimizing industrial systems, we decided to use mainly positive polarity which constitutes the most critical situation regarding breakdown phenomena.

In the following text without special indication, breakdown results correspond to our "standard" conditions: d = 5 cm, r = 0.5 mm and positive polarity.

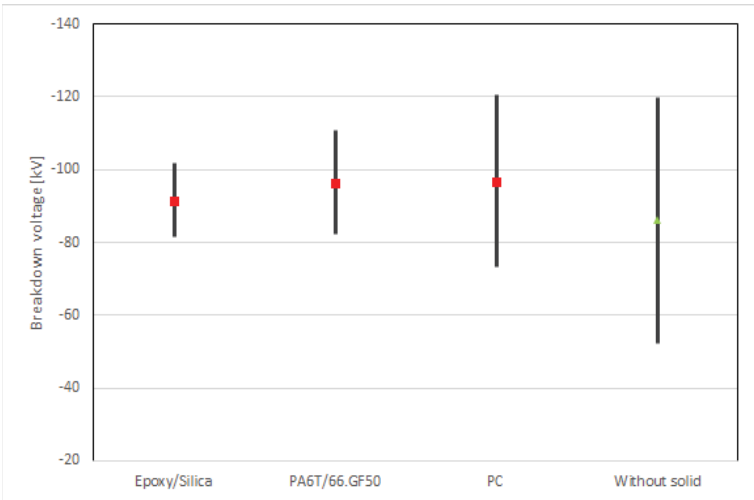

Fig. 30: Breakdown voltages for dry materials in negative polarity (parallel field, d = 5 cm, r = 0.5 mm).

4.4. Influence of pressure, comparison with SF_6

This work constitutes part of a more global project aiming at the replacement of SF_6. However, the study of various gases to replace SF_6 was not in the scope of our study. Measurements were performed in air to characterize and understand the influence of solid materials on creeping discharges. As explained in *Chapter 1*, air constitutes an alternative to SF_6 in several industrial cases. Nevertheless, some measurements were also carried out with SF_6 for comparison.
Fig. 31 and Fig. 32 show breakdown measurements in SF_6 and air with and without solids at different pressures. Values were as expected higher at atmospheric pressure for SF_6 than in air. The main difference, already observed in previous studies, comes from the influence of

pressure: in air a marked increase is observed, whereas in SF_6 a slight decrease is recorded in this pressure range (an increase should be however observed at higher pressures) [6].

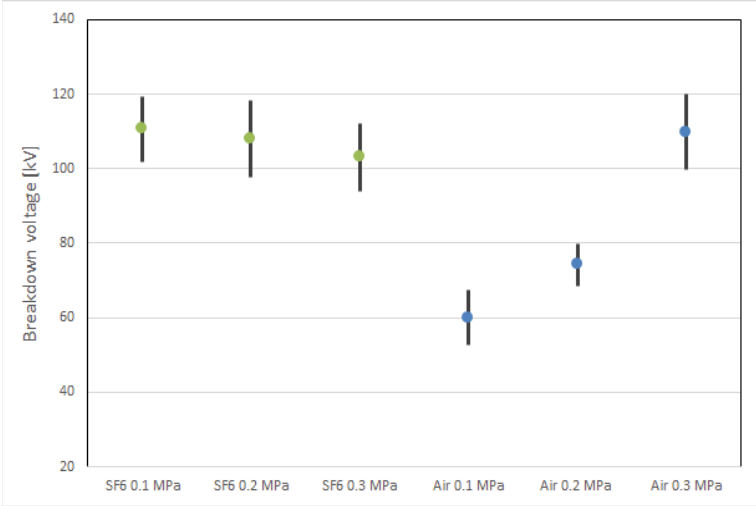

Fig. 31: Breakdown measurements in SF_6 and air without solid (d = 5 cm, r = 0.5 mm).

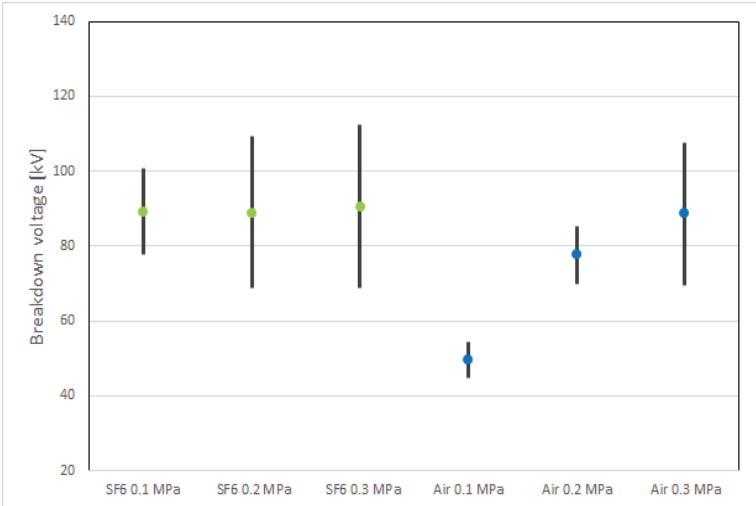

Fig. 32: Breakdown measurements in SF_6 and air with Epoxy/Silica (parallel field, d = 5 cm, r = 0.5 mm).

The impact of solids is similar in both gases, with a decrease of the breakdown voltage in the presence of a solid. Error bars were also larger in the case of SF_6. Although it leads to higher breakdown voltages, SF_6 was not studied in detail here since it should be replaced in future applications. Three pressures were investigated here: 0.1, 0.2 and 0.3 MPa. The maximum pressure of 0.3 MPa was selected since air pressure must be raised to 0.3 MPa in order to reach the same breakdown voltage than in SF_6 (see Figs. 31, 32).

5. Breakdown measurements

With the test conditions selected in *section 4*, it's now possible to investigate the influence of solid's nature on breakdown voltage.

5.1. Parallel field configurations

5.1.1. Atmospheric pressure measurements

In the first measurement series dedicated to study the influence of a large variety of solids, a large number of breakdown measurements were carried out at atmospheric pressure with the “parallel” point-plane system of Fig. 12A.

Point-plane electrodes

On figures, mean values of breakdown voltages are plotted together with error bars showing the standard deviation. Fig. 33 shows the reduction of the breakdown voltage in the presence of a dry solid insulator (about 9 kV, i.e. - 16 % of the breakdown voltage in air alone). Despite the large difference in chemical composition of materials, minimal differences were observed between materials. Scatter bars show a comparable uncertainty of the breakdown phenomenon with and without solids.

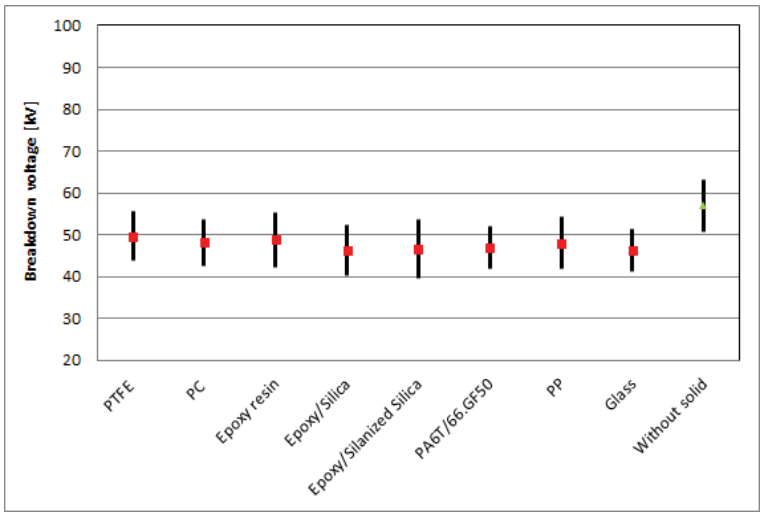

Fig. 33: Breakdown voltages in parallel field for dry materials (d = 5 cm, r = 0.5 mm).

Breakdown measurements of identical materials saturated of water (62 %, 70 °C) were also performed (Fig. 34). For a fixed material, no clear influence of water is seen, even when the water content exceeded 1.4 % in some materials. Just like for chemical nature, water content has no clear influence on breakdown voltage.

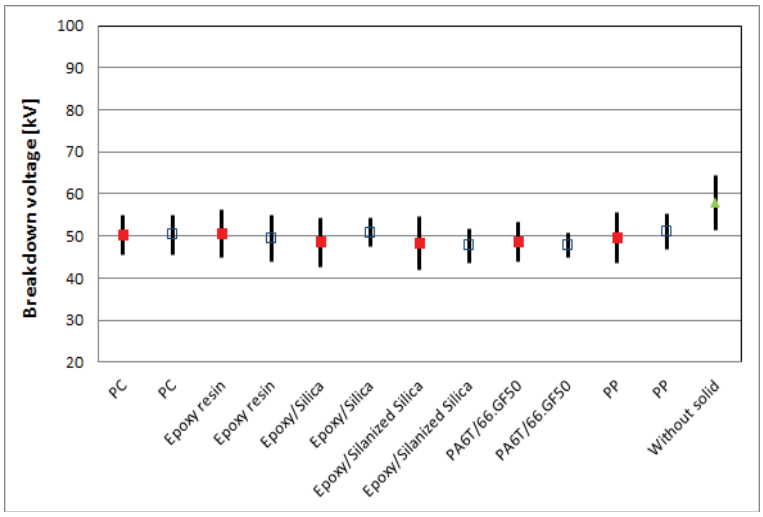

Fig. 34: Breakdown voltages in parallel field for dry (full dots) and wet (open dots) materials (d = 5 cm, r = 0.5 mm).

In *Chapter 2*, spectroscopy measurements were performed to determine the relative permittivity of each material at 1 MHz and 20 °C. From these results, it's possible to plot breakdown voltage versus relative permittivity (Fig. 35). In this figure, the range of permittivities was enlarged compared to Fig. 33, by adding measurements carried out with glass (ε_r = 5), alumina ceramic (ε_r = 9), and air alone (ε_r = 1). Fig. 35 shows a weak decrease of breakdown voltage, with a uniform tendency when permittivity is increased. This suggests that chemical nature and water content of materials have mainly an indirect effect on breakdown voltage, by changing the value of permittivity.

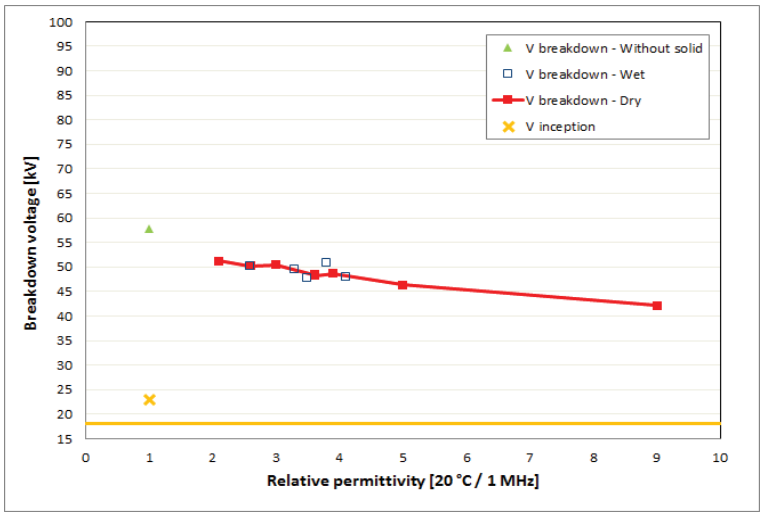

Fig. 35: Breakdown voltages in parallel field versus relative permittivity measured at 1 MHz (d = 5 cm, r = 0.5 mm).

In air without solid, the discharge inception voltage quoted (23 kV) was well below the breakdown voltage. In the presence of solids, the inception voltage was < 20 kV and couldn't

be precisely quantified, because of the limitation of the minimum voltage applicable with the Marx generator (15 kV).

Some results were also obtained in order to evaluate the influence of the surface roughness on the breakdown voltage. Two surface conditioning were tested: smooth and rough. The rough surface was obtained after the use of sand blasting on the polycarbonate (PC) surface. Fig. 36 shows that the surface roughness has no clear influence on the breakdown voltage.

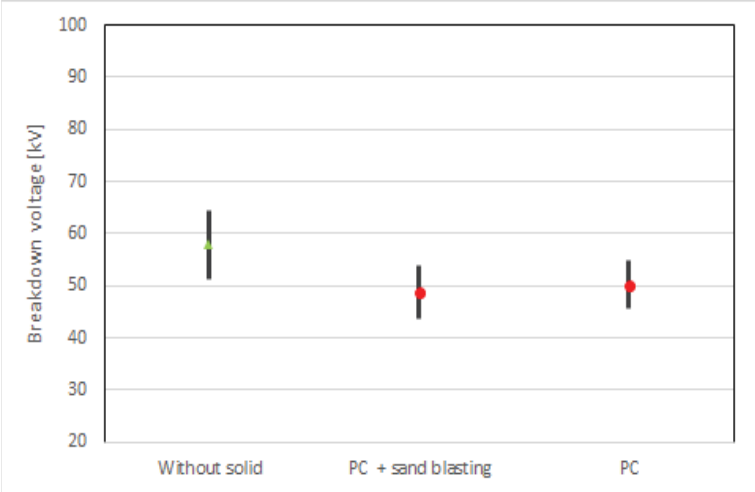

Fig. 36: Breakdown voltages in parallel field for sand blasted PC (d = 5 cm, r = 0.5 mm).

Some measurements were carried out with a larger gap (d = 9 cm), in order to check the influence of this parameter. By increasing the gap distance, breakdown voltage logically increase (Fig. 37). Fig. 37 shows a similar influence of relative permittivity than for 5 cm gap.

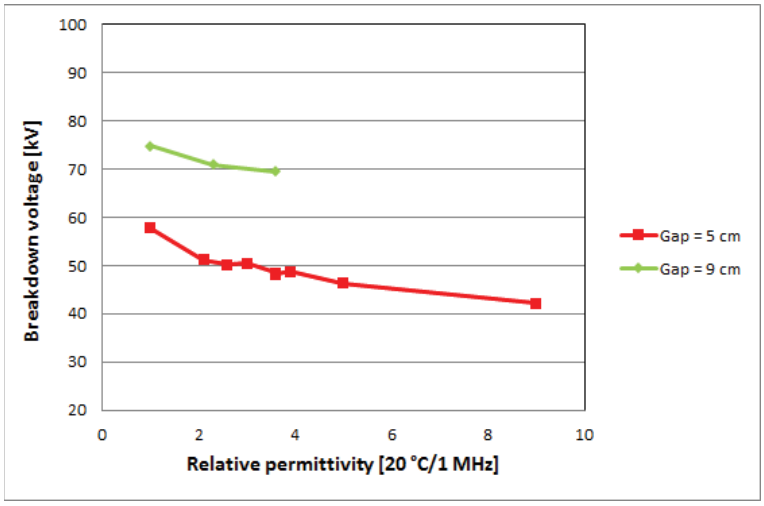

Fig. 37: Breakdown voltages in parallel field for dry materials with a gap between electrodes of d = 5 cm and d = 9 cm. (r = 0.5 mm).

Location of breakdown sparks

With the gated camera, it's possible to observe the breakdown spark by attenuating the light with crossed polarizers, in order to avoid saturating the camera with the intense spark light. By turning the sample, we can obtain front and side views. With the side view, we can observe the localization of the breakdown spark. Breakdown can occur on the surface of the solid (Fig. 38 A), in the gas volume above the surface (B), or sometimes in both (C). On Fig. 38 B) and C), on the left-hand side of photograph, a reflection of the spark light on the smooth solid surface is seen.

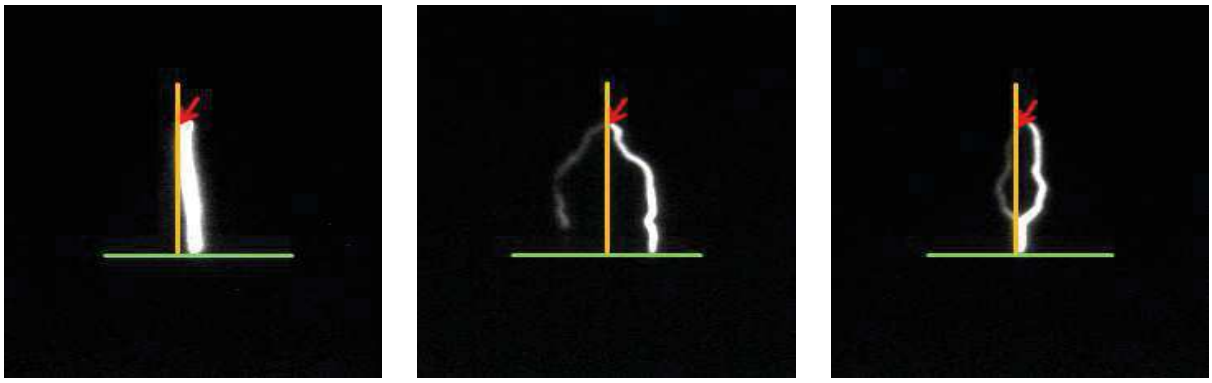

A) B) C)

Fig. 38: Time-resolved photographs of breakdown sparks (side view) with Epoxy/Silica. A) Surface breakdown B) Volume breakdown C) Surface and volume breakdown. The arrow represents the point, the vertical line shows the solid surface, and the horizontal line the grounded plane (parallel field, d = 5 cm, r = 0.5 mm).

Many breakdown measurements have been achieved with a large range of solid materials. From these measurements, we can extract the Tab. 2 showing the occurrence probability of surface and volume sparks. Breakdowns developing both on the solid surface and in the air (Fig. 38 C) are not counted.

Localization	Probability of occurrence
Surface	56 %
Volume	44 %

Tab. 2: Probability of breakdown occurrence extracted from 61 breakdown measurements.

There is no clear tendency of localization of the breakdown spark. Breakdown slightly more develops on the surface of the solid. The solid's nature doesn't influence the localization of breakdown. This result can be correlated to the rather low influence of solids on breakdown voltage. No correlation could be established between the localization of the spark and the value of breakdown voltage.

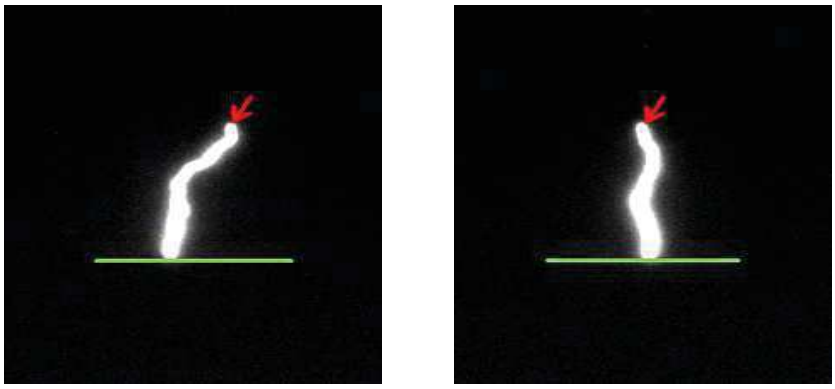

A) B)

Fig. 39: Time-resolved photographs of breakdown (front view) with Epoxy/Silica solid (gap distance = 5cm). A) 53 kV B) 49 kV.

Front view visualizations (Fig. 39) show that sparks take the form of a unique luminous channel. This conductive channel doesn't cross the gap straight and follows random direction until the grounded plane.

Sphere-plane configuration

Several breakdown measurements were also carried out with another electrode configuration: sphere-plane, described in Fig. 13. With this system, discharges are initiated due to the field enhancement at the triple junction between the sphere of 5 mm radius, and the insulating solid (Fig. 19). Due to the 10 times larger radius of the electrode, the field at this place is significantly lower compared with the 0.5 mm point. The electric field gets a value of 9 kV/mm instead of 38 kV/mm with PP insulator ($\varepsilon_r = 2.3$).

Fig. 40 shows that breakdown voltage in air without solid has a large scatter. Recordings with the photomultiplier showed that without solid there were no partial discharge occurring at voltages lower than breakdown voltage (Fig. 41). Therefore, the initiation of the discharge in this configuration controls the breakdown.

Conversely, in the presence of solid, partial discharges could be recorded at voltages slightly lower than breakdown voltage (Fig. 41). Logically, the inception voltage decreases when permittivity is increased, since the field at the triple junction region increases (Fig. 42). The main difference with the point-plane geometry comes from the much lower difference between inception and breakdown voltages: more than 30 kV with $\varepsilon_r = 2.6$ with the point (Fig. 35), down to 5 kV with the sphere (Fig. 43).

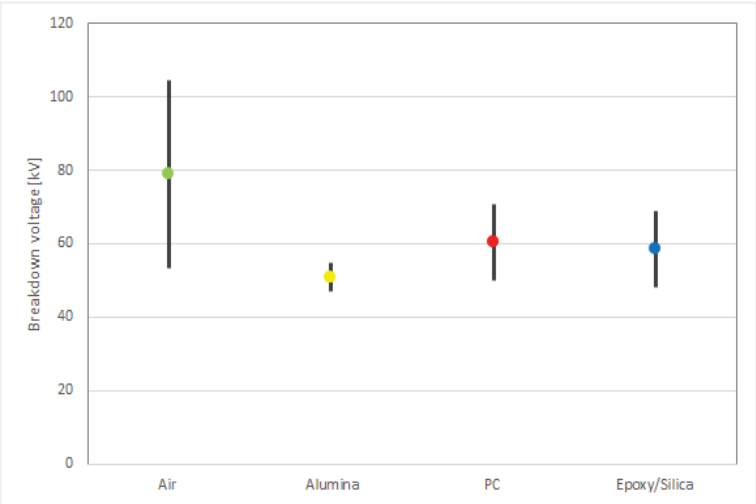

Fig. 40: Breakdown voltages for dry materials in sphere-plane geometry (parallel field, d = 5 cm, r = 5 mm)

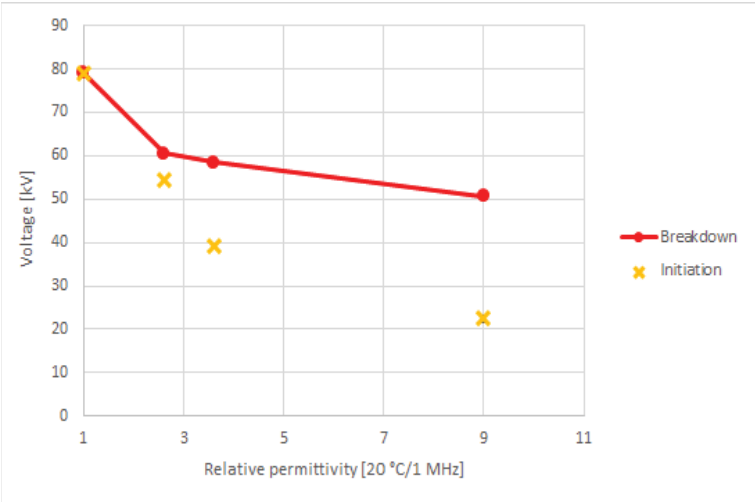

Fig. 41: Breakdown and PD initiation voltages for dry materials (parallel field, d = 5 cm, r = 5 mm).

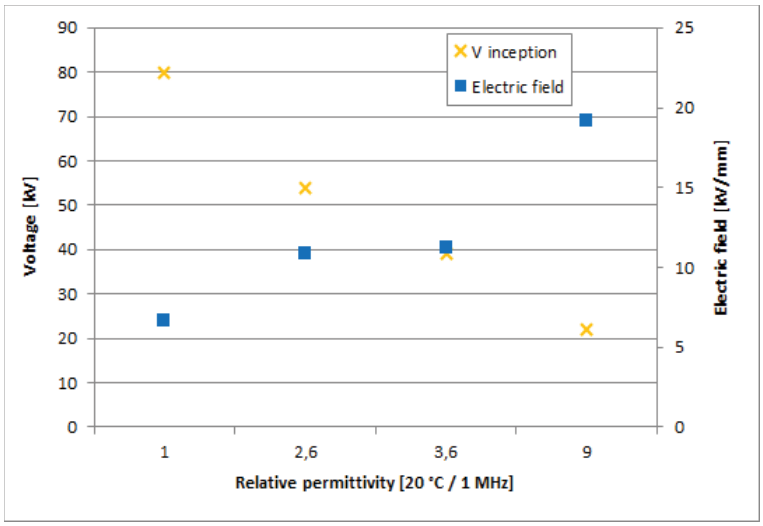

Fig. 42: Initiation voltages and maximum electric field at the triple point for dry materials (parallel field, d = 5 cm, r = 5 mm).

When breakdown voltages are plotted versus relative permittivities (Fig. 43), the figure shows that values are lower with the point. However, a nearly identical degradation of breakdown voltage in the presence of solid occurs with the sphere compared to the point. The point in air alone with the sphere must not be considered here, since breakdown is controlled by initiation, and the meaning of the breakdown voltage is thus different.
These results are interesting since they show that when the field is parallel to the surface, the classification of materials and the influence of permittivity on the breakdown voltage remain nearly unchanged when the electrode (and field) geometry is changed. Therefore, this allows us extrapolating results obtained in point-plane geometry (Fig. 33, 34) to other geometries such as those found in practical systems, provided the main direction of the field is parallel to the surface.

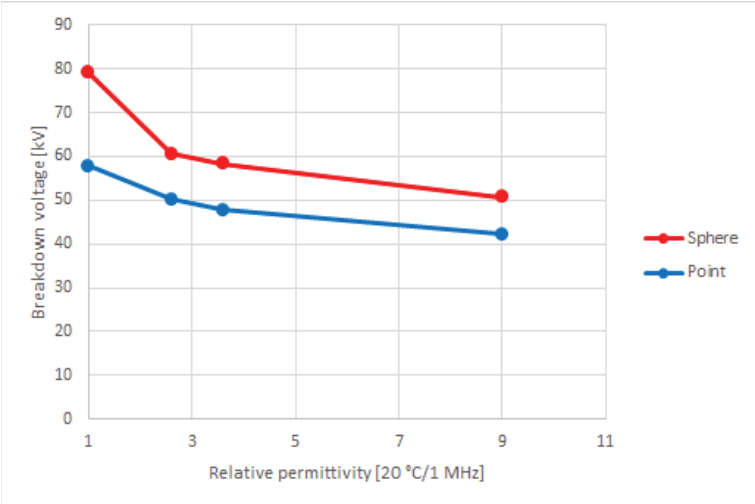

Fig. 43: Comparison of breakdown voltages with point and sphere configurations (parallel field, d = 5 cm).

Summary of breakdown results with parallel field in ambient air

Summary of breakdown measurements in parallel field, in ambient air are listed below:

- Moderate decrease with technical materials.
- Impossible to identify a clear influence of material nature and presence of water: only relevant parameter: permittivity, indirect influence of nature & water.
- Influence of water: impossible to evidence the influence of accumulated charges during measurements.
- Experiments in different geometries (distance, sphere) show that results can be extrapolated to different geometries.
- Chap 4 will show that measured breakdown voltages do not represent the voltage required for streamer initiation, nor propagation, but the voltage required to induce transition from streamers to spark.
-

5.1.2. Measurements under pressure

Same types of breakdown measurements were performed under pressure up to 0.3 MPa with dry synthetic air. After mounting the solid sample in the pressure test cell, the test cell was first placed under vacuum, then rinsed with dry synthetic air, and filled at the desired pressure.

The goal is to verify if the influence of solid's nature on breakdown voltage observed in ambient air can be extrapolated to higher pressures. Fig. 44 and 45 shows that complex (and sometimes contradictory) tendencies were observed at different pressures.

Fig. 44 first shows that at atmospheric pressure in ambient air, and in synthetic dry air at 0.1 MPa, we obtained the same breakdown voltages in air alone, and with Epoxy/Silica. We can conclude that the relative humidity present in the ambient air has a negligible impact on our measurements. This is consistent with the observation that even a large sample water content (e.g. > 1.4 % in PA6T/66.GF50) had a limited influence on measurements (Fig. 34).

Fig. 44 shows that with technical materials (Epoxy/Silica, PA6T/66.GF50, PC) an increase of breakdown voltage versus pressure can be observed, such as in air alone. However, a reversed influence was recorded between 0.2 and 0.3 MPa with high permittivity materials (glass, alumina).

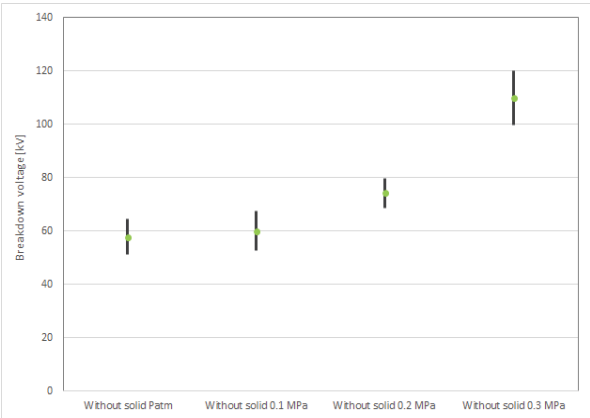

Air

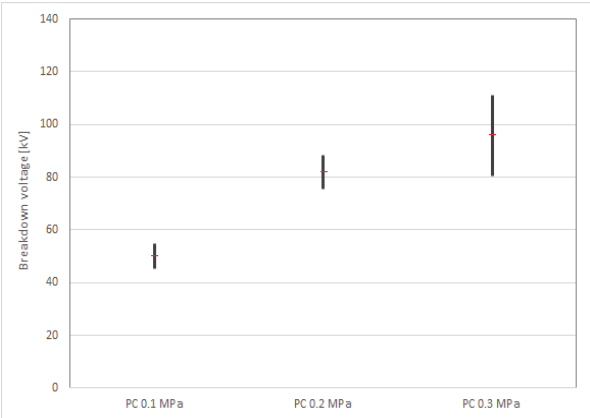

PC (ε_r = 2.6)

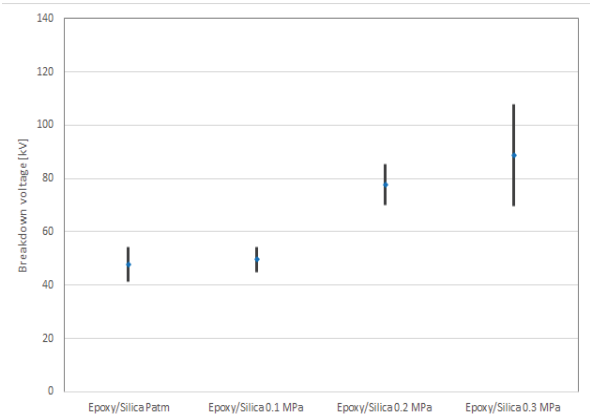

Epoxy/Silica (ε_r = 3.6)

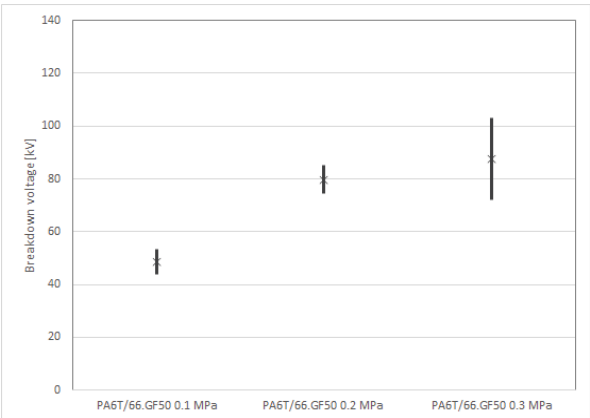

PA6T/6T.GF50 (ε_r = 3.9)

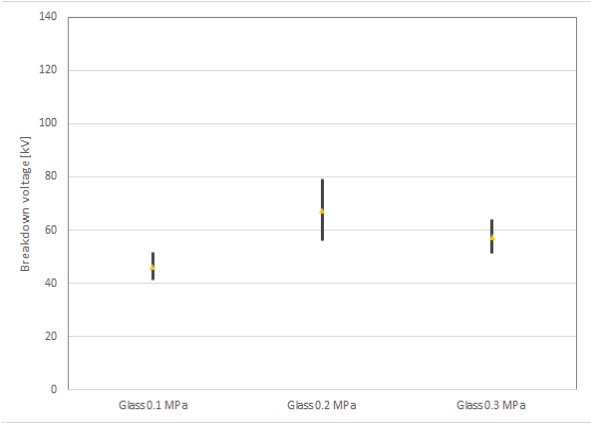

Glass (ε_r = 5)

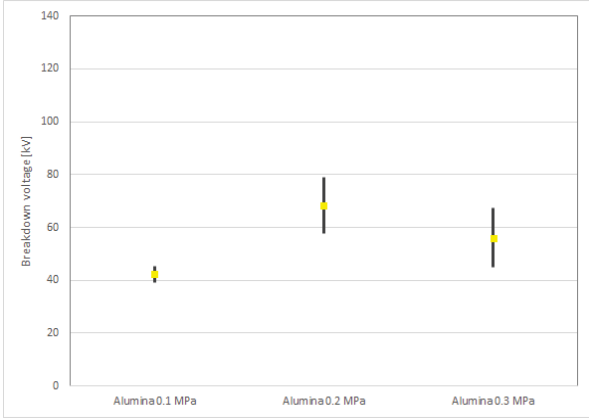

Alumina (ε_r = 9)

Fig. 44: Breakdown voltages for dry materials at atmospheric pressure, 0.1 MPa, 0.2 MPa and 0.3 MPa. (Parallel field, d = 5 cm, r = 0.5 mm)

When results are plotted versus permittivity (Fig. 45), a similar influence (i.e. a global decrease of breakdown voltage versus permittivity) is observed at 0.1 and 0.3 MPa. In contrast, at 0.2 MPa the decrease due to solids compared to the gas alone is not clearly evidenced.

At 0.3 MPa with technical materials (ε_r < 4), a regular decrease of breakdown voltage versus permittivity was recorded (- 31 %), larger than that observed at atmospheric pressure (- 17 %). With high permittivity materials (glass and alumina) a sudden large drop is recorded (such as at 0.2 MPa), the breakdown voltage becomes independent on the permittivity, and larger values are observed at 0.2 MPa compared to 0.3 MPa.

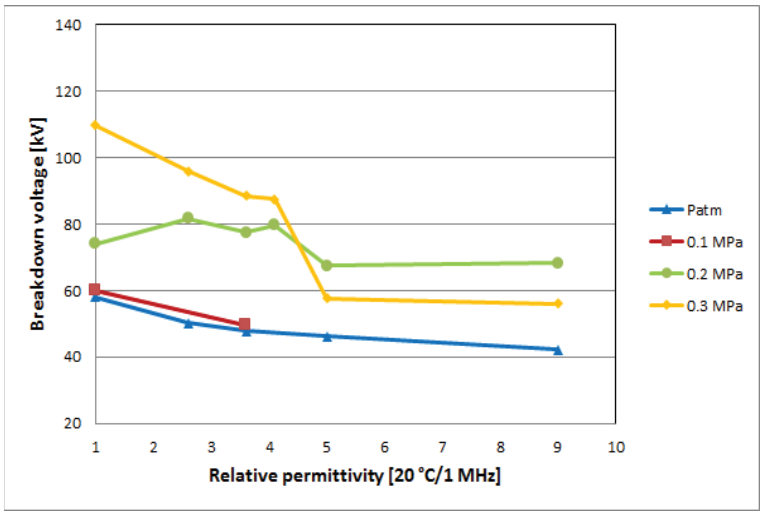

Fig. 45: Breakdown voltages versus relative permittivity and pressure (parallel field, d = 5 cm, r = 0.5 mm).

Visualizations of breakdown sparks were performed under pressure. Tab. 3 shows that at 0.2 and 0.3 MPa, most of sparks now occur on the solid surface. Pressure clearly promotes the

occurrence of breakdown on the surface compared to atmospheric pressure condition. This behavior will be more clearly illustrated and explained in *Chapter 4*.
No satisfactory explanation for the erratic behavior observed at 0.2 MPa can be found.

Pressure [MPa]	Localization	Probability of occurrence
0.2	Surface	**93 %**
	Volume	7 %
0.3	Surface	**82 %**
	Volume	18 %

Tab. 3: Probability of breakdown occurrence extracted from 60 breakdown measurements (0.2 MPa) and 56 breakdown measurements (0.3 MPa).

5.2. Perpendicular field configuration

5.2.1. Atmospheric pressure measurements

With the perpendicular field configuration, we observe larger differences between materials (Fig. 46). PTFE and PP show a higher breakdown voltage than other materials. Materials such as PA6T/66.GF50 and Epoxy/Silica get nearly the same breakdown voltage, even if their chemical compositions are very different.

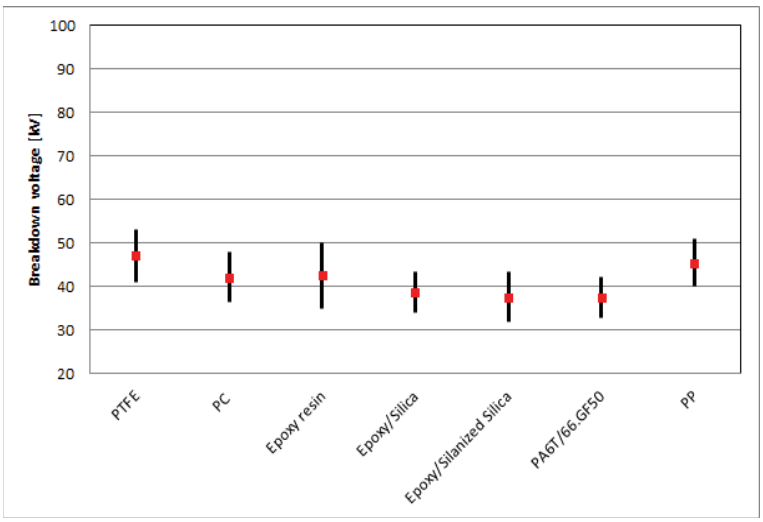

Fig. 46: Breakdown voltages in perpendicular field for dry materials (perpendicular field, d = 5 cm, r = 0.5 mm).

For PC and Epoxy/Silanized silica, the wet materials show the same (or slightly higher) breakdown voltage (Fig. 47). For Epoxy resin and PA6T/66.GF50, a significant reduction is observed in the presence of water. These results are consistent with the fact that PA6T/66.GF50 and Epoxy resin absorb larger amounts of water compared to PC, Epoxy/Silica and Epoxy/Silanized silica.

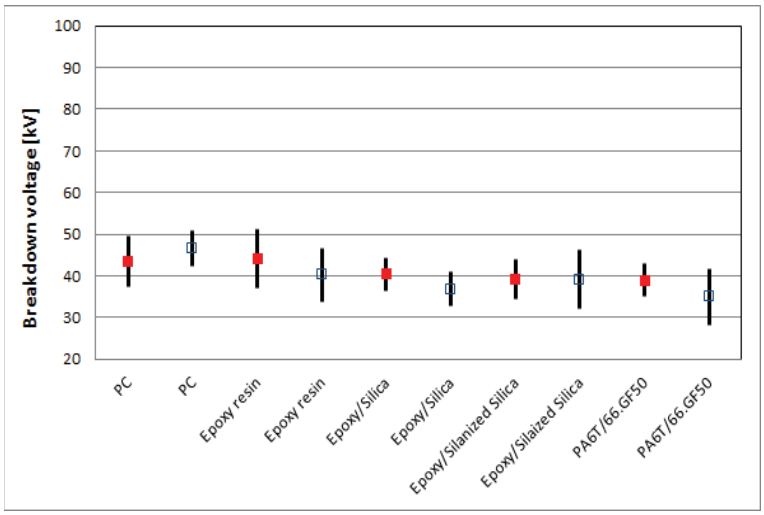

Fig. 47: Breakdown voltages in perpendicular field for dry (full dots) and wet (open dots) materials (perpendicular field, d = 5 cm, r = 0.5 mm).

Fig. 48 shows the plot of breakdown voltage versus permittivity. A marked decrease of breakdown voltage versus permittivity is now observed. Once again, permittivity appears to be the only significant parameter able to characterize the behavior of solids, either dry or wet. The material chemical nature mostly shows an indirect influence on breakdown voltage via variations of the permittivity. In a similar way, water content only gets an indirect influence, by increasing slightly the relative permittivity.

Since the “perpendicular” field geometry is identical to that used in Surface Potential Decay experiments (*Chapter 2*), one can conclude that the accumulation of surface charges during breakdown measurements has a negligible impact. A very large difference of Surface Potential Decay time was observed between wet and dry materials, especially with PA6T/66.GF50. In wet PA6T/66.GF50, the surface potential dropped within a few seconds, i.e. a very short time compared to the interval between successive shots (30 s).
In a similar way, no large difference was observed between Epoxy/silica and PA6T/66.GF50, whereas these materials showed large differences in SPD measurements (charges on dry epoxy may remain for days).

Similar conclusions can be derived from “parallel” field measurements, whereas the field geometry was somewhat different from that of SPD.

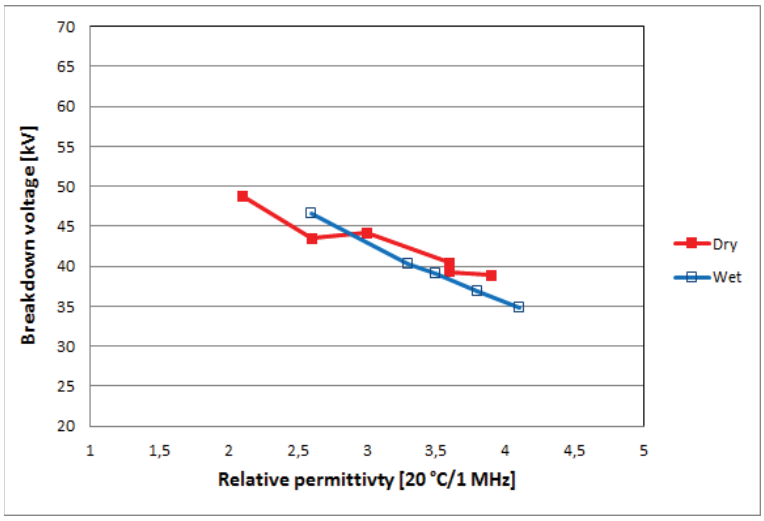

Fig. 48: Breakdown voltages versus relative permittivity (at 1 MHz). Perpendicular field, d = 5 cm, r = 0.5 mm.

Fig. 49 shows the compared influence of permittivity in perpendicular and parallel fields. From this figure, it is clear that the influence of permittivity is larger in perpendicular field configuration.

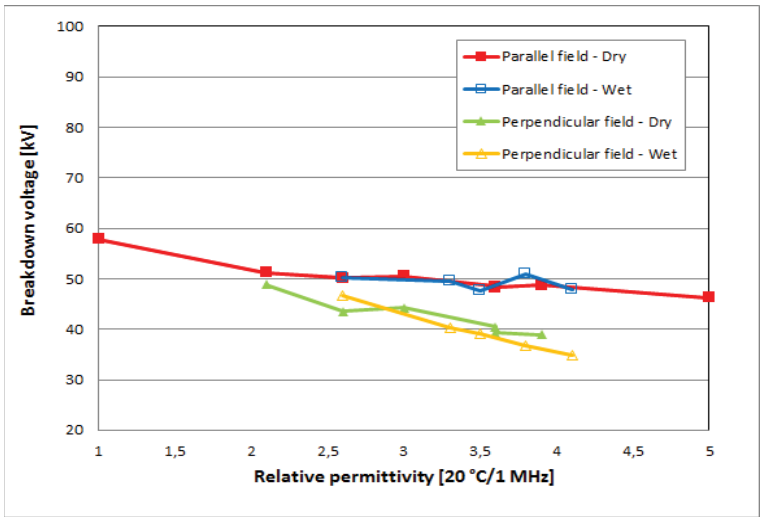

Fig. 49: Breakdown voltages versus relative permittivity (at 1 MHz) in parallel and perpendicular field. (d = 5 cm, r = 0.5 m).

In the perpendicular field configuration, breakdown always occurred on the surface (Tab. 4). This result is consistent with the fact that the field perpendicular to the surface prevents the discharge from propagating in other directions, above the surface. However, these results should be interpreted with caution because they are extracted from only ten breakdown measurements.

Localization	Probability of occurrence
Surface	100 %
Volume	0 %

Tab. 4: Probability of breakdown occurrence extracted from 10 breakdown measurements.

5.2.2. Pressure measurements

Some experiments were carried out in perpendicular field configuration at different pressures. For all pressures tested, the solid's permittivity has nearly the same influence on breakdown voltage (Fig. 50). A major difference with parallel field is that the breakdown voltage is now nearly independent of pressure, considering the scatter of measurements. On average, the best results are obtained with 0.2 MPa.

All measurements at various pressures up to 0.3 MPa in this geometry provide lower breakdown voltage compared to the case of parallel field at atmospheric pressure (Fig. 45). From the point of view of applications, the perpendicular field geometry constitutes a critical situation, and no large beneficial effect is observed when pressure is increased.

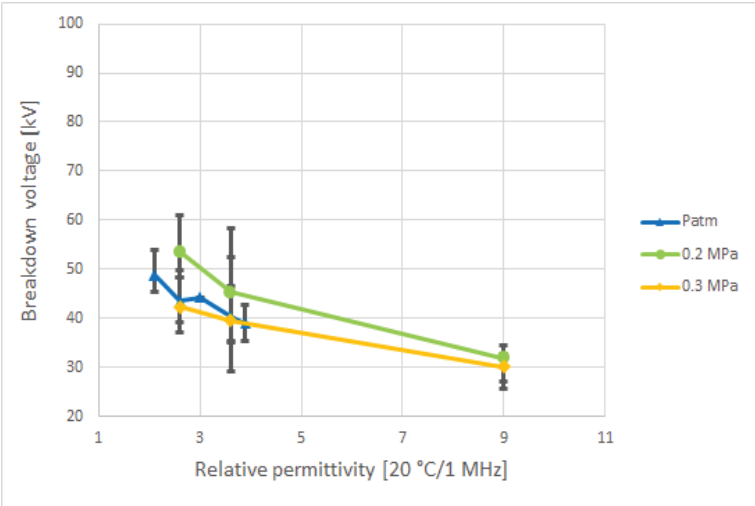

Fig. 50: Breakdown voltages versus relative permittivity and pressure. Perpendicular field, d = 5 cm, r = 0.5 mm.

In Tab. 5, with obtain the same conclusions than for atmospheric pressure measurements. For all measurements, the breakdown always occurred on the solid's surface.

Pressure [MPa]	Localization	Probability of occurrence
0.2	Surface	**100 %**
	Volume	0 %
0.3	Surface	**100 %**
	Volume	0 %

Tab. 5: Probability of breakdown occurrence extracted from 22 breakdown measurements (0.2 MPa) and 6 breakdown measurements (0.3 MPa).

6. Conclusion

In this chapter, a rather large range of materials were tested to study the influence of solid's nature on breakdown measurements. An adequate electrode system was selected to get breakdown voltage relevant of discharge propagation and transition to breakdown, rather than discharge initiation (presence of partial discharges at voltage lower than breakdown).
Two typical field geometries were investigated, with the field either parallel or perpendicular to the solid surface. The actual field in applications is usually between these extreme situations.

From these results, it appears that the breakdown voltage is mainly a function of the relative permittivity of materials. The chemical nature and water content have only an indirect influence on breakdown, by changing the permittivity. In all geometries investigated an increase of permittivity induces a reduction of breakdown voltage. Only one exception was observed with measurements in "parallel" field at 0.2 MPa.
In the presence of a solid, pressure has a positive impact mainly in the "parallel" field geometry, and almost no influence in "perpendicular" field. Since lower breakdown voltages are always measured in this geometry, this situation clearly represents the most critical one.

The influence of sample water content is evidenced only via its influence on the permittivity. This indicates that charge accumulation on the solid during breakdown measurements has a negligible impact on the breakdown process. This conclusion is based on the fact that water has a large impact of surface potential decay (chapter 2). The same conclusion can be obtained from breakdown measurements carried out with different materials with a rather different Surface Potential Decay.
In the next chapter, pre-breakdown phenomena will be investigated. This will provide a better insight about the process actually involved in breakdown experiments, and about the influence of solid surfaces.

Bibliography

[1] L. Caliap, « Etude de l'optimisation des isolants d'un point de vue diélectrique pour les contraintes du GIS », Thèse de doctorat (institut polytechnique de Grenoble), Septembre 2010.

[2] E. Marx, "Versuche über die Prüfung von Isolatoren mit Spannungsstößen", Electrotech. Z. ETZ, 45, pp. 652-654, 1924.

[3] "High-speed gated image intensifier V3063U", Technical Data Sheet, Hamamatsu.

[4] IEC 60060-1, CEI 60060-1: 2010-09, p.65.

[5] F. Mauseth, J. S. Jorsatd and A. Pedersen, "Streamer inception and propagation for air insulated rod-plane gaps with barriers", IEEE, 2012.

[6] L. Niemeyer, L. Ullrich and N. Wiegart, "The Mechanism of Leader Breakdown in Electronegative Gases", IEEE Transactions on Electrical Insulation, Vol. 24 No. 2, April 1989.

Chapter 4: Pre-breakdown streamers: study of initiation and sequence of events leading to breakdown

In this last chapter, we will study pre-breakdown phenomena in more details, using transient current measurements and time-resolved visualization. In *Chapter 3* several conclusions were obtained regarding the influence of solid's nature on the breakdown voltage, in different conditions of pressure and electrode geometry. We concluded that measured breakdown voltages are influenced by the solid's nature mainly in an indirect way, by changing the permittivity of the solid. Further investigations will be done in this chapter to better define the three different steps of the discharge process leading to breakdown: streamer initiation, propagation, and transition from streamer to breakdown spark.
We will see that depending on conditions (gap geometry, pressure), measured breakdown voltages represent the voltage required to either initiate the discharge, of propagate it up to the grounded electrode, or induce the transition from a streamer to a spark. The two last phenomena (propagation and transition to a spark) are properly characterized by breakdown voltages already measured in *Chapter 3*. In this chapter, the first step (initiation) will be studied in more details, by investigating the influence of the solid's nature on it.

1. Experimental setup

1.1. Transient current measurements

The experimental setup used in this chapter is basically the same as the one used in *Chapter 3*. Only the tip holder containing the transient current measurements system will be explained here. Under impulse voltage, the large transient current flowing during the voltage rise (due to charging of electrodes capacitance) usually constitutes a severe limitation for the measurement of small discharge currents, superimposed to this large charging current. The arrangement used (Fig. 1), similar to that described in [1] allowed to considerably reducing the detrimental influence of the charging current.

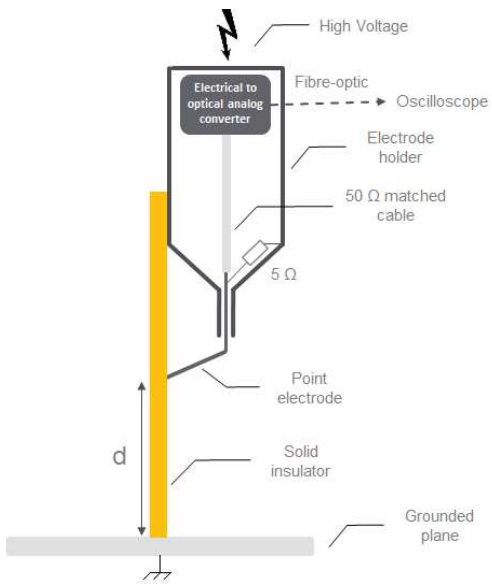

Fig. 1: Principle of the transient current measurement system.

Currents flowing through the point at high voltage are measured via a 5 Ω resistor located inside the tip holder (Fig. 1), and sent to the oscilloscope via a 100 MHz bandwidth analog optical fiber link. Since only the extremity of the point emerges from the point holder, the measured charging current during the voltage rise (a few mA) is negligible compared to discharge currents. It becomes then possible to detect discharge inception with a high sensitivity, even during the voltage rise.
Correlated to current measurements, pre-breakdown streamers were visualized with the fast gated intensified camera, equipped with quartz optics (UV sensitivity down to 200 nm).

1.2. Surface charge measurements

The existence and measurement of surface charges remaining on the insulator after discharges was studied with two different electrostatic probes, either measuring the electric field induced by charges, or the surface potential.

1.2.1. Electric field probe

A portable electrostatic fieldmeter model 257D from Monroe Electronics was used (Fig. 2). To measure the electrical field, a vibrating electrode “senses” the field to be measured through the aperture in the probe gradient plate. The AC signal induced on this electrode is proportional to its excursion path, and to the strength of the ambient field. After calibration, the measured field is displayed by the LCD meter [2]. The main drawback of this probe is its large diameter (4 cm, see Fig. 2), which prevented from scanning it over the sample surface (only the average field at the center of the point-plane gap was measurable).

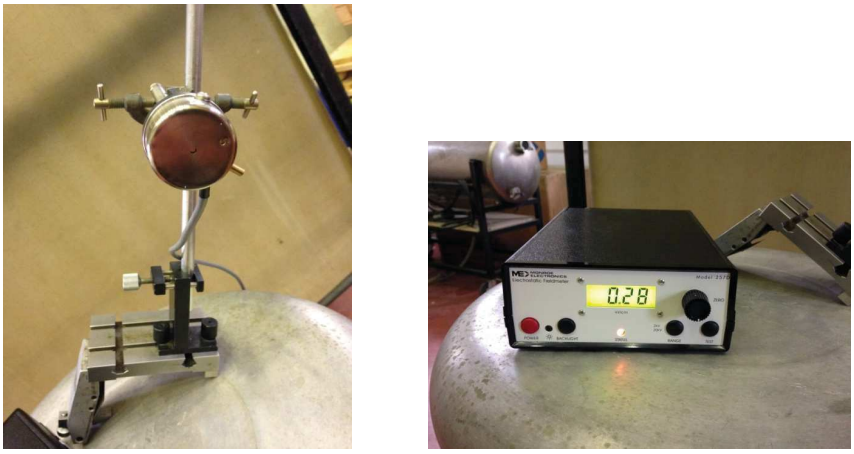

Fig. 2: Field probe and measurement unit.

1.2.2. Surface Voltage Probe

The TREK 341B (Fig. 3) electrostatic voltage probe was used [3]. It’s a high-voltage electrostatic voltmeter up to +/- 20 kV, which can make non-contact surface voltage

measurements. The 314B employs a field-nulling technique that achieves DC stability and high accuracy even if the probe-to-surface spacing changes. This permits measurements of either stationary or moving surfaces, without the need to establish fixed spacing to maintain accuracy. The smaller size of the probe (12 x 12 mm) allowed scanning it over the solid surface.

Fig. 3: Trek 341B electrostatic voltage probe.

2. Characterization of pre-breakdown streamers

The objective of this part was to investigate the different steps of pre-breakdown phenomena leading to breakdown in air. To this end, we performed time-resolved visualization with and without solids in the two electrical field configurations, in positive and negative polarity, and under pressure. For reasons of time, availability of equipment, and technical problems, measurements of streamer transient currents were only done in parallel field under positive polarity, using a variety of different insulating solids.

2.1. Parallel field, positive polarity, and atmospheric pressure

2.1.1. Without solid

The first measurements were performed in air at atmospheric pressure without solid. These experiments provide basic information that will be later compared to experiments with a solid. Recordings B, C and D on Fig. 5 correspond to photographs B, C and D on Fig. 4. The opening time of the intensifier is shown on oscilloscope recordings (lower trace). Transient currents get a negative sign due to the measurement system used.

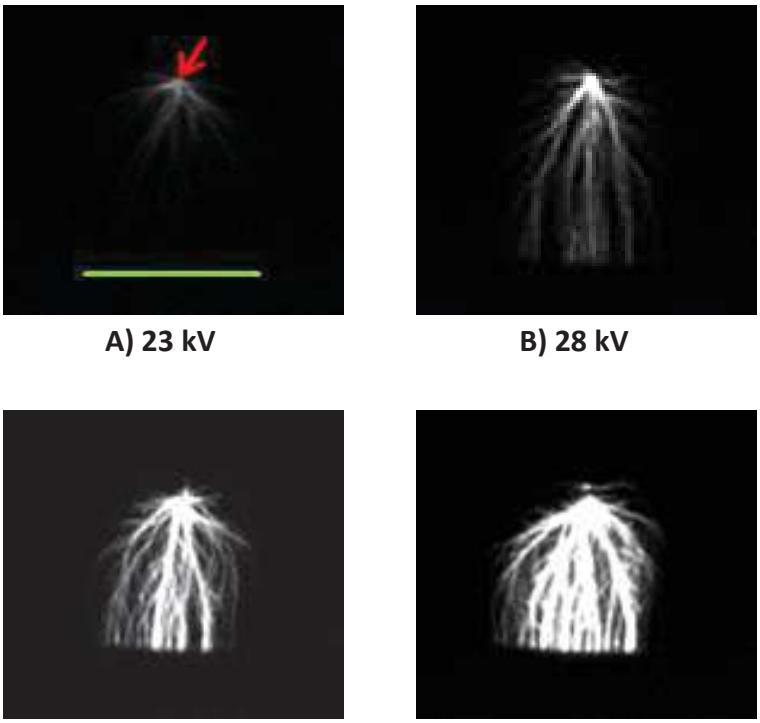

Fig. 4: Time-resolved photographs of streamers in the air alone (without insulating solid) versus voltage (gap distance = 5 cm). The arrow represents the point and the horizontal line the grounded plane.

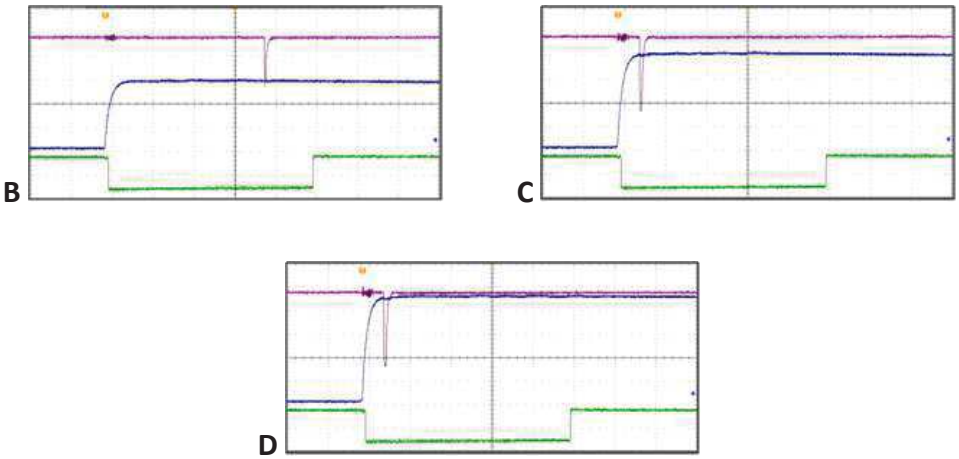

Fig. 5: Oscilloscope recordings corresponding to Fig. 4B, C and D. Upper trace: current (200 mA/div.). Middle: voltage (10 kV/div.). Lower: intensifier's gate. Horizontal scale: 2 µs/div.

Fig. 4 shows typical images of streamers obtained in air without solid. At low voltage (Fig. 4A), a PD close to the point is observed. The applied voltage is not high enough for streamers to reach the grounded plane. Fig. 4B shows the propagation of a streamer to grounded plane. This streamer is composed of several branches. There is no transition to breakdown at this voltage. Its propagation is correlated to a current pulse (Fig. 5B), about 400 ns in duration and 400 mA in amplitude, occurring on the voltage plateau (i.e. after the risetime).

By increasing voltage (Fig. 4B), branches of the streamer are getting more and more luminous, until breakdown occurs (at higher voltage than 45 kV).

2.1.2. With Epoxy/Silica solid

Time-resolved photographs were taken together with transient current measurement (Fig. 6 and 7). Recordings B, C, and D on Fig. 7 correspond to photographs B, C and D on Fig. 6. On the left hand side of photographs, a reflection of the streamer light on the smooth solid surface is seen. The optical gain of the intensifier in Fig. 6 A and B was larger than in figures C and D.

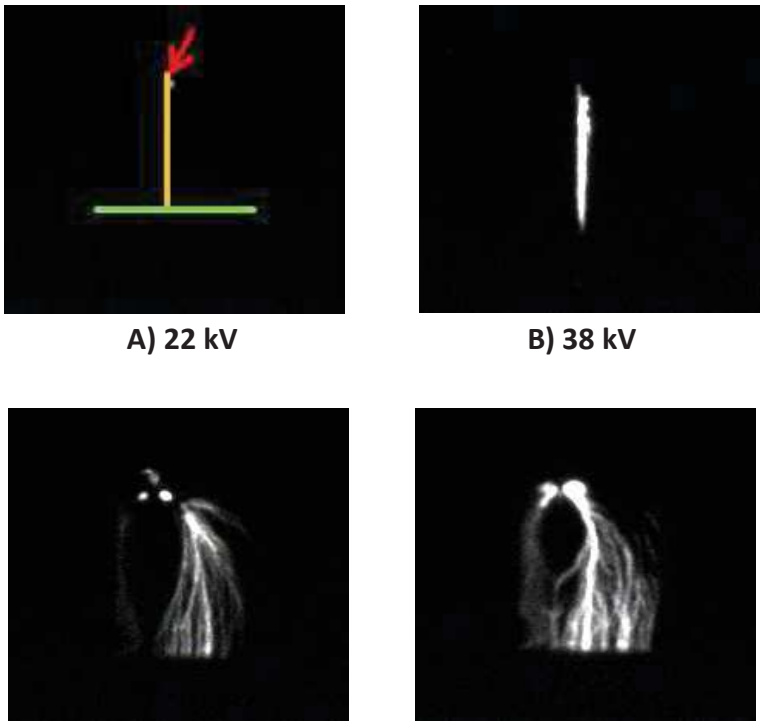

Fig .6: Time-resolved photographs of streamers (side view) with Epoxy/Silica solid, versus voltage (gap distance = 5 cm). The arrow represents the point, the vertical line shows the solid surface, and the horizontal line the grounded plane. Opening time of intensifier's gate is shown in Fig. 7.

At low voltage (Fig . 6), a luminous spot is observed at the point tip. No propagation occurs at this voltage. At higher voltage (B), the propagation of a weakly luminous streamer along the solid surface up to the plane electrode is observed. Its propagation is correlated to a fast-current pulse (Fig. 7B), about 20 ns in duration and 200 mA in amplitude, occurring during the voltage rise at an instantaneous voltage lower than the maximum value. There is no transition to breakdown. Compared to the case without solid, the minimum instantaneous voltage required to allow streamer propagation up to the plane is slightly higher (30 kV instead of 28 kV without solid).

Fig. 8 (front view) shows that surface streamers are constituted by several branches initiated from the point, and spreading over the surface. Only some of these branches reach the grounded plane electrode.

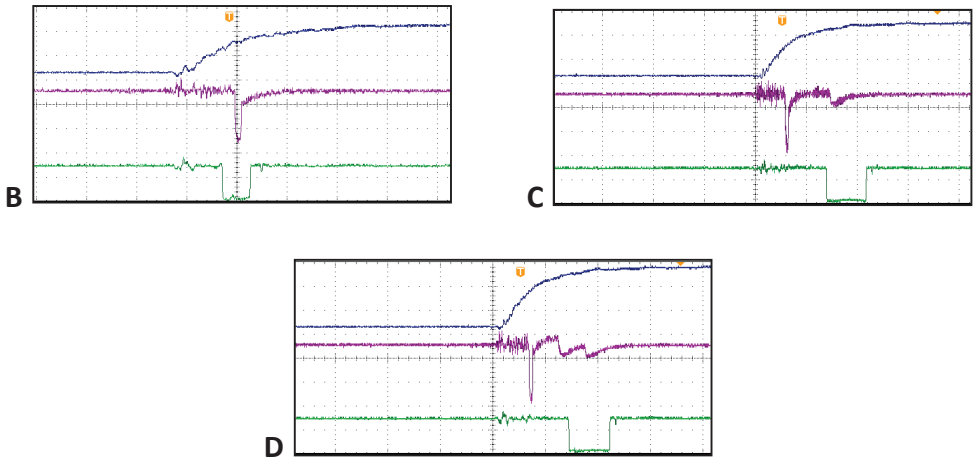

Fig. 7: Oscilloscope recordings corresponding to Figure 6B, C and D. Upper trace: voltage (20 kV/div.). Middle: current (100 mA/div.). Lower: intensifier's gate. Horizontal scale: B: 200 ns/div., C, D: 400 ns/div.

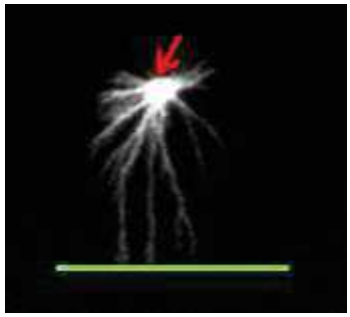

Fig.8. Photograph of surface streamer (parallel field, front view) on Epoxy/Silica at 31 kV.

At higher voltage, a second streamer type follows the first surface discharge. It is composed by more luminous filaments propagating in the air volume above the surface (Fig. 6C). It is correlated to a second current pulse occurring at higher instantaneous voltage, of lower amplitude (50 mA) and longer duration (200 ns) compared to the first surface streamer. Breakdown is still not observed. When voltage is further raised (Fig. 6D) several streamer filaments propagating above the surface become much more luminous, multiple current pulses are recorded, and breakdown rapidly follows. Just below the breakdown voltage, some luminous filaments may re-adhere to the solid surface close to the plane.

The fact that the duration of the current pulse corresponding to the surface discharge (20 ns) is much shorter than in air (200 ns) is probably correlated to the highest velocity of surface streamers. Correlated to the gap distance (5 cm), a duration of 20 ns corresponds to an estimated propagation velocity about 2.5 10^6 m/s, in agreement with measured velocities of surface streamers (*Chapter 1*).

2.1.3. Sequence of pre-breakdown events at atmospheric pressure

Time-resolved recordings obtained here allow describing the sequence of streamers leading to breakdown when the applied voltage is raised. It is slightly different in air alone and in the presence of a solid.

Air alone: 1: streamer initiation;
2: streamers propagation to the plane;
3: transition to breakdown spark.

With solid: 1: streamer initiation;
2: surface streamer propagating to the plane;
3: subsequent streamers propagating in air over the surface;
4: transition to breakdown spark.

With the 0.4 µs voltage rise time used, the streamer sequence in the presence of a solid starts during the voltage rise at an instantaneous voltage lower than the crest applied voltage, while phenomena in air alone occur mainly on the voltage plateau. Detailed measurements of instantaneous inception voltages with various solids will be presented in next sections.
The existence of streamer filaments propagating either along the surface or in the air volume above the surface agrees with previous observations [4,5,6]. The fact that streamers can propagate up to the plane electrode without inducing breakdown agrees with other observations. This agrees with the fact that streamers are constituted by a “cold” and weakly ionized plasma. The value of the minimum propagation voltage (about 28 kV at d = 5 cm gap in air alone) agrees with previous values of the “stability field” of streamers in ambient air, from 0.4 to 0.6 kV/mm according to experimental conditions (air humidity, voltage shape, etc.) [7]. The fact that surface streamers reach the plane at identical voltage (28 kV) show that the mechanisms involved are basically identical to those occurring in air alone.

However, in a number of papers the streamer propagation up to the plane is considered as a sufficient criterion to predict breakdown, especially in numerical simulations developed to predict breakdown [8]. From our measurements, and from several other similar experimental studies [9], this criterion appears insufficient since a rather large difference exists at atmospheric pressure between the minimum voltage required for streamers to propagate up to the plane (e.g. 28 kV), and the breakdown voltage measured in the same situation (48 kV, see *Chapter 3*).

Therefore, when breakdown voltages in ambient air are measured in divergent fields (i.e. when inception voltage is significantly lower than breakdown voltage), and in conditions

close to our experiments, the measured breakdown voltage represents the voltage required for the transition from a streamer to a breakdown spark. It does not represent the voltage required for streamer propagation up to the plane, as quoted in several papers. At atmospheric pressure, the situation may however change when conditions are changed, e.g. at much larger gap distances and voltage, when pre-breakdown discharges change from streamers to leaders. In this case, the leader channel is much more conductive (inner voltage drop of 0.1 – 0.2 kV/mm [7]) and breakdown occurs as soon as the discharge reaches the plane. This situation was not investigated in this study. Measurements under AC show the inception of leaders in ambient air at distances larger than 10 cm, and corresponding breakdown voltages above 70 kV [7]. Similar leader phenomena occur in electronegative gases (e.g. in SF_6) at much lower voltage and distance.

In Fig. 6C and D, subsequent streamers propagate mostly in air above the surface, probably because of positive surface charges left by the first surface streamer. These charges contribute to lower the field on the surface. Subsequent streamers leading to breakdown propagate by getting around the charged zone.

2.2. Parallel field, positive polarity, and pressure up to 0.3 MPa

The pressure is affecting the development of the discharge. Visualisations and transient current measurements were performed in dry air without solid, and in the presence of Epoxy/Silica at 0.2 and 0.3 MPa.

2.2.1. In dry air without solid

Pressure hampers the development of streamers until the grounded plane. Higher voltages must be applied to observe luminous phenomena and the transition to breakdown (Figs. 9, 10). Fig. 9 shows streamers at 0.2 MPa without solid in dry air. Such as at atmospheric pressure, streamers propagate to the grounded plane without transition to breakdown. Compared to atmospheric pressure, the minimum voltage required for propagation up to the plane (Fig. 12) is larger (52 kV at 0.2 MPa and 110 kV at 0.3 MPa instead of 28 kV). By increasing the applied voltage, streamers are getting more and more luminous.

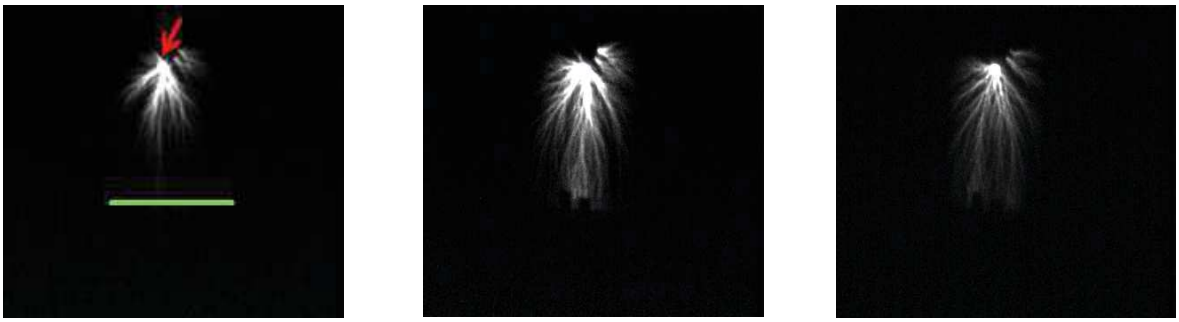

A) 52 kV **B) 59 kV** **C) 70 kV**

Fig. 9: Time-resolved photographs of streamers in air versus voltage (gap distance = 5 cm) at 0.2 MPa. The arrow represents the point and the horizontal line the grounded plane.

At 0.3 MPa, Fig. 10 shows that at 106 kV, i.e. slightly below the breakdown voltage (110 kV), streamers did not reach the grounded plane. This result strongly suggests that at this pressure, propagation of streamers up to the plane now directly leads to breakdown when the streamer reaches the plane. We can hypothesize that contrarily to 0.1 MPa and 0.2 MPa, the propagation to the plane can constitutes a sufficient criterion to ensure breakdown. At this pressure, we can admit that propagation controls breakdown.

A) 54 kV **B) 80 kV** **C) 106 kV**

Fig. 10: Time-resolved photographs of streamers in air versus voltage (gap distance = 5 cm) at 0.3 MPa. The arrow represents the point and the horizontal line the grounded plane.

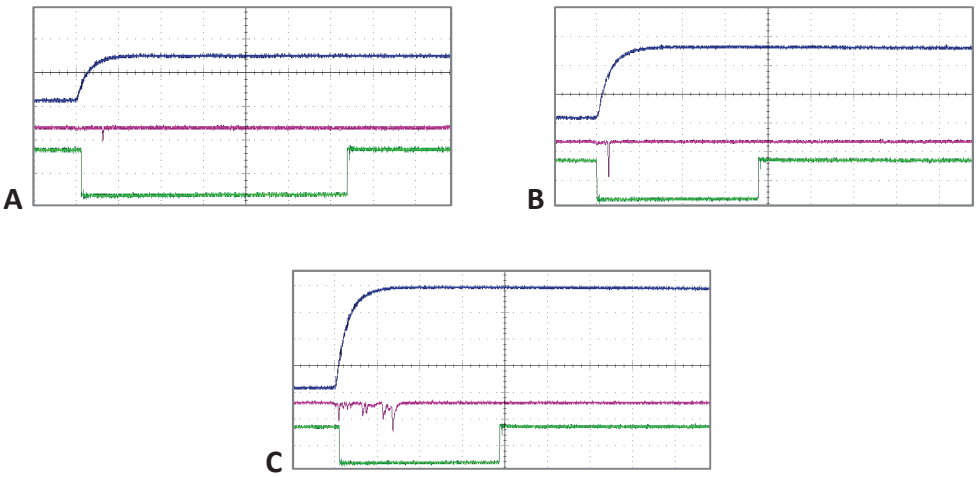

Fig. 11: Oscilloscope recordings corresponding to Fig. 10A, B and C. Upper trace: voltage (30 kV/div.). Middle: current (200 mA/div.). Lower: intensifier's gate. Horizontal scale: B, C and D: 400 ns/div.

On Fig. 12 the breakdown criterion is indicated (T^V: streamer to spark transition in air volume, P^V: propagation in air).

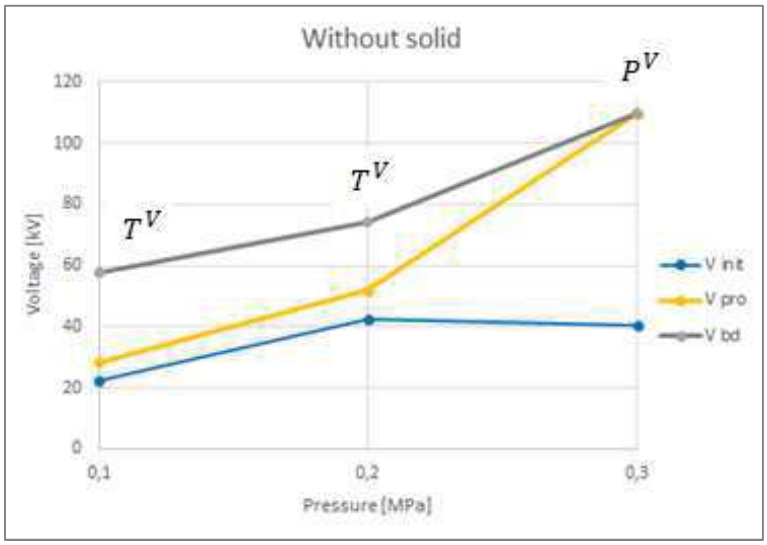

Fig. 12: Initiation, propagation and breakdown voltage for three different pressures without solid.

2.2.2. In dry air with solid

Compared to atmospheric pressure measurements (Fig. 6), surface and volume streamers are still observed at 0.2 and 0.3 MPa (Fig. 13, 15). The voltage required for propagation (Fig. 16) increases with pressure.

At 0.2 MPa, such as at atmospheric pressure, the voltage required to reach the grounded plane with solids (74 kV) is larger compared to air alone (52 kV). The solid appears to restrain streamer propagation. Such as in air alone at the same pressure, streamers can reach the plane without inducing breakdown. Fig. 13C shows that slightly below breakdown voltage, surface streamers reached the plane, whereas volume streamers did not. This constitutes a large difference with atmospheric pressure (Fig. 6).

A) 38 kV **B) 59 kV** **C) 75 kV**

Fig. 13: Time-resolved photographs of streamers (side view) on Epoxy/Silica in parallel field versus voltage (gap distance = 5 cm) at 0.2 MPa. The arrow represents the point, the vertical line shows the solid surface, and the horizontal line the grounded plane.

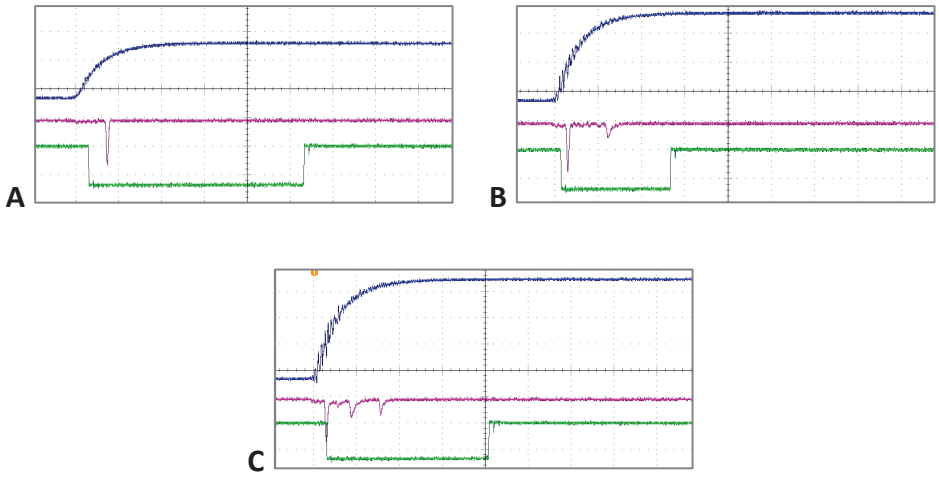

Fig. 14: Oscilloscope recordings corresponding to Fig. 12A, B and C. Upper trace: voltage (20 kV/div.). Middle: current (200 mA/div.). Lower: intensifier's gate. Horizontal scale: B, C and D: 400 ns/div.

At higher pressure (0.3 MPa), a reversed influence of the solid is observed: propagation voltage with solid (74 kV) is now lower than without solid (110 kV). The solid now appears to strongly favour discharge propagation. Contrarily to air alone, at 0.3 MPa streamers can now reach the grounded plane at 74 kV without inducing breakdown (Fig. 16). Such as at 0.2 MPa, the surface streamer propagates to the plane while the volume streamer is much shorter (Fig. 14C).

The reversed influence of the solid at 0.3 MPa suggests that a sudden change in the pre-breakdown mechanism occurred in these conditions. At this pressure, a sudden drop of breakdown voltages also occurred with solids of high permittivity (glass, Alumina, *Chapter 3* Fig. 45). The possibility that this transition could be associated with the propagation of leaders instead of streamers should be considered. It agrees with previous observations showing that the formation of leaders in air is favoured along dielectric surfaces [10]. Furthers investigations should be carried out to ascertain this hypothesis.

These observations are also consistent with the fact that at 0.2 and 0.3 MPa, breakdown sparks always occurred on the surface (*Chapter 3*). At atmospheric pressure, both surface and volume streamers propagate at voltage lower than the breakdown voltage (Fig. 6). This explains that sparks can occur either on the surface, or in the volume (*Chapter 3*).

With solid, the breakdown criterion at all pressures is the transition to a spark.

A) 26 kV **B) 59 kV** **C) 74 kV**

Fig. 15: Time-resolved photographs of streamers (side view) on Epoxy/Silica in parallel field versus voltage (gap distance = 5 cm) at 0.3 MPa. The arrow represents the point, the vertical line shows the solid surface, and the horizontal line the grounded plane.

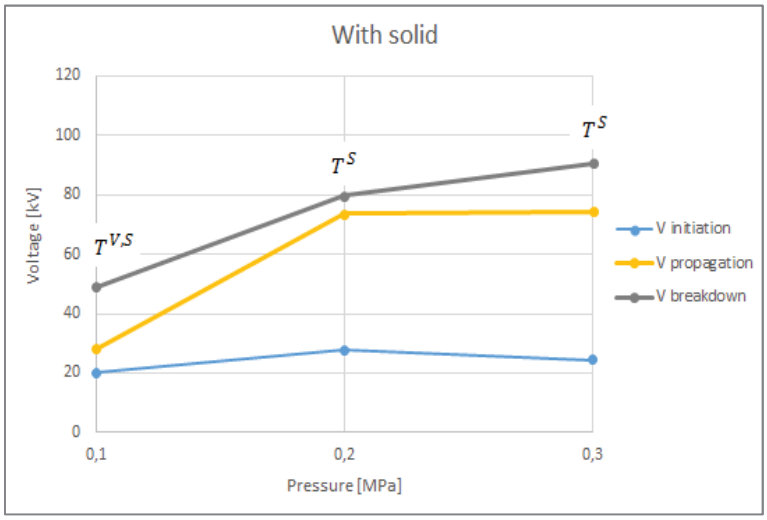

Fig. 16: Initiation, propagation of surface streamers and breakdown voltage for three different pressures with solid.

	Solid			Without solid		
	Patm	**0.2 MPa**	**0.3 MPa**	**Patm**	**0.2 MPa**	**0.3 MPa**
V inception [kV]	< 20	28	24	23	43	41
V propagation [kV]	28	74	74	28	52	110
V breakdown [kV]	49	75	77	58	74	

Tab. 1: Summary of average voltage corresponding to the different steps of development of the discharge.

2.3. Perpendicular field, positive polarity, and atmospheric pressure

In this geometry, only visualizations with solids could be performed. Attempts to measure transient currents were hindered by large parasitic perturbations occurring during the voltage rise. These perturbations probably result from the larger inter-electrode capacitance, which in turn induces a larger charging current.

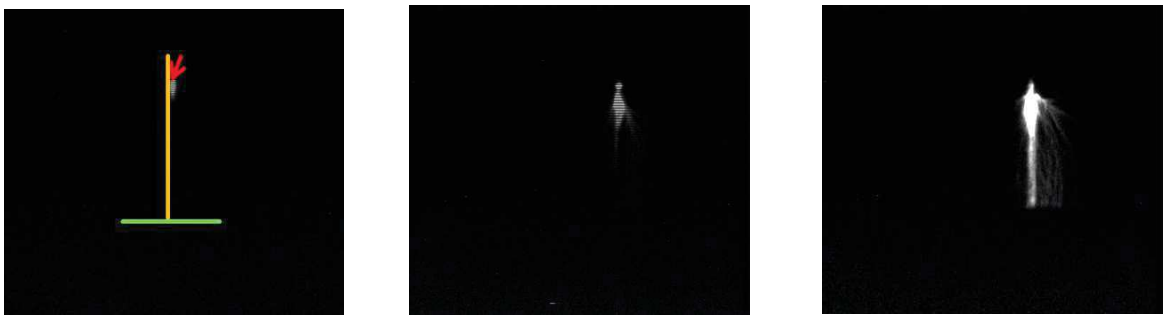

A) 21 kV **B) 34 kV** **C) 39 kV**

Fig. 17: Time-resolved photographs of streamers (side view) on Epoxy/Silica in perpendicular field versus voltage (gap distance = 5 cm). The arrow represents the point, the vertical line shows the solid surface, and the horizontal line the grounded plane.

Time-resolved photographs shows that streamers propagating on the surface and above in the gas volume also exist in this geometry (Fig. 17). The main difference with parallel field comes from the fact that luminous streamers observed at high voltage, responsible for the transition to breakdown, occur now on the surface instead of above the surface. Here again, streamers at atmospheric pressure were seen touching the plane without breakdown (Fig. 17C). However, the difference between propagation and breakdown voltage is lower compared to parallel field (5 kV instead of 21 kV). Therefore, measured breakdown voltage also represent the transition from streamer to breakdown (and not the propagation voltage).

2.4. Parallel field, negative polarity, and atmospheric pressure

A few comparative measurements were carried out in negative polarity. Streamers are much less ramified and take the form of few luminous large branches (Fig. 18). Compared to positive polarity, a higher voltage needs to be applied so that streamers reach the grounded plane and induce breakdown. These results agree, with the higher breakdown voltage measured in *Chapter 3*.

A) – 35 kV **B) – 47 kV** **C) – 62 kV**

Fig. 18: Time-resolved photographs of streamers in air without solid versus voltage (gap distance = 5 cm) in negative polarity. The arrow represents the point and the horizontal line the grounded plane.

A) – 35 kV **B) – 45 kV** **C) – 65 kV**

Fig. 19: Time-resolved photographs of streamers in air with PC versus voltage (gap distance = 5 cm) in negative polarity. The arrow represents the point, the vertical line shows the solid surface, and the horizontal line the grounded plane.

2.5. Influence of solid permittivity on the transition to breakdown

To explain the transition from streamer to breakdown, the models developed in the literature consider the mechanism of thermal runaway of streamer channels (see *Chapter 1*). It is difficult from the data obtained here to establish a quantitative model on this process. This would require knowing the amount of electrical energy dissipated within channels, and its variation with parameters (applied voltage, permittivity). Such investigations were out of the scope of the present work. It is however possible, based on simplified electrical model, to simply assess that the discharge current (and hence energy), increases with solid permittivity. In geometry identical to the "perpendicular" field used here, a formula of the total charge of creeping streamers was established [10]:

$$Q = \frac{2\pi\varepsilon}{d}\left[\frac{Ul^2}{2} - \frac{El^3}{3}\right] \qquad (1)$$

With Q: streamer charge, ε: solid permittivity, d: solid thickness, U: applied voltage, l: streamer length, E: voltage drop per unit length along the streamer channels. From this formula, it appears that the charge (and hence current and dissipated energy) corresponding to the streamer propagation is simply proportional to the solid permittivity. This provides a qualitative explanation for the marked decrease of breakdown voltage versus permittivity in this geometry (Fig. 48, *Chapter 3*). An increase of the streamer current and energy should favour the temperature rise, and the transition to a spark. In "parallel" field, a similar model would require a more complex 3D numerical calculation of the charge.

3. Investigations on streamer initiation in the presence of solids

3.1. Measurement procedure

Starting from 15 kV, the applied voltage was raised by 2 kV steps until breakdown. At each step, ten measurements were done. Fig. 20 shows a typical recording of voltage and current with a solid. The figure shows the instantaneous inception voltage V_i^s and time delay t^s of the first surface discharge. The time delay is arbitrarily counted from the beginning of voltage rise. The second instantaneous voltage V_i^v quoted corresponds to the inception of streamers in the air above the surface (volume streamer). The influence of several different solids was investigated with this method.

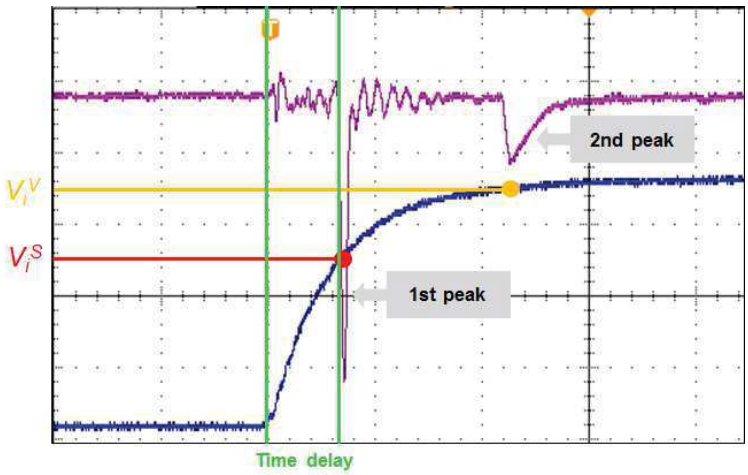

Fig. 20: Oscilloscope recording showing the measurement of instantaneous inception voltages and delays. Upper trace: current (50 mA/div.). Lower: voltage (10 kV/div.). Horizontal scale: 400 ns/div.

3.2. Ambient air

Measurements were first carried out in air alone without solid, in order to obtain reference measurements. On Fig. 21, mean values of instantaneous inception voltages in air (V_i^{air}) are plotted versus maximum applied voltage (V_a), with error bars showing maximum and minimum values. The red line corresponds to $V_i = V_a$. Consequently, data points located on that line correspond to streamers occurring on the voltage plateau at the maximum voltage, while data points below the line correspond to streamers occurring at lower voltage during the voltage rise. Fig. 22 shows the discharge inception delay time versus V_a. The red line corresponds to the rise time of the impulse voltage. Data points below the line correspond to discharges occurring during the voltage rise, and above the line during the voltage plateau.

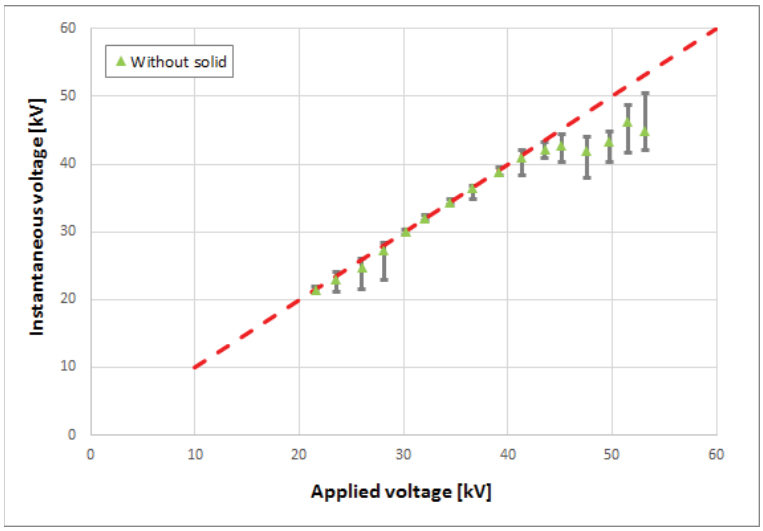

Fig. 21: Instantaneous inception voltage of discharge without solid (V_i^{air}). (d = 5 cm, r = 0.5 mm, 0.1 MPa).

In air, streamers appear at the voltage V_i^{air}, quite close to the maximum applied voltage V_a up to about 40 kV (i.e. streamers appear on the voltage plateau). Above 40 kV, V_i^{air} is slightly below V_a, i.e. streamers appear at the end of voltage rise.

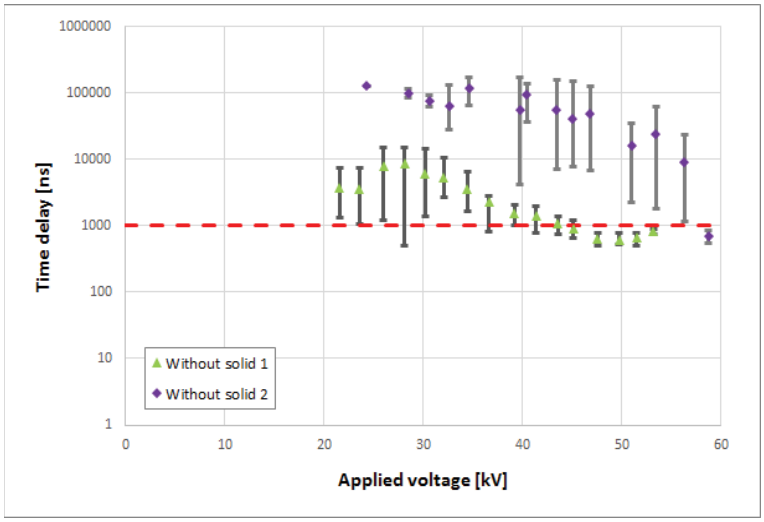

Fig. 22: Time delay for streamer without solid (t_d^{air}). (d = 5 cm, r = 0.5 mm, 0.1 MPa).

Fig. 22 shows time delays for streamers in the air (t_d^{air}). A very large scatter is typical for this statistical time delay, especially at low voltage. Furthermore, by repeating the measurements in air alone at different days with the same electrode, rather different results with a large scatter are obtained. Time delay can increase/decrease by one order of magnitude from day to day. In series 2, quite few discharges were observed at the lowest voltage (≤ 30 kV), this explains the small scatter bars. In the following, measurements of series 1 will be used as a basis for comparison with solids.

3.3. Comments about streamer inception in ambient air

In these measurements, time delays may last up to 100 µs at low voltage. The random character is reduced when the applied voltage is raised. The usual hypothesis to explain the scatter is that the delay time corresponds to the statistical time necessary to get a charge (electron) within some critical volume around the point, to initiate the streamer. By increasing the applied voltage, the critical volume increases, and the statistical delay decreases. The origin of the large variation observed from day to day is not known. It is usually considered that charges able to initiate discharges have various origins: ionization by cosmic rays, detachment from ions due to the applied field. Since experiments were carried out in ambient air, we may also suppose that other parameters also may participate to the observed variations (small changes in pressure, temperature, humidity, electrode surface condition ?).

When streamers appear on the voltage plateau (up to 40 kV in series 1), Fig. 22 shows the variation of random inception delays (up to 100 µs in series 2) when a constant voltage (and hence field) is applied. When streamers appear during the voltage rise, the measured delay does not any more represent only a statistical “waiting time”, but also depends on the time required to reach the inception voltage. A proper measurement of the inception delay under constant voltage would require a faster rise time, lower than the measured delay. The random character of measured delays nearly disappears at high voltage when streamers appear during the voltage rise.

When measurements are carried out with a standard 1.2/50 µs lightning impulse, the rapid decay of voltage prevents from obtaining such data. Under lightning impulse, the probability to observe a discharge results from a complex convolution between the probability to get a discharge versus voltage, and the decay of voltage. Measurements are thus very difficult to interpret. It can be anticipated that in the case of measurements of series 2, a lightning impulse should provide a lower inception probability compared to our long duration impulse (0.4/1400 µs) at the same voltage. Such time-dependent effects do not exist with a long duration impulse, which constitute more favourable conditions to study independently the variations of inception delay and inception voltage when conditions are changed (e.g. when solids will be introduced).

3.4. Epoxy/Silica

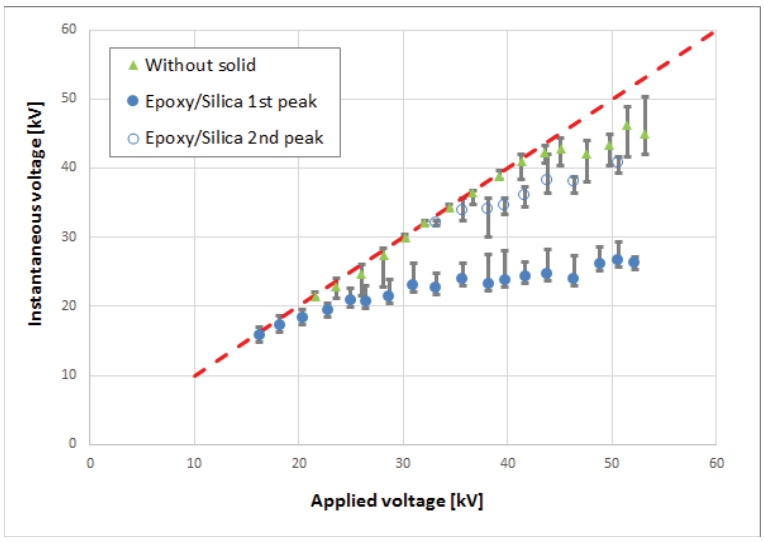

Fig. 23: Instantaneous inception voltage of first discharge without solid (V_i^{air}). First (surface, V_i^s) and second (volume, V_i^v) discharges with solid. (parallel field, d = 5 cm, r = 0.5 mm, 0.1 MPa).

Epoxy/Silica is the reference material of Schneider Electric. Fig. 23 shows that the first surface streamer on Epoxy/Silica appears at an instantaneous voltage V_i^s lower than the maximum voltage V_a (i.e. discharges mostly appear during the voltage rise). The corresponding delay time t_d^s are much lower than in air (about 1 order of magnitude) and show a much lower scatter, excepted when streamers appear on the voltage plateau (i.e. at the lowest voltage investigated < 20 kV), such as in air. The minimum voltage to observe discharges is also reduced: discharges are already observed at the minimum voltage allowed by the Marx generator (about 15 kV). Unfortunately, due to this limitation, it was not possible to obtain a precise value of the minimum discharge inception such as in air.

The subsequent "volume streamer" propagating above the solid surface starts after a time delay t_d^v. These streamers also occur during the voltage rise. As compared to air alone, delays t_d^v and scatter bars are smaller. This shows that even if this second streamer develops in the air and resemble those observed in air alone, it is however influenced by the previous surface streamer. It is interesting to note that the minimum voltage required to observing a second streamer (33 kV on Fig. 23) is much larger than in air alone (22 kV). This is certainly due to the influence of surface charges left by the first surface streamer, which reduce the electric field at the point.

3.5. Discussion about streamer inception with Epoxy/Silica solid

These results show that in presence of a solid, the inception of the first streamer is considerably facilitated. The first reason for this is the field enhancement due to the solid, close to the contact point between solid and point extremity. Field calculations of *Chapter 3*

show that with Epoxy/Silica of permittivity ε_r = 3.6, the maximum field is increased by a factor (x 2.5) compared to air alone. It is interesting to observe that to get the same delay (e.g. 1 µs on Fig. 23), nearly the same factor exists between the voltage in air alone (40 kV) and with Epoxy/Silica (16 kV). This comparison is however not totally conclusive since streamer inception not only depends on the maximum field value, but also on the spacial field distribution, which is modified in the presence of a solid.

Moreover, experiments carried out with other solids (PP, PTFE) in the next sections will show that initiation is not only controlled by the electric field, but also by other factors linked to the solid nature. In the case of Epoxy/Silica, the influence of the material nature in addition to that of permittivity cannot be clearly evidenced.

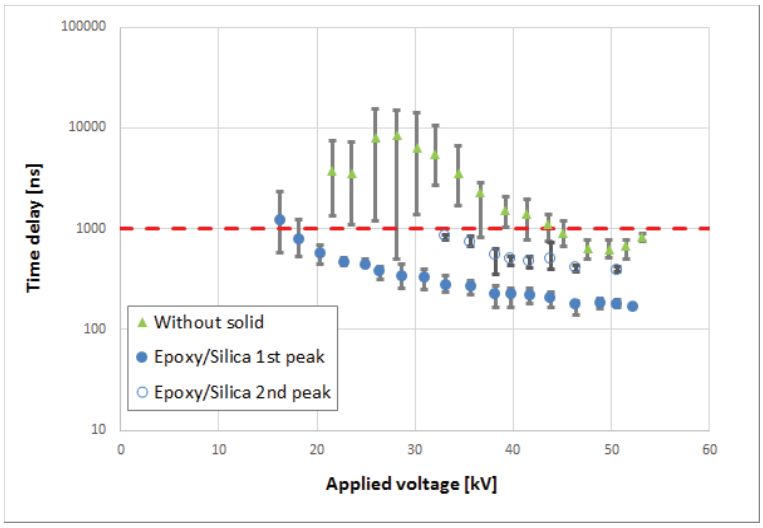

Fig. 24: Time delay for streamer without solid (t_d^{air}), and with Epoxy/Silica (t_d^{s} and t_d^{v}).

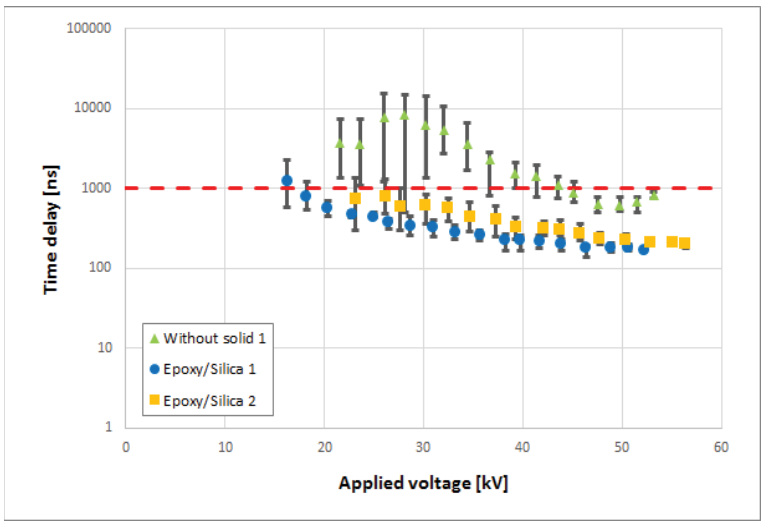

Fig. 25: Time delay for first streamers without solid (t_d^{air} , measurement at different days), and with Epoxy/Silica (t_d^{s}, measurement of different solids at different days).

Second volume streamers appear after the surface streamer, at an instantaneous voltage V_i^v slightly lower than in air alone. Photographs show that in many cases, these streamers do not originate from the triple point region, but from the electrode at some distance from this point (Fig. 6C, D, Fig. 10B, C). This was not observed in air alone. In a similar way, they do not propagate over the surface, and the final breakdown spark frequently occurs above the surface. All these results can probably be explained by charges left on the solid surface by the first surface discharge that modify the field distribution.

3.6. Others materials: PPA, PC, Epoxy resin

We performed the same measurements on several other materials (presented in *Chapter 2)* to determine if the same degradation of voltage and time to initiate the discharge is observed.

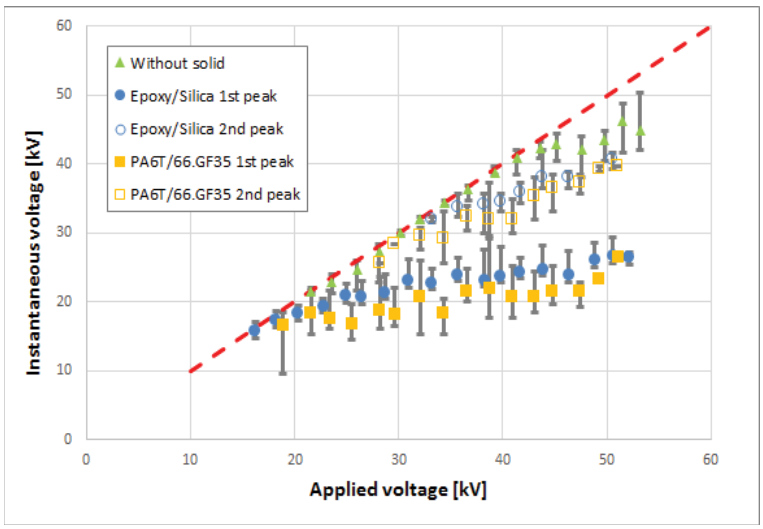

Fig. 26: Instantaneous inception voltage of first discharge without solid (V_i^{air}). First (surface, V_i^s) and second (volume, V_i^v) discharges with two different solids.

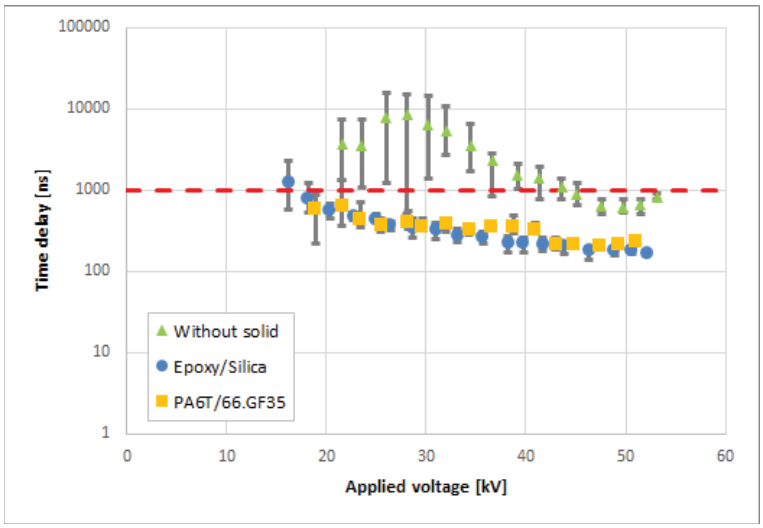

Fig. 27: Time delay for first streamers without solid, with Epoxy/Silica and with PA6T/66.GF35.

Fig. 26 and 27 show that PA6T/66.GF35 has the same behaviour than Epoxy/Silica. The surface discharge initiates at nearly the same voltage, as well as the second volume streamer.

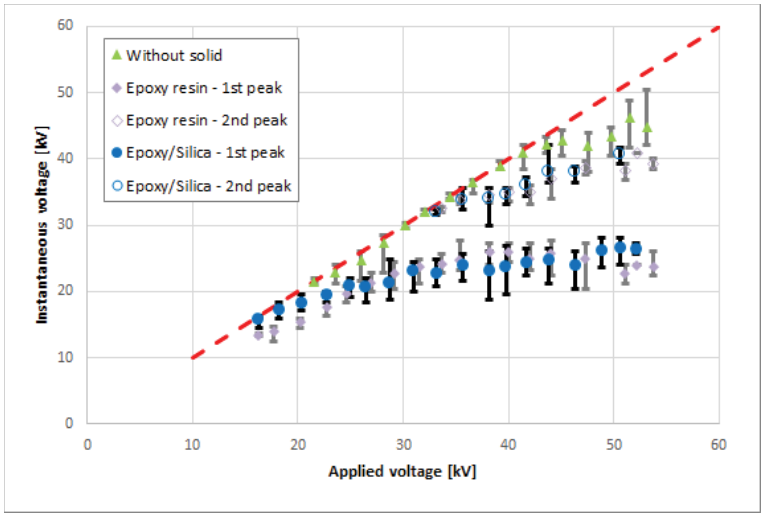

Fig. 28: Instantaneous inception voltage of first discharge without solid (V_i^{air}). First (surface, V_i^s) and second (volume, V_i^v) discharges with Epoxy/Silica and Epoxy resin.

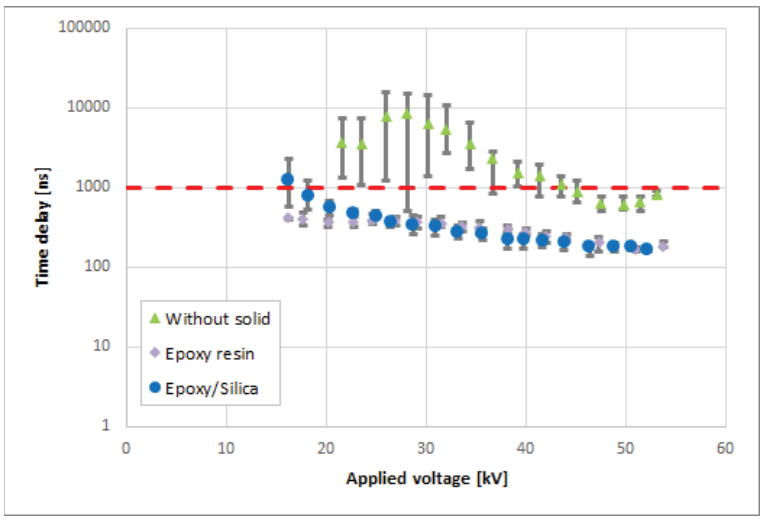

Fig. 29: Time delay for first streamers without solid, with Epoxy/Silica and with Epoxy resin.

Figs. 28, 29 show the influence of silica particles in Epoxy resin on initiation of the discharge. Same results are obtained for both material. The presence of silica in the resin has no influence on the discharge's occurrence.

The polycarbonate was also investigated, with two different surface roughnesses to check the influence of this parameter on initiation (Fig. 30 and 31). The first PC sample has a smooth surface and the second one presents a much higher surface rugosity due to the sand blasting carried out.

Fig. 30 shows that the average values of the instantaneous initiation voltages for the surface discharge for PC with and without sand blasting are the same. The only difference was a higher scatter of statistical time with the sand blasted surface, also correlated to a larger scatter of initiation voltage. The second streamer in the air volume has the same behaviour for both PC.

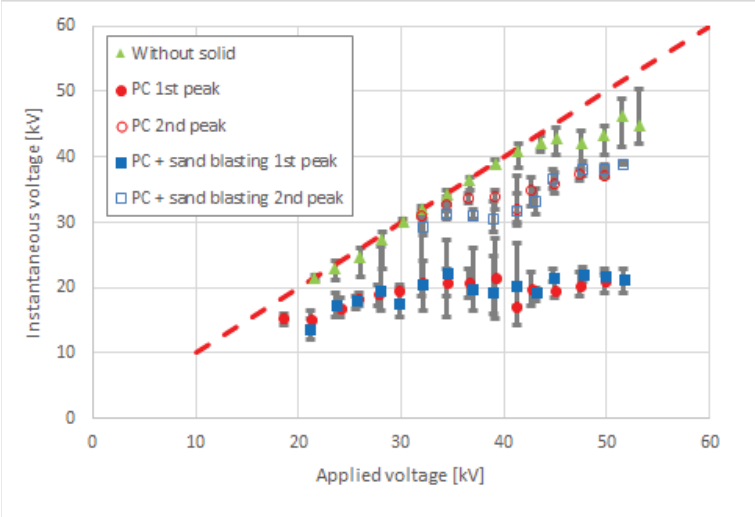

Fig. 30: Instantaneous inception voltage of first discharge without solid. First and second discharges with PC with and without sand blasting.

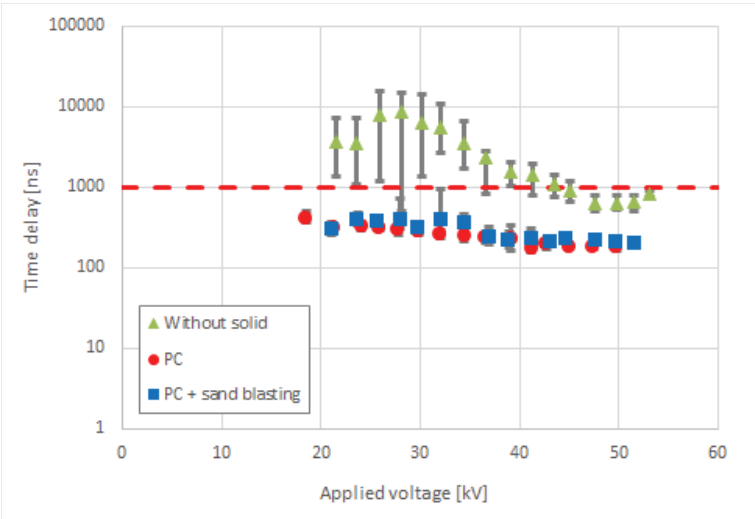

Fig. 31: Time delay for first streamers with PC with and without sand blasting.

The main conclusion obtained from these measurements is that it is very difficult to evidence clear differences between these materials. No clear ranking can be established considering the permittivities from ε_r = 2.6 (PC) to ε_r = 3.9 (PPA). Even measurements carried out with glass of higher permittivity (ε_r = 5) show no clear differences (*Annex 2*).

3.7. Polypropylene (PP), polytetrafluoroethylene (PTFE)

These materials showed a rather different behaviour compared to the previous ones. Fig. 31 shows that the voltage inception of the surface discharge with PP is almost the same than in air alone, considering the large scatter usually observed in these conditions. The inception voltage of the second streamer is nearly identical to the first surface discharge. Both streamers appear during the voltage "plateau", not during the voltage rise. Such as in air, inception delays show a large scatter (Fig. 33). On this figure larger delays were observed with PP, but this conclusion is not totally conclusive since in air alone a large instability exists.

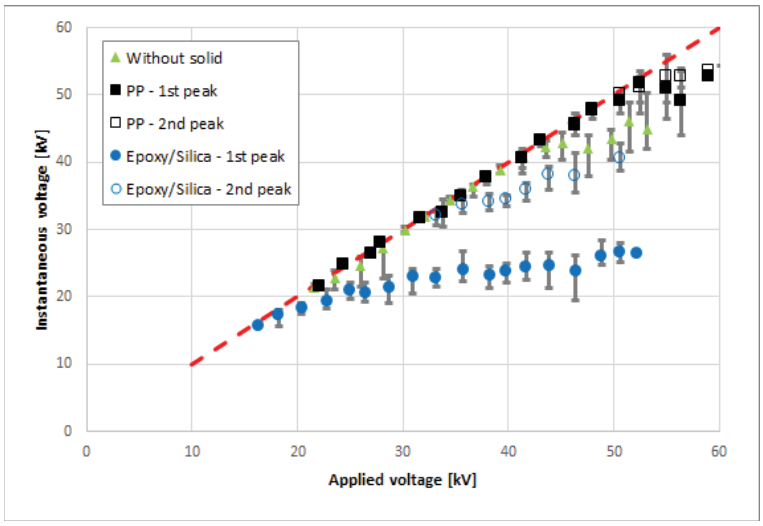

Fig. 32: Instantaneous inception voltage of first discharge without solid, with Epoxy/Silica and PP.

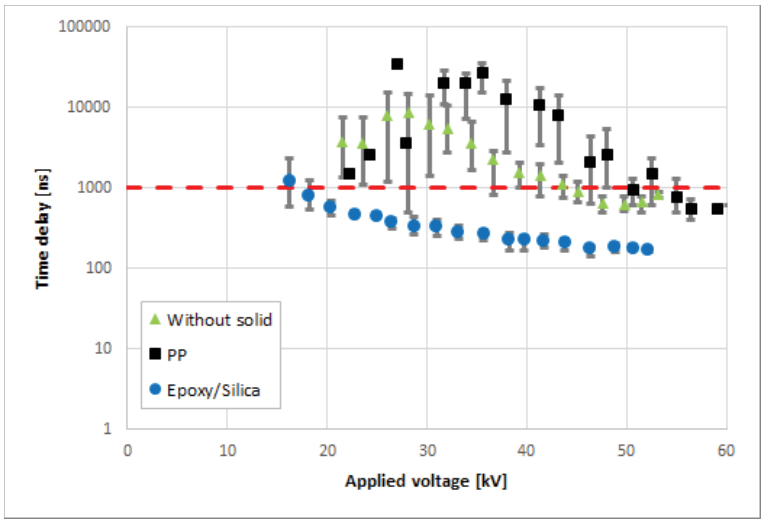

Fig. 33: Time delay for first streamers without solid, with Epoxy/Silica and PP.

Same measurements were performed with PTFE (Figs. 34, 35). This material shows an intermediate behaviour between PP and the other materials. Surface streamers are developing at a voltage higher on average than for others materials, but lower than with PP

or air. A much larger scatter than in other materials is however observed. Large error bars span between the behaviour of epoxy and that of air. This means that from shot to shot, a large instability is observed. The same applies with the inception time, higher on average compared to other materials. However, from shot to shot streamers with PTFE can either appear during the voltage rise, or on the plateau.

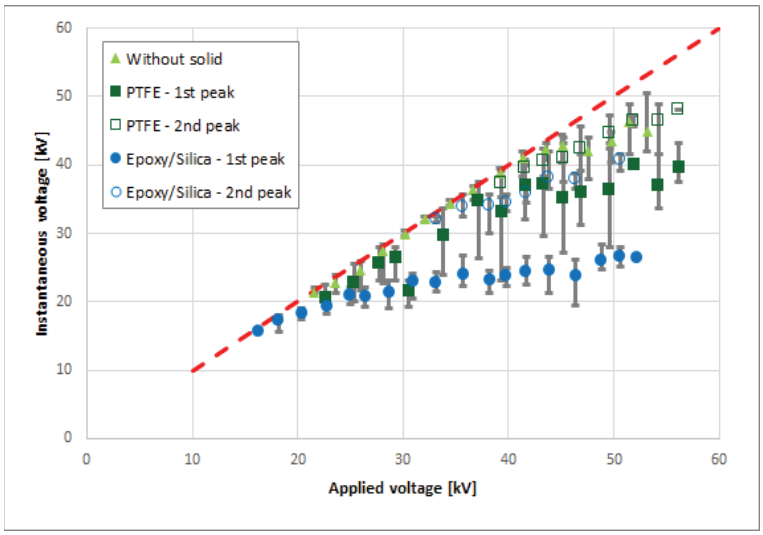

Fig. 34: Instantaneous inception voltage of first discharge without solid. First discharge with Epoxy/Silica and PTFE.

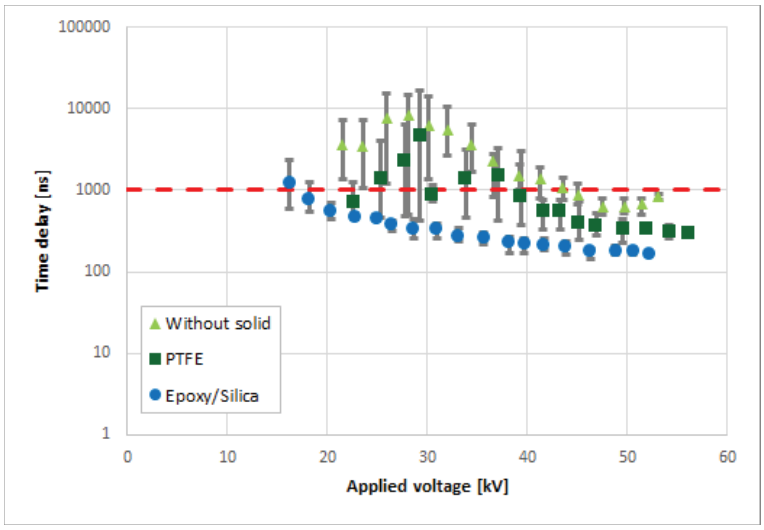

Fig. 35: Time delay for first streamers without solid, with Epoxy/Silica and PTFE.

3.8. Comments about measurements in PP

The results obtained with PP, compared to other materials such as Epoxy resin or PC, show that the influence of solids cannot be attributed solely to the field enhancement occurring at the triple point. PP shows almost no difference with air alone, in spite of the field enhancement at the triple point due to its permittivity, about twice that of air. We can conclude that the inception of the discharge is also influenced by the solid's nature. With PP

(and also with PTFE), some unknown mechanism seems to compensate the influence of field enhancement, by restraining discharge initiation. Tentative mechanisms can be invoked:

- The influence of surface charges remaining in the triple point region could induce a field reduction. However, it is very difficult to evidence the influence of surface charges on inception (see next section 4);
- It is striking to observe that PTFE and PP show unusual tribo-electric properties, compared to other solids such as PC [11]. These materials show a high ability to "catch" electrons, characterized by a high Affinity parameter (PTFE: -190 nC/J, PP: -90nC/J) compared to other materials (PC: -5 nC/J). Other materials show a positive affinity (such as glass: + 25nC/J), meaning that they easily provide electrons. The "catching" of electrons by PP or PTFE surfaces could explain that discharge inception is restrained with these materials;
- PP and PTFE are the only materials tested showing no double bond and/or aromatic rings in their molecule (*Chapter 2*).

3.9. Influence of the contact between electrode and solid

In order to check the influence of the contact between electrode and solid material, some experiments were done with the point at some distance (120 µm) from the solid surface (Fig. 36).

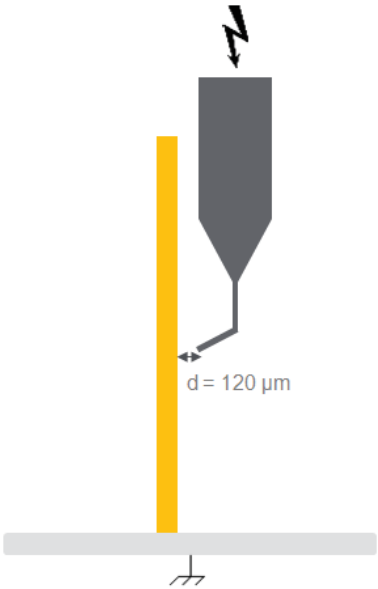

Fig. 36: Electrodes setup in parallel field with the point at some distance (120 µm) from the insulator's surface.

Fig. 37 shows that moving the point-electrode away from the surface at a short distance (120 µm) strongly affects the initiation conditions. Photographs show that first streamers still develop on the surface, but not any more during the voltage rise, and with a time delay comparable to air (Fig. 38).

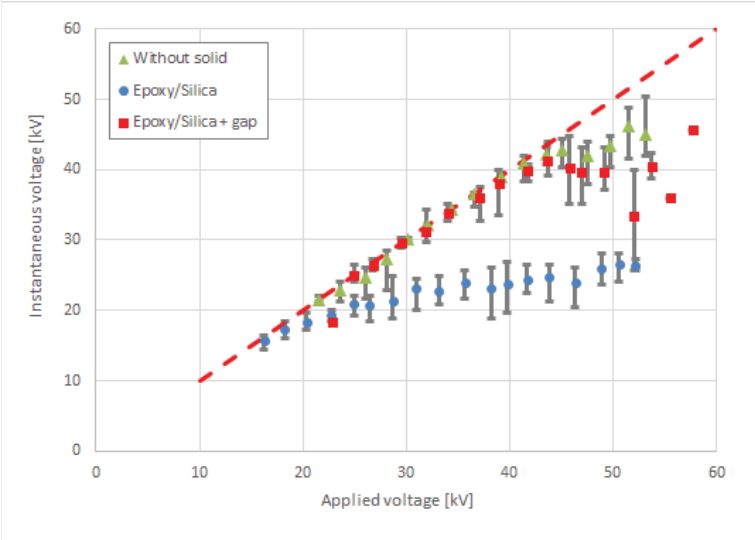

Fig. 37: Instantaneous inception voltage of first discharge without solid and with Epoxy/Silica.

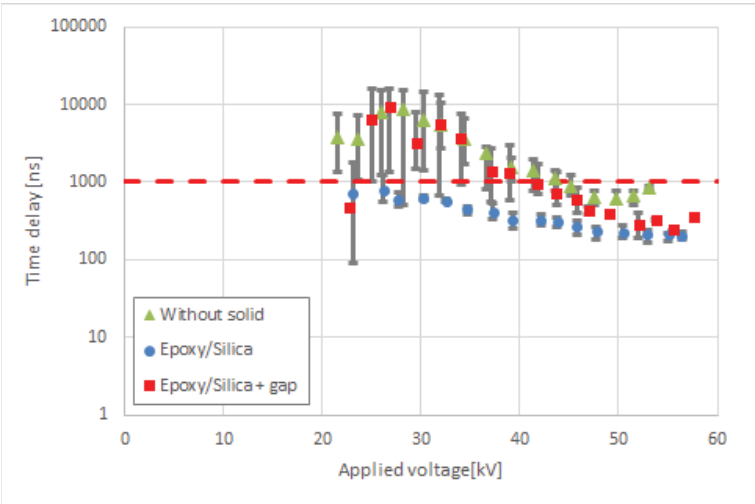

Fig. 38: Time delay for first streamers without solid and with Epoxy/Silica at 120 µm from the point.

These results show that the region around the triple point causing a large degradation of the inception voltage is quite small, around the contact point metal/solid. When the point touches the solid, a gas wedge exists, and PD's occur in this wedge at some distance from the contact point, due to the mismatch of permittivities (*Chapter 1*, Fig.19). If this wedge is enlarged, the maximum field is reduced and discharge inception voltage should increase.

3.10. Influence of pressure

Measurements under pressure in dry synthetic air were first performed in air without solid (Fig. 39). The comparison between ambient air and dry air at 0.1 MPa shows a large scatter in both cases (Fig. 40). In dry air, time delays strongly increase with the pressure, with about two decades difference between 0.1 and 0.3 MPa. Pressure has a positive impact on the initiation of the discharge without solid (Fig. 40).

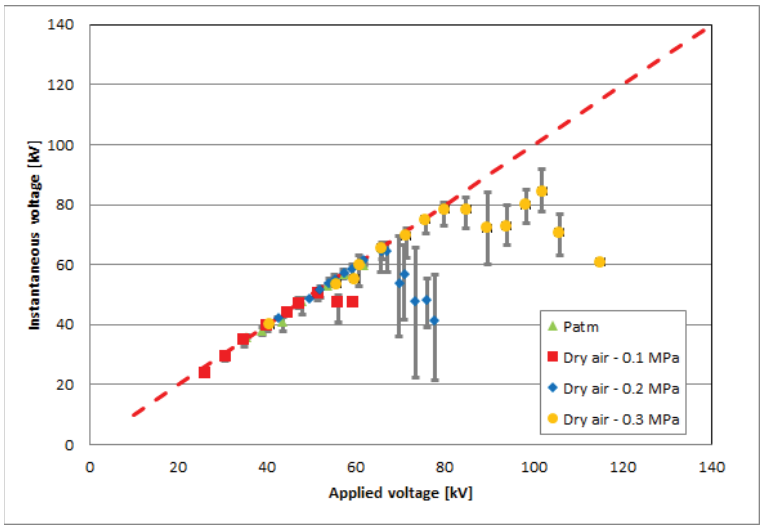

Fig. 39: Instantaneous inception voltage of first discharge without solid at different pressures.

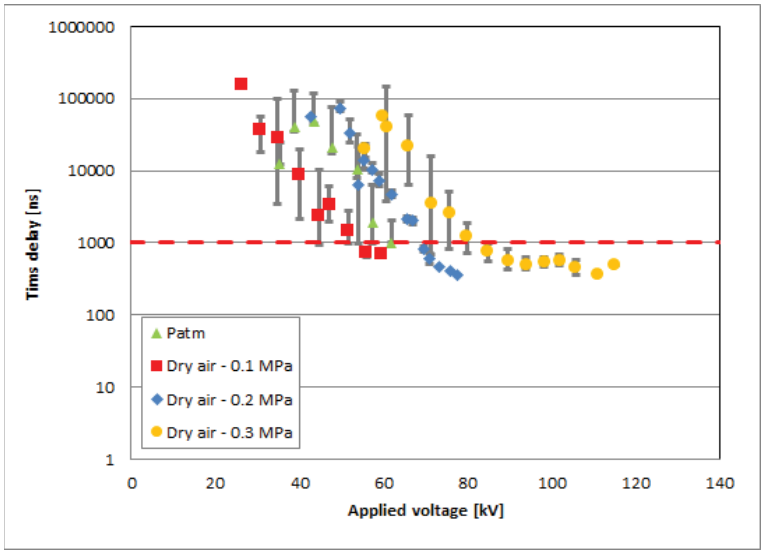

Fig. 40: Time delay for first streamers without solid at atmospheric pressure and dry air (0.1, 0.2 and 0.3 MPa).

With Epoxy/Silica (Figs. 41, 42), pressure doesn't have the same influence than without solid. The inception voltage and time are the same for 0.2 and 0.3 MPa. Pressure has a low influence on the initiation of the discharge in dry air with Epoxy/Silica.

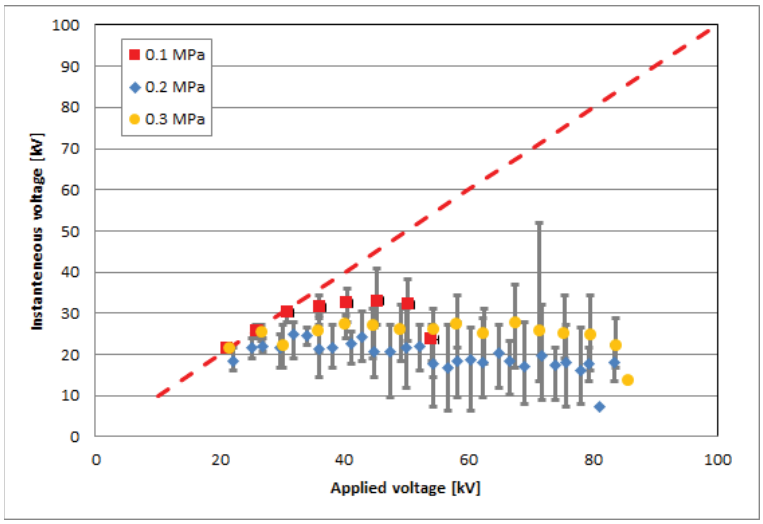

Fig. 41: Instantaneous inception voltage of first discharge with Epoxy/Silica at different pressures.

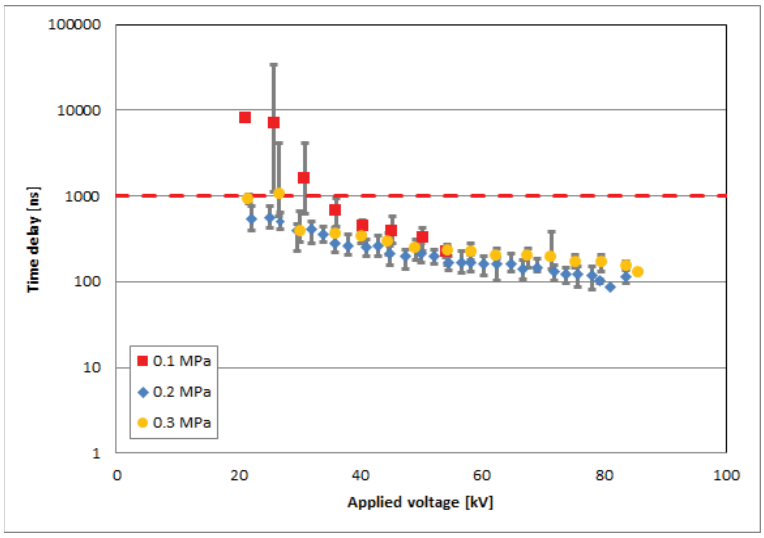

Fig. 42: Time delay for first streamers with Epoxy/Silica at 0.1, 0.2 and 0.3 MPa.

Fig. 43 and 44 show that at 0.3 MPa, the inception voltage and time of the discharge are the same for Epoxy/Silica and PA6T/66.GF35. These measurements are consistent with the ones obtained at atmospheric pressure, with a time delay higher without solid and with a strong decrease of this time is the presence of a solid. The solid's nature has no influence on the inception under pressure. These results agree with atmospheric pressure measurements.

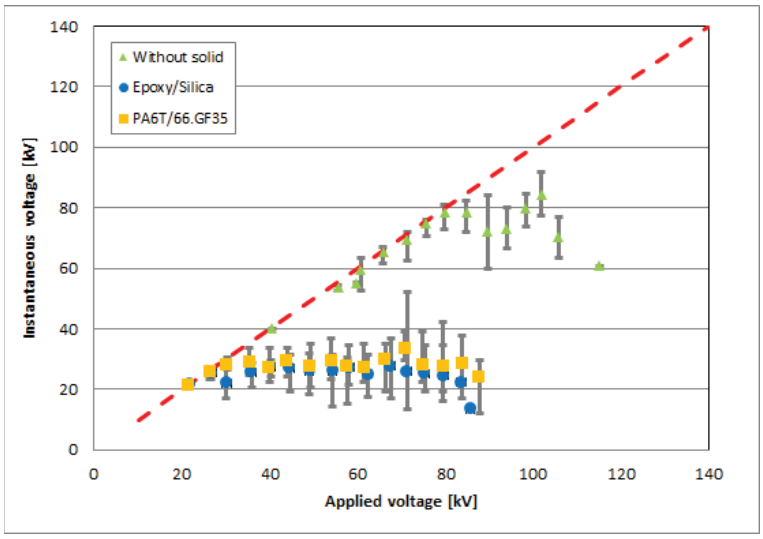

Fig. 43: Instantaneous inception voltage of first discharge without solid and with Epoxy/Silica and PA6T/66.GF35 at 0.3 MPa.

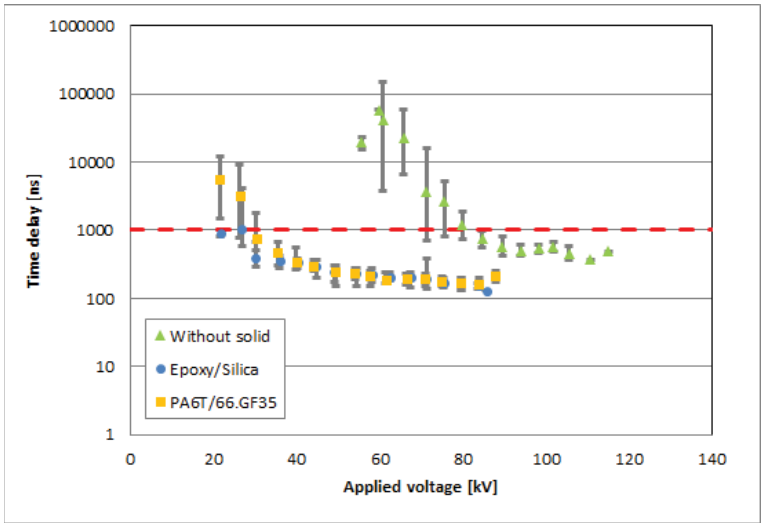

Fig. 44: Time delay for first streamers without solid, with Epoxy/Silica and PA6T/66.GF35 at 0.3 MPa.

3.11. Correlation with breakdown measurements

In breakdown measurements carried out in divergent field (point-plane) in *Chapter 3*, the discharge inception voltage was much lower than the breakdown voltage. Consequently, the inception conditions did not influence the breakdown voltage (*Chapter 3*). However, with less divergent fields such as with the sphere electrode (*Chapter 3*, Fig. 41) the difference between inception voltage and breakdown voltage is much reduced. With low permittivity solids (ε_r = 2.5), they become nearly identical, and breakdown becomes then controlled by discharge initiation. In these conditions, initiation conditions should become of major importance in breakdown measurements. This point was not investigated in detail in this work. We may however anticipate that the nature of solid could get a much larger influence compared to our breakdown measurements. This point should be checked in future measurements.

4. Evidence of charges remaining on the solid surface after discharges

The role of charges remaining on the solid insulator during breakdown measurements was estimated in *Chapter 3* via the influence of the sample water content. Since almost no influence of water was observed, while water strongly accelerates surface potential decay, it was concluded that charges that may accumulate on solids when series of impulses are applied has a minor influence on the breakdown process. In order to get a better insight on this question, several complementary measurements were carried out by measuring the surface potential after streamers or breakdown with electrostatic probes.
All measurements were performed at atmospheric pressure for technical reasons (it was not possible to introduce field and voltage probes in the high pressure test cell). Two different probes were used to measure either electrical field or surface potential induces by charges.

4.1. Field probe

After a series of impulses at fixed voltage, the probe was placed after 30 s in front of the solid insulator center, at a fixed distance (2 cm). Measurements were performed on Epoxy/Silica (Tab. 2), PA6T/66.GF35 (Tab. 3), and PP (Tab. 4). From field measurements and from the distance between probe and surface, values of the surface potential were calculated.

	Potential [kV]		
Voltage [kV]	**1 shot**	**5 shots**	**10 shots**
-22	- 4.8	- 5.0	- 4.7
-36	- 5.0	- 5.2	- 4.9
-47	- 6.6	- 5.7	- 5.3
-69	- 4.5	- 7.5	- 5.4
-91	- 7.4	- 0.4	-
-101	-	- 0.1	- 0.1
+ 26	+ 1.8	+ 1.9	+ 2.0
+ 37	+ 1.9	+ 2.2	+ 2.3
+ 48	+ 2.1	+ 0.5	-
+ 55	+ 0.2	+ 0.1	+ 0.2

Tab. 2: Potential measurements on Epoxy/Silica (parallel field) in negative and positive polarity. Red values correspond to the breakdown.

	Potential [kV]		
Voltage [kV]	**1 shot**	**5 shots**	**10 shots**
- 25	- 1.7	- 2.1	- 2.5
- 36	- 4.1	- 4.0	- 4.0
- 47	- 4.9	- 7.5	- 6.4
- 70	- 8.7	- 8.4	- 7.8
- 92	- 7.0	- 0.2	-
- 109	- 0.2	- 0.4	- 0.8
+ 26	+ 1.1	+ 1.9	+ 2.7
+ 34	+ 2.7	+ 3.1	+ 2.7
+ 48	+ 2.5	+ 0.2	-
+ 54	+ 0.0	- 0.0	+ 0.0

Tab. 3: Potential measurements on PA6T/66.GF35 (parallel field) in negative and positive polarity. Red values correspond to the breakdown.

Tab. 2, 3 and 4 first show that charges of the same polarity of the impulse can be detected. They also show that series of 1, 5, or 10 shots inducing streamers provide almost the same final value of the surface potential. No clear effect of accumulation during series of streamers can be evidenced. When breakdown occurs, surface potential measured immediately after is close to zero: almost no charges remain on the solid's surface.
Comparing the results of Tab. 2, 3, 4 shows no obvious influence of the solid's nature.

Contrarily than with Epoxy/Silica and PA6T/66.GF35, measurements with PP were performed with the probe placed at a distance of 7 mm from the solid.

	Potential [kV]		
Voltage [kV]	**1 shot**	**5 shots**	**10 shots**
+ 25	+ 1.7	+ 2.5	+ 2.5
+ 37	+ 1.6	+ 1.8	+ 1.9
+ 48	+ 2.2	- 0.1	-

Tab. 4: Potential measurements on PP (parallel field) in positive polarity. Red values correspond to the breakdown.

4.2. Surface potential probe

This probe of smaller size could be scanned over the sample surface. Fig. 45 shows the trajectory of the probe over the solid surface. The probe was placed at 3 mm from the surface. Measurements were also done 30 s after high voltage shots.

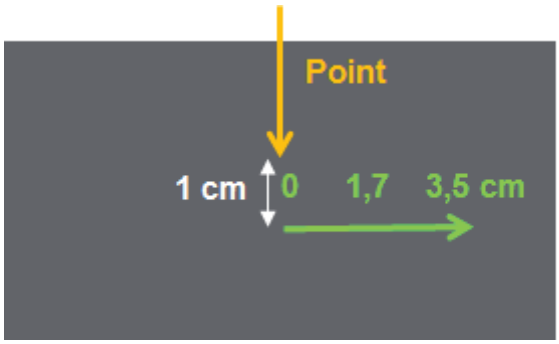

Fig. 45: Protocol of potential probe's movement.

On Fig. 46, we can observe that by increasing the applied voltage, the surface potential at the sample edge (3.5 cm) also increases. Closer to the point (0 and 1.7 cm) a sudden drop is observed when the potential exceeds about 9 kV (corresponding to an applied voltage above 33 kV). The potential close to the point then drops to about 5 kV. The same is also observed on Fig. 47.

When breakdown occurs, the surface potential drops to 0 V, excepted at 3.5 cm (i.e. far from the breakdown spark).

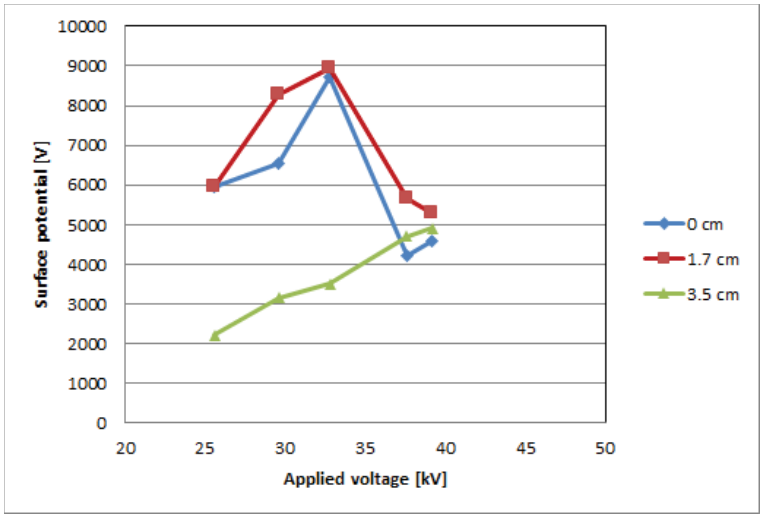

Fig. 46: Surface potential measurements on Epoxy/Silica in parallel field.

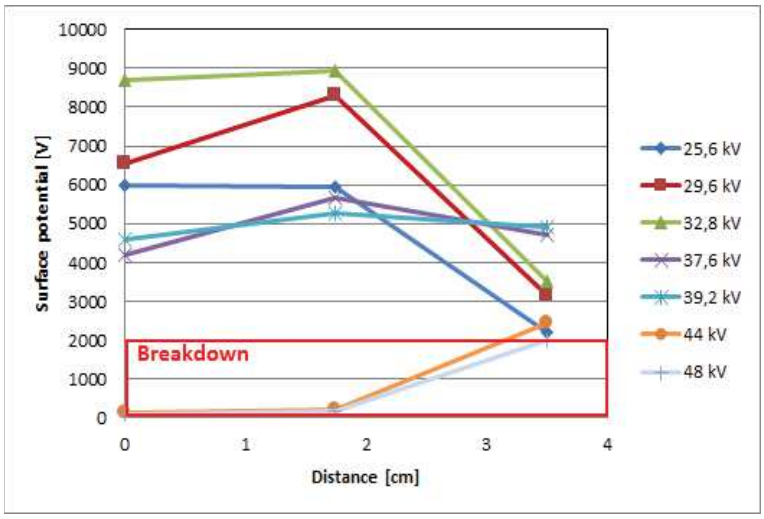

Fig. 47: Surface potential measurements on Epoxy/Silica in parallel field.

Figs. 48, 49 shows the same measurements on PA6T/66.GF35. With this solid, nearly identical potential is measured at the sample edge compared to Epoxy/Silica. Close to the point, lower values of potential are measured (e.g. 5 kV instead of 9 kV at 0 cm / 33 kV). At 0 cm (i.e. below the point) instead of first rising up to 9 kV and then dropping to 5 kV, the potential seems to saturate at this value since the lowest applied voltage. When it occurs, breakdown also removes accumulated charges.

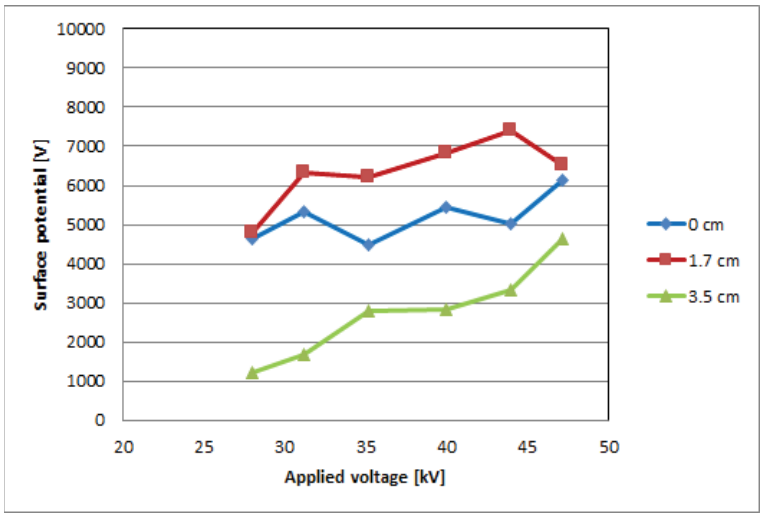

Fig. 48: Surface potential measurements on PA6T/66.GF35 in parallel field.

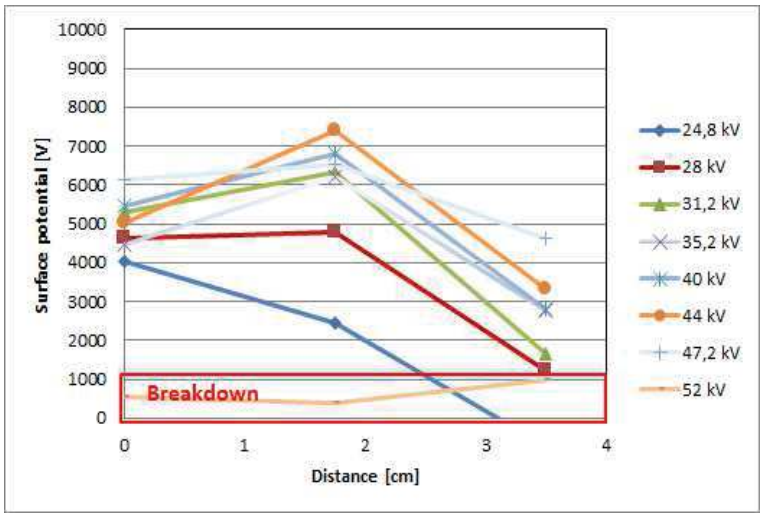

Fig. 49: Surface potential measurements on PA6T/66.GF35 in parallel field.

4.3. Discussion about influence of surface charges

These experiments provide an evidence of surface potential (and hence charge) induced by streamers, with the same sign of applied voltage. Breakdown sparks are observed to erase this charge. The absolute value of measured potentials (up to 10 kV) is not negligible compared to the applied voltage. These observations agree with previous similar measurements in air [12, 13].

Unfortunately, the size of probes prevents from obtaining precise data in the region of the triple point. The first measurements are located 1 cm from this point. Measurements also cannot be done during the voltage impulse, but only when the applied voltage is back to zero.

The influence of water in breakdown experiments provided some evidence that accumulated charges before the impulse play a minor role in the breakdown process. In a similar way, measurements dealing with inception voltage (*Section 2* above) with solids did not provide evidence of the influence of accumulated charges in the triple point region. As compared with the case of air alone, where no charge accumulation occurs, higher inception voltages should occur with solids, since accumulated charges on the surface should reduce the field on the electrode. However, in our measurements, inception voltages with solids were lower in most cases (or equal in the case of PP).

The main reason for this is probably that surface charges induced by streamers during the impulse in the immediate vicinity of the triple point are quickly neutralized when the voltage comes back to zero. When voltage drops to zero, the surface charge left by streamers induces a high reverse field close to the electrode, which may induce:

- either a surface conduction current (such as in Potential Decay experiments) leading to removal of charges;
- or even a “back discharge” if the reverse field is high enough.

This hypothesis is supported by:

- the observation by [14] showing logically no charges or potential in the immediate vicinity of the high voltage electrode after the impulse;
- the detection of “back discharges” in a triple point geometry, of opposite polarity of the impulse voltage, when the impulse voltage goes back to zero [12].

The sudden drop of surface potential close to the point when this potential exceeds some critical value (9 kV) supports the hypothesis of a “back discharge”. Since this potential was measured at 1 cm from the point, a reverse field of 10 kV/cm constitutes a sufficient value able to induce a surface “back discharge”. The fact that the triple point region could be “discharged” after each impulse can explain that no evidence of charge accumulation on inception voltage could be obtained.
Conversely, static charges remaining in the middle of the gap prior to impulses may influence the propagation of the first surface discharge. None of the measurements carried out here allow evidencing such influence.

5. Conclusion

In this chapter, pre-breakdown phenomena were studied. Visualizations were performed to describe the steps of development of the discharge without and with solid. Before breakdown, two streamers are developing: a “surface” streamer and a “volume” streamer.

Breakdown phenomena are complex with and without solid. Several modes of breakdown were observed depending on the pressure, material and electrode geometry. With our setup, PDs always occur before breakdown, the initiation of the discharge is not controlling the breakdown voltage. Streamers are propagating to the grounded plane without breakdown. We can conclude that propagation of streamers is not the adapted criterion to control the breakdown. It is when there is the transition from streamer to spark, that breakdown occurs. However, this result is not valid at 0.3 MPa without solid. In this case, streamers propagation is controlling the breakdown voltage.
In the presence of a solid, for all pressures tested, it is the transition from streamer to spark which is controlling the breakdown.

In the second part of this chapter, we studied the initiation of surface and volume streamers. This initiation of the surface streamer is dependent on the solid nature in the case of PP and PTFE. We could also observe that with these two materials, time to initiate is strongly delay compared to Epoxy/Silica. These results can be significant and can influence the breakdown voltages if measurements are performed with standard lightning impulse (shorter tail).

Bibliography

[1] P. Rain and O. Lesaint, “Prebreakdown phenomena in mineral oil under step and AC voltages in large gap divergent fields”, IEEE Trans. On Diel. And Elec. Insul., vol.1, n°4, pp.692-701, 1994.

[2] Stat-Arc™ hand-held electrostatic fieldmeter Model 255, Monroe Electronics.
Link: http://www.monroe-electronics.com/ESD/pdf/255_ob-manual.pdf

[3] Trek website, Measuement and Power Solutions™.
Link: http://www.trekinc.com/products/341B.asp

[4] L. A. Lazaridis and P. N. Mikropoulos, “Flashover along cylindrical insulating surfaces in a non-uniform field under positive switching impulse voltages”, IEEE Transactions on Dielectrics and Electrical Insulation, Vol. 15, No. 3, June 2008.

[5] V. V. Timatkov, G. J. Pietsch, A. B. Saveliev, M. V. Sokolova and A. G. Temnikov, “Influence of solid dielectric on the impulse discharge behaviour in a needle-to-plane air gap”, J. Phys. D: appl. Phys. 38 877-886, 2005.

[6] L. Trémas, O. Lesaint, N. Bonifaci, B. Ohl and F. Gentils, “Breakdown in air along insulating solid surfaces of different natures, parallel or perpendicular to the field direction”, IEEE Conf. on Elec. Insul. and Diel. Phen. (CEIDP), Toronto (Canada), Oct. 16-19, 2016.

[7] A. Pedersen, T. Christen, A. Blaszczyk and H. Boehme, “Streamer inception and propagation models for designing air insulated power devices”, Proc. of the Conference on Electrical Insulation and Dielectric Phenomena, 2009.

[8] F. Mauseth, J. S. Jorstad and A. Pedersen, “Streamer inception and propagation for air insulated rod plane gaps with barriers,” CEIDP CEIpp. 732-739, 2012.

[9] R. Ono and T. Oda, “Formation and structure of primary and secondary streamers in positive pulsed corona discharge-effect of oxygen concentration and applied voltage”, J. Phys. D: Appl. Phys., 36(16):1952-1958, 2003.

[10] P. Atten and A. Saker, “Streamer propagation over a liquid/solid interface”, IEEE Transactions on electrical insulation, 28(2), 230-242, 1993.

[11] AlphaLab Inc.
Link: https://www.trifield.com/content/tribo-electric-series/

[12] L. Caliap, « Etude de l'optimisation des isolants d'un point de vue diélectrique pour les contraintes du GIS », Thèse de doctorat (institut polytechnique de Grenoble), Septembre 2010.

[13] J. Deng, A. Kumada, K. Hidaka, G. Zhang and H. Mu, "Residual charge density distribution measurement of surface leader with feedback electrostatic probe", Appl. Phys. Lett., vol. 100, p. 192906, May 2012.

Conclusions and Perspectives

The context of this work is the SF_6 replacement for global warming reason. Several medium voltage devices are concerned by the substitution of SF_6 by alternative gases. In several cases, compressed air can constitute a possible solution, and this study was mainly devoted to this gas. When the gas nature is changed from SF_6 to air, the dielectric withstand may decrease, and some creeping discharges and tracking phenomena can occur if the system was not properly redesigned. To solve this problematic, it is important to work upstream on the creeping discharge phenomena in air, to get a better overview of mechanisms occurring at medium voltage at the gas/solid interface.
Before starting this work, we have reviewed several physical phenomena involved in creeping discharge phenomena. First we detailed the development of discharges in gas, which is rather well known. From this point, it was possible to analyze the different previous studies carried out on the complex phenomena of discharges in the presence of solid insulator. Several physical processes induced by the presence of an insulating solid occur, such as the distortion of the electric field at the triple point, and the possible presence of charges remaining on the dielectric. Some features of pre-breakdown phenomena on dielectric surfaces were described: localizations of streamers, streamer velocity and streamer length. The last point of this review was the work carried out on breakdown voltage measurements, essential for the design of medium voltage apparatus. The influence of solid nature on breakdown voltage appeared still under debate: it remained difficult to provide a general interpretation of parameters such as permittivity or material nature, since contradictory results were available. Furthermore, several other questions such as the influence of surface charges or the sequence of pre-breakdown phenomena in a wide range of conditions remained without answer. Based on this review, we have defined experimental investigations which allows a better comprehension of the creeping discharge phenomena.

We first selected a large range of insulating solids: Epoxy/Silica which is the material of reference for Schneider Electric, new industrial material: PA6T/66.GF50, and several materials selected for their various permittivity (Alumina, glass, PC, …). We characterized them with Surface Potential Decay, dielectric spectroscopy and absorption current measurements. From these measurements, we could correlate some material's properties with breakdown and pre-breakdown measurements, such as the influence of surface charges (strongly modified by the presence of water), and permittivity.
A test setup allowing to measure breakdown voltage due to creeping discharge propagation was developed. Indeed, with some setups used in literature (uniform field and weakly divergent field) the breakdown voltage is dependent on the initiation of the discharge, and breakdown measurements cannot be properly compared with other studies. Two types of electrode systems were selected: a point-plane non-uniform field (0.5 mm radius, 5 cm distance), and another less divergent with a 5 mm sphere. We also defined two electric field configurations: "parallel" and "perpendicular", representing two extreme cases in apparatus.

Breakdown measurements were performed, and it appeared that relative permittivity is the only adequate parameter that impacts the dielectric withstand in all geometries: water content and chemical nature have only and indirect influence. We could also conclude that surface charges have no large influence on the breakdown process, since no obvious influence of the water content was recorded, except that due to a small modification of permittivity.

The “perpendicular” field configuration appeared to constitute by far the most critical one for applications: the lowest breakdown voltages were recorded in this geometry, and almost no beneficial effect was observed when pressure was increased up to 0.3 MPa. In “parallel” field, breakdown voltages were higher and a positive impact of pressure was recorded. Results obtained at 0.2 MPa were the only one showing no influence of the material nature. No convincing reason for this abnormal behavior was found. A dependence of the localization of the breakdown spark on pressure was also evidenced.

The last investigations concerned pre-breakdown streamers, with a detailed study of initiation, and of the sequence of events leading to breakdown. Transient current measurements were performed with a setup allowing measuring low discharge currents under impulse voltage, correlated with fast visualizations. From visualizations, we can describe the sequence of streamers leading to breakdown in the parallel field geometry.

At atmospheric pressure without solid, streamers initiate, propagate to the plane, and breakdown occurs at even higher voltage required for streamer to spark transition. With solid, the scenario is slightly different: surface streamers first propagate during the impulse rise time, followed by volume streamers at slightly higher voltage. As in air at atmospheric pressure, the transition from streamers to spark occurs at higher voltage, and determines the breakdown voltage. Since both surface and volume streamers propagate below the breakdown voltage, the breakdown spark can randomly occur from either type of surface or volume streamers.

By increasing pressure, other breakdown modes were observed. Both surface and volume streamers were recorded, but it was observed that surface streamer propagation was favored compared to volume: at the same voltage, volume streamers were much shorter than surface ones. It is possible to conclude that depending on the setup and the experimental conditions, breakdown voltage can be controlled by different steps of development of the discharge.

From voltage and time to initiate the discharge, we could observe that the presence of most of solids studied degraded the inception voltage of the discharge, compared to the case without solid. This degradation is surely due to the local field enhancement at the triple point formed by the point, the solid and the air. However, with two solids (PP and PTFE), a reversed behavior was observed, with inception voltages equal or even higher than in air alone. Based on these observations, we can conclude that the field enhancement at the triple point is not the only mechanism affecting discharge initiation. In these experiments,

the material nature induces a specific modification of the initiation process, which tends to compensate the deleterious influence of the field enhancement due to permittivity.

In this experimental study, several materials properties were observed to get an influence on the creeping discharge process. Different breakdown modes were highlighted with a description of steps leading to breakdown from 0.1 to 0.3 MPa. However, a large number of experiments could be performed to get a further comprehension of the physical process involved, and try to verify several hypotheses. A non-exhaustive list of questions could be addressed:

- Breakdown measurements could be carried out with a less divergent field (such as the sphere-plane system used here), in order to further document the influence of solid's nature on initiation. For instance with solids such as PP, we may expect a subsequent increase of breakdown voltage compared to other materials;
- In which conditions does the transition from streamer to leader occur ? Several papers as well as results obtained here at high pressure and high permittivity suggest that this process could explain transitions in the breakdown voltage in these conditions. The physical nature of pre-breakdown events could be further documented by a spectroscopic study of emitted light, as well as by time resolved measurements of propagation velocities and transient currents;
- The use of a standard lightning impulse (1.2/50 µs), closer to the applications test methods, could induce slightly different results in conditions where long inception delay times were recorded (e.g. in air alone or with PP);
- Other solids known to get a high electron affinity (e.g. PVC) could be investigated to check the hypothesis of the possible correlation between tribo-electric properties and initiation.

List of publications during Ph. D. work

L. Trémas, O. Lesaint, N. Bonifaci, B. Ohl and M. Hassanzadeh, “Measurements of surface potential decay on polyphthalamide (PPA) composite”, IEEE Conf. on Diel. (ICD), Montpellier (France), July 3-7, 2016.

L. Trémas, O. Lesaint, N. Bonifaci, B. Ohl and F. Gentils, “Breakdown in air along insulating solid surfaces of different natures, parallel or perpendicular to the field direction”, IEEE Conf. on Elec. Insul. and Diel. Phen. (CEIDP), Toronto (Canada), Oct. 16-19, 2016.

L. Trémas, O. Lesaint, N. Bonifaci, B. Ohl and F. Gentils, “Creeping discharge in air: streamers visualizations and transient current”, International Symposium on High Voltage Engineering (ISH), Buenos Aires (Argentina), August 28 – September 1, 2017.

L. Trémas, O. Lesaint, N. Bonifaci, B. Ohl and F. Gentils, “Inception of the solid material nature on the inception of creeping discharges in air”, IEEE Conf. on Elec. Insul. and Diel. Phen. (CEIDP), Fort Worth (U. S. A.), Oct. 22-25, 2017.

Annex 1

Sample conditioning: drying and impregnation by water

To evaluate the effect of water present in the material bulk on dielectric properties and breakdown voltages, two extreme conditions were used: either thoroughly dried or impregnated with water. As we will see later, the presence of water has a large influence on the material conductivity, and hence on its ability to either store or quickly dissipate surface charges. The presence of water will be later used to check the influence of accumulated surface charges on the creeping discharge process.

Drying procedure

At atmospheric conditions, materials contain an unknown amount of water. To control this amount of water in the material, a drying procedure was undertaken.

After molding, surface of samples is cleaned with ethanol to remove impurities. To remove water content within the material bulk, samples were placed in a vacuum oven at 90 °C. The variations of water content were then monitored by periodic weighing with a high-resolution balance (0.1 mg sensitivity). The stabilization of the weight provided a criterion to stop the drying procedure.

Fig. 1 shows that the time required to dry a sample depends on its nature. For Epoxy/Silica, Epoxy/silanized silica, Epoxy resin and PC, a stabilization is observed after two days. In contrast, PA6T/666.GF50 is completely dry after twelve days (due to a larger initial amount of water in the bulk, compared to other materials). This procedure was carried out on two different samples of each type to validate these results.

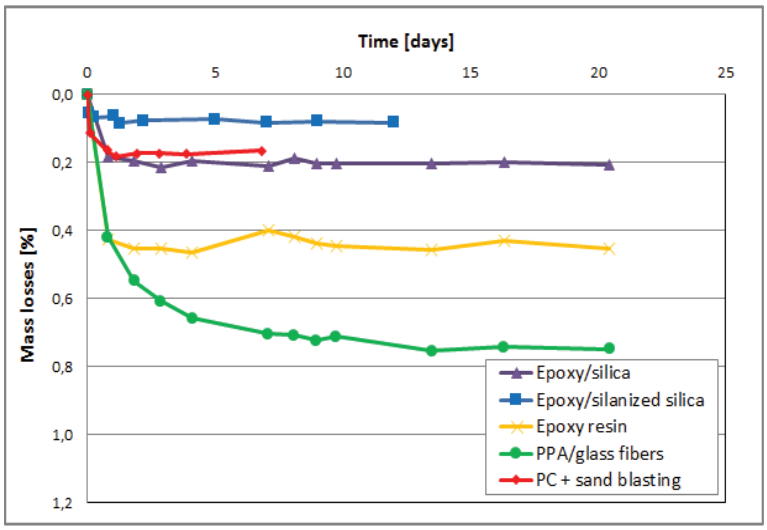

Fig. 1: Drying procedure according to solids' nature.

Impregnation procedure

Following the drying procedure, materials were then placed in a climatic chamber at 70 °C and 62 %RH (relative humidity), according to the ISO-1110 standard.

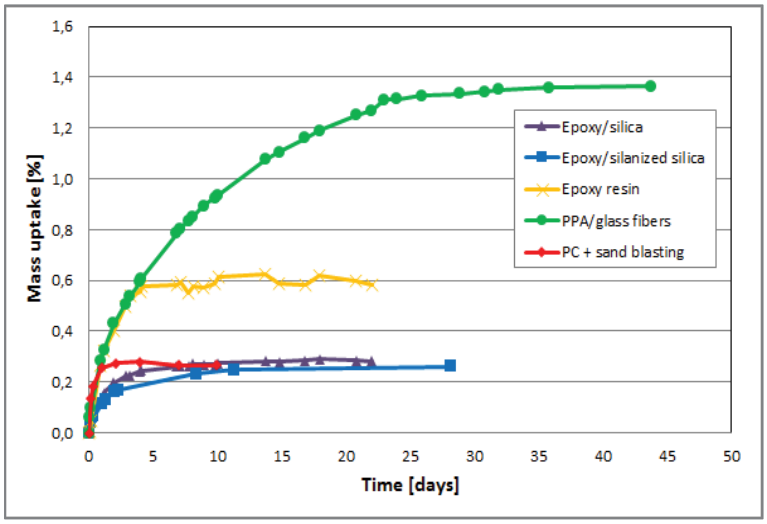

Fig. 2: Moisture uptake procedure according to solids' nature.

From Fig. 2, the classical Fick's diffusion law can be plotted, to describe diffusion of water in various materials. Fig. 3 shows an example of Fick's plot for PA6T/66.GF50. Similar results were obtained with others material of Fig. 2. The diffusion behavior of water may be considered to follow the Fickian-type diffusion. The solution for Fick's law at short times is reduced to the equation (1) for the initial stage of diffusion [1]:

$$\frac{M_t}{M_\infty} = 2\left(\frac{Dt}{\pi l^2}\right)^{1/2} \qquad (1)$$

Where M_t is the mass gain at short time, M_∞ is the maximum mass gain at the equilibrium state, and l is half the thickness of the sample.

Coefficients of Fick's law can be determined from the slope of the normalized weight change. In Fig. 3 it is possible to observe at short times a linear relationship between the increase of mass and the square root of time. From this linear part, it is possible to calculate the diffusivity with the slope.

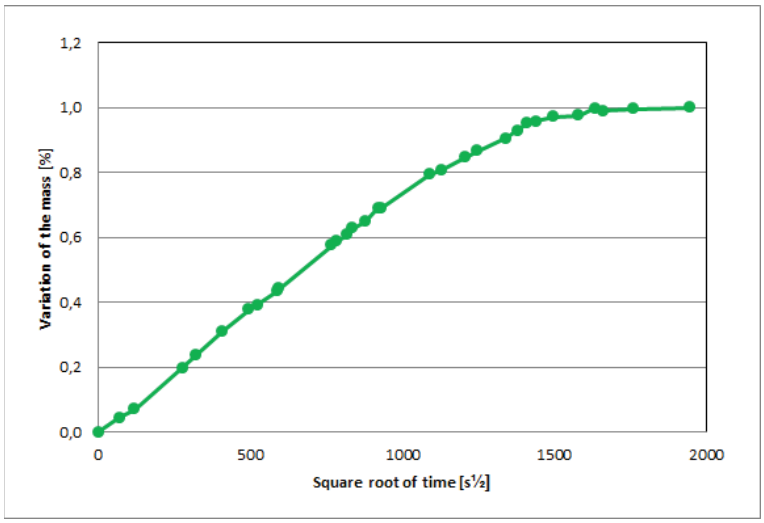

Fig. 3: Example of Fick's plot for PPA/Glass fibers.

The diffusion coefficient can be used to compare the diffusion rates of materials and to estimate how much time is needed to reach moisture saturation of a sample.
Tab. 1 summarizes the diffusion coefficients obtained for all samples tested. For each material, water uptake was carried out for two samples. Values in Tab. 1 correspond to an average of the two calculated diffusion coefficients. The three kinds of Epoxy get nearly the same diffusion coefficient. PA6T/66.GF50 shows the slowest diffusion coefficient, this explains the waiting time of forty days required to reach saturation.

	Epoxy resin	**Epoxy/Silica**	**Epoxy/Silanized silica**	**PA6T/66.GF50**
Diffusion coefficient $\left[\frac{m^2}{s}\right]$	3.8×10^{-12}	5.2×10^{-12}	3.3×10^{-12}	8.4×10^{-13}

Tab. 1: Diffusion coefficients for several materials.

Physico-chemical properties

This series of tests submitted materials to a large range of temperature. The material will go through different steps of transformation, depending of its nature. Several parameters can be measured, such as glass transition and loss weight.

Differential Scanning Calorimetry (DSC)

DSC measures the amount of energy absorbed or released by a sample when it is heated or cooled. The main goal is to study phase transitions, such as melting, glass transitions, or crystallization. In our case, only the glass transition was of interest.

Experimental system

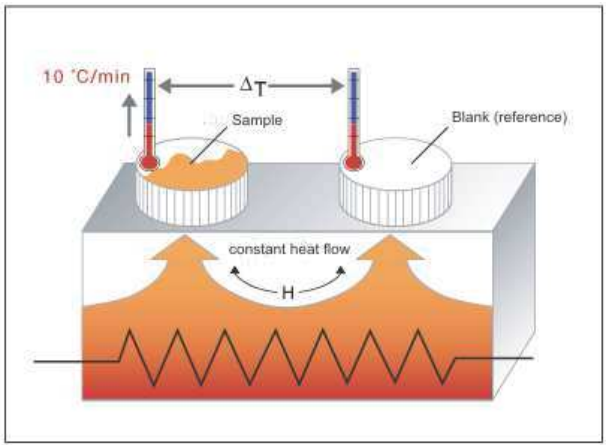

Fig. 4: Diagram of DSC set-up [2].

The sample is placed inside a crucible which is then placed inside the measurement cell (furnace) with a reference (Fig. 4). A temperature program is applied to the cell. Difference in temperature between the material and the reference is measured as a function of temperature.

Results

The measurement starts at 40 °C and finishes at 350 °C. The temperature gradient is 10 °C / min. Fig. 5 shows the result of a typical DSC experiment, the curve represents a heat flow versus temperature. It can be used to calculate enthalpies of transitions. This is done by integrating the peak corresponding to a given transition.

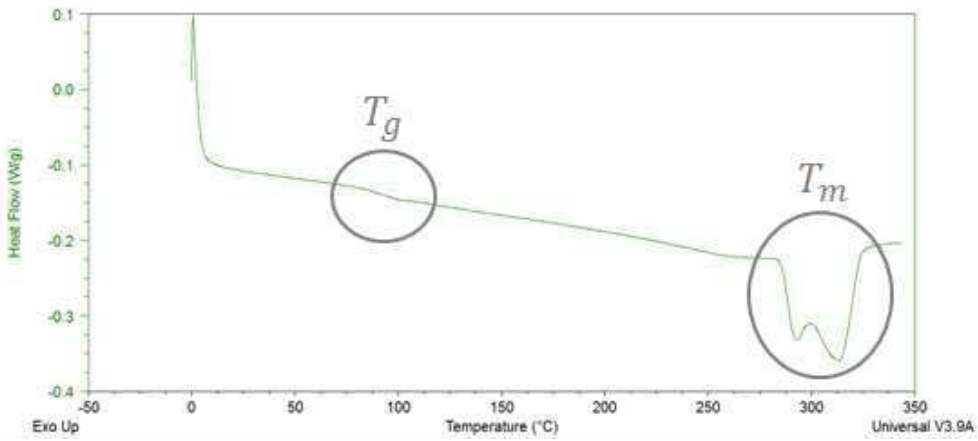

Fig. 5: Example of DSC curve for undried PA6T/66.GF50.

From Fig. 5, it's possible to extract the glass transition temperature (T_g) and melting temperature (T_m) of the material. T_g may occur as the temperature of an amorphous solid is increased. T_g is always lower than the melting temperature. These transitions appear as a step in the baseline of the recorded DSC signal. This is due to the sample undergoing a change in heat capacity.

Dry materials	Tg
Epoxy/Silica	129 °C
Epoxy resin	124 °C
PA6T/66.GF50	95 °C

Tab. 2: Values of glass transition temperatures for three dry materials.

Tab. 2 shows the glass transition temperatures for three different materials. Epoxy/Silica has the highest glass transition. Epoxy resin has a T_g value close to Epoxy/Silica. PA6T/66.GF50 shows the lowest value with a T_g of 95 °C. It was important to measure these values because in most of our experiments, materials were first placed in a vacuum oven at 90 °C. We must ensure that this temperature is high enough to dry materials, without reaching their glass transition temperature (and hence possibly modifying their structure).

Thermal Gravimetric Analysis (TGA)

Thermogravimetric analysis measures weight/mass change (loss or gain), and the rate of weight change as a function of temperature and time. In our study, this experiment can provide information concerning the thermal stability of materials.

Experimental system

On Fig. 6, the diagram of the experimental set-up consists of a furnace to control the heating rate, a thermocouple to measure the change in temperature, and a balance arm to measure the mass of the sample. The balance operates on a null-balance principle. At the zero, equal amounts of light shine on the two photodiodes. If the balance moves out of the null position, an unequal amount of light shines on photodiodes. Current is then applied to the meter movement to return the balance to null position. The amount of current applied is proportional to the weight loss or gain [3].

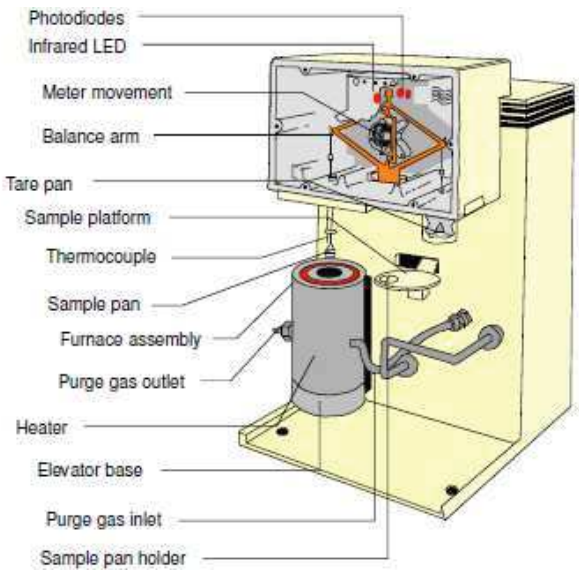

Fig. 6: Diagram of experimental set-up for TGA.

Results

The measurement starts at 40 °C and finished at 180 °C. Fig. 7 shows an example of TGA on PA6T/66.GF50 without preconditioning (undried). Variation of mass is weak (< 0.3 %) from 40 °C to 180 °C. Weight loss can come from several phenomena listed below:

- Decomposition: breaking of chemical bonds
- Evaporation: loss of volatiles compounds at elevated temperature
- Reduction: interaction of sample to a reducing atmosphere
- Desorption of water

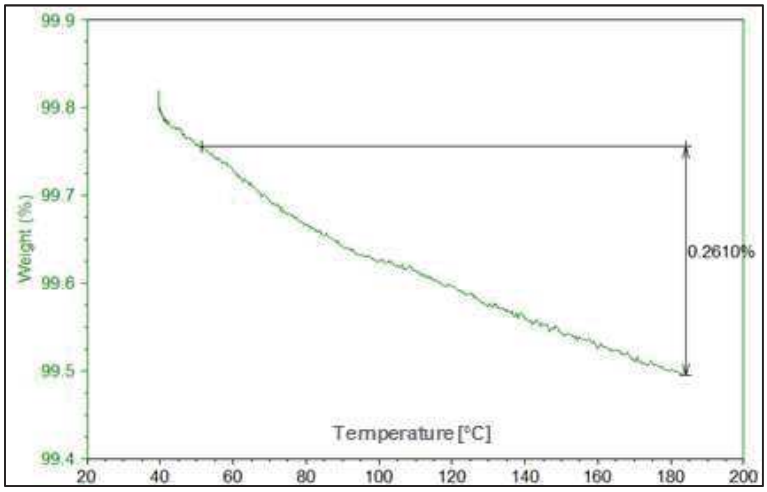

Fig. 7: Example of TGA for undried PA6T/66.GF50.

TGA measurements have been done with dry materials and undried materials. All the results are presented in Tab. 3 following.

	PA6T/66.GF50	Epoxy resin	Epoxy/Silica
Dry	0.0032 %	0.0308 %	0.0295 %
Undried	0.2610 %	0.2301 %	0.0684 %

Tab. 3: Weight loss for three materials with dry/undried conditions (max temperature: 180 °C)

The lowest weight variations concern dried samples. Indeed, the desorption process already took place during the drying procedure, so it's obvious that the loss of weight is less important than for undried samples. For undried conditioning, epoxy/silica has the smallest relative weight variation, surely coming from the high percentage of silica (60 %).

Bibliography

[1] N. Abacha, M. Kubouchi, T. Sakai, « Diffusion behavior of water in polyamide 6 organoclay nanocomposites », eXPRESS Polymer Letters Vol. 3, No. 4 245-255, 2009.

[2] Institut für Technische Chemie, Technische Universität Braunschweig.
Link: http://www.itc.tu-bs.de/Abteilungen/Makro/Methods/dsc.htm

[3] K. Mohomed, "Thermogravimetric analysis (TGA), Theory and applications", TA Instruments.

Annex 2

Investigations on streamer initiation in the presence of solids.

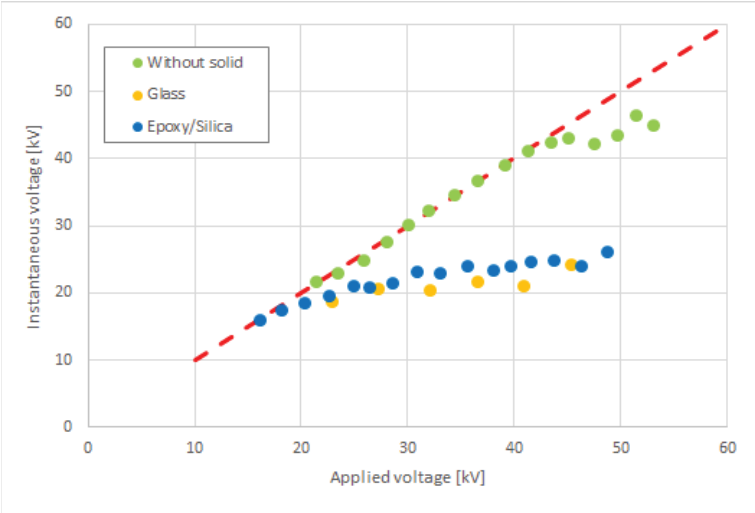

Fig. 1: Instantaneous inception voltage of first discharge without solid, with glass and Epoxy/Silica (parallel field, d = 5 cm, r = 0.5 mm, 0.1 MPa).

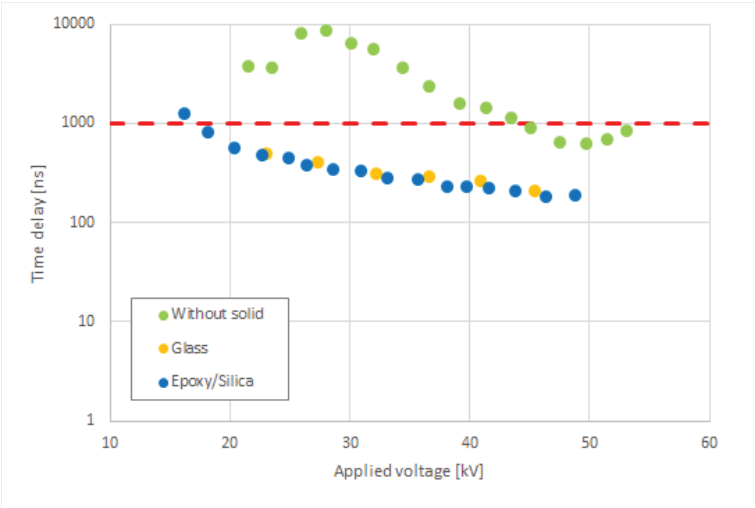

Fig. 2: Time delay for streamer without solid, with glass and Epoxy/Silica.

Pre-breakdown and breakdown phenomena in air along insulating solids

In the context of SF_6 replacement in medium-voltage apparatus, a study of mixed electrical insulation (gas (air) / insulating solid) was carried out. The aim is to determine the influence of the nature of the solid on breakdown voltage. For this purpose several materials have been selected such as epoxy / silica (reference material of Schneider Electric), PA6T / 66.GF50 (new material for this application) and several other materials allowing a better understanding of the phenomenon (PTFE, PC, PP, ...). The dielectric characterizations allowed us to measure potential decay, currents and permittivities according to the nature of the materials. From this data, breakdown measurements have been carried out. Two configurations of electric field were tested (parallel and perpendicular to the solid). The "point-to-plane" geometry was selected, allowing the observation of partial discharges before breakdown and therefore a study of the propagation of the discharge and not of the initiation. These measurements show the influence of the solid on the breakdown voltage, with an indirect influence of the nature of the material and its water content. In our configuration, the presence of a solid insulator lowers the dielectric strength. The relative permittivity is the main parameter influencing the breakdown voltage, with a reduction of it in the presence of materials with high permittivity (alumina). It was not possible to establish a link between surface potential decay measurements and breakdown voltages. In order to characterize the development of the electric discharge along the solid insulation, visualizations and transient current measurements were achieved. The visualizations allowed the observation two types of discharges before the breakdown. First, the development of a surface discharge "surface streamer", followed by a discharge in the gas "volume streamer". These observations lead us concluding that streamers leading to breakdown develop predominantly in air above the surface in the parallel field configuration. Current measurements provide information on the initiation of the discharge. There exists a reduction of voltage and initiation time of the discharge in the presence of a solid. Similar results have been obtained for a wide range of materials. However, several low permittivity materials (PTFE, PP) show a different behaviour, with higher and scattered time delay and initiation voltage, similar to those obtain in air without solid. It has been shown that initiation and propagation do not influence the breakdown voltage in point-plane geometry. The transition to breakdown mainly determines the breakdown voltage.

Key words: medium voltage apparatus, breakdown voltage, dielectric characterization, streamers, transient currents, visualizations.

Phénomènes de pré-claquage et claquage dans l'air le long d'isolants solides

Dans le cadre du remplacement du SF_6 dans les appareils moyenne tension, une étude de l'isolation électrique mixte (gaz (air) / solide isolant) a été réalisée. L'objectif étant de déterminer l'influence de la nature du solide sur la tenue au claquage. Pour cela plusieurs matériaux ont été sélectionnés tel que l'époxy / silice (matériau de référence chez Schneider Electric), le PA6T/66.GF50 (nouveau matériau pour cette application) ainsi que plusieurs autre matériaux permettant une meilleure compréhension du phénomène (PTFE, PC, PP, …). Les caractérisations diélectriques ont permis de mesurer des déclins de potentiel, des courants volumiques ainsi que des permittivités en fonction de la nature des matériaux. A partir de ces données, des mesures de claquage ont été effectuées. Deux configurations de champ électrique ont été testées (parallèle et perpendiculaire au solide). La géométrie « pointe-plan » a été sélectionnée, permettant l'observation de décharges partielles avant le claquage et donc une étude de la propagation de la décharge et non de l'initiation de celle-ci. Ces mesures ont permis de déterminer l'influence du solide sur la tension de claquage, avec une influence indirecte de la nature du matériau et sa teneur en eau. Dans notre configuration, la présence d'un isolant solide dégrade la tenue diélectrique. La permittivité est le paramètre influençant la tension de claquage, avec une réduction de celle-ci en présence de matériaux à forte permittivité (comme l'alumine). Aucun lien n'a pu être mis en évidence entre les mesures de déclin de potentiel et les tensions de claquage. Pour caractériser le développement de la décharge électrique le long de l'isolant solide, des visualisations et des mesures de courant ont été réalisés. Les visualisations ont permis d'observer deux types de décharges menant avant le claquage. Dans un premier temps le développement d'une décharge en surface « streamer de surface », puis celui d'une décharge dans le gaz « streamer de volume ». Ces observations ont permis de conclure que le streamer menant au claquage se développe majoritairement dans l'air en configuration de champ parallèle. Les mesures de courant ont apporté des informations sur l'initiation de la décharge, en montrant une réduction de la tension et du temps d'initiation de la décharge en présence d'un solide. Des résultats semblables ont été obtenus pour une large gamme de matériaux. Cependant certains matériaux de faible permittivité (PP, PTFE) se distinguent avec des tensions et des temps d'initiation retardés et aléatoires, semblables à ceux obtenus dans l'air sans solide. Il a été montré que l'initiation et la propagation n'influencent pas la tension de claquage en géométrie pointe-plan. Celle-ci est déterminée par la transition au claquage.

Mots-clés : appareillages moyenne tension, tension de claquage, caractérisation diélectriques, streamers, courant transitoires, visualisations.

Résumé en français

Introduction

Ce travail s'inscrit dans le cadre de la problématique du remplacement du SF_6 dans les appareils moyenne tension. Malheureusement, le SF_6 est le gaz à effet de serre le plus puissant et doit être remplacé dans les appareils moyenne tension dans les années à venir. Parmi les différents gaz qui pourraient être utilisés comme bons substituts du SF_6, l'air comprimé peut être une alternative acceptable dans plusieurs cas. En effet, des phénomènes de décharge très différents se produisent lorsque le SF_6 est remplacé par d'autres gaz, et par conséquent les règles de conception doivent être adaptées et redéfinies en conséquence.
A l'interface entre le gaz, le solide diélectrique et le métal (appelé "point triple"), l'initiation des décharges est favorisée. Il est également généralement admis que la propagation des décharges est favorisée le long des surfaces diélectriques (décharges rampantes).
Il reste nécessaire de travailler sur la problématique des points triples, des décharges rampantes et des phénomènes de claquage, notamment en étudiant une large gamme de matériaux isolants. C'est l'objet principal de cette thèse. Cette question sera abordée principalement à titre expérimental, car aucun modèle n'est aujourd'hui en mesure de prédire le comportement des décharges rampantes sur un matériau spécifique. Les expériences incluront une étude détaillée des étapes conduisant au claquage sous choc de foudre (phénomènes de "pré-claquage"). Il sera également essentiel de bien caractériser les matériaux solides afin de comprendre l'influence de paramètres tels que la permittivité, la teneur en eau ou les charges de surface sur les phénomènes de décharge et de claquage.

Chapitre 1 : Etat de l'art sur les décharges rampantes sur isolant solide

Dans ce chapitre, nous avons examiné plusieurs aspects liés aux décharges rampantes : la physique de base des décharges dans l'air et les observations antérieures sur les décharges rampantes. Ce sujet a été abordé depuis longtemps, mais des études détaillées restent cependant nécessaires pour mieux caractériser, comprendre et modéliser les processus physiques complexes impliqués. Par rapport au cas d'une décharge se développant dans le gaz seul, la présence d'un isolant solide induit plusieurs effets différents, qui peuvent influer à la fois sur l'initiation de la décharge (modification de la géométrie du champ au point triple gaz/métal/solide isolant) et sur sa propagation lorsque la décharge se propage sur le solide. Il reste cependant difficile de fournir une interprétation générale à partir des expériences publiées, car les phénomènes de pré-claquage sont fortement dépendants des conditions utilisées (géométrie des électrodes, forme de l'impulsion de tension, etc.). De nombreuses questions restent sans réponse claire :

- Influence de la charge de surface lors des essais de claquage ?

- Influence du solide sur les différentes étapes du processus de claquage (initiation, propagation, transition vers le claquage) ?
- Influence de la géométrie du champ ? La plupart des expériences ont été obtenues avec une surface parallèle au champ, mais dans les systèmes réels beaucoup d'autres géométries sont présentes.
- Influence de la pression du gaz ? Cette question a été abordée dans très peu d'articles.
- Quels sont les paramètres solides pertinents ? Nature chimique ? Permittivité ? Teneur en eau ?

L'objectif premier de ce travail est d'étudier l'influence de la nature du solide sur la tension de claquage et d'essayer d'établir une classification des solides. Cette question sera abordée de manière expérimentale, en accordant une attention particulière à plusieurs points :

- L'étude de la séquence des événements de pré-claquage (initiation, propagation, transition au claquage) dans différentes conditions de champ et de pression. Objectif : pouvoir étudier sélectivement l'influence des solides sur chacune de ces phases.
- Le contrôle des charges de surface restantes par le contrôle de la teneur en eau de l'échantillon. Des expériences antérieures avec des époxy composites ont montré que l'évacuation des charges de surface peut être considérablement modifiée par la présence d'eau.
- Sélection et caractérisation d'une large gamme de solides, comprenant à la fois des composites industriels et des matériaux purs.

Chapitre 2: Les isolants solides : sélection et caractérisation

Dans ce chapitre, plusieurs matériaux ont été sélectionnés pour étudier plusieurs de leurs propriétés supposées avoir une influence sur le processus de décharge rampante : permittivité, conductivité, présence d'eau, capacité de stockage ou de dissipation des charges de surface. À partir de ces résultats, nous serons en mesure d'établir une corrélation entre les mesures de claquage et les mesures de pré-claquage des chapitres 3 et 4.

Le déclin de potentiel de surface met en évidence les différences entre les matériaux en ce qui concerne le comportement des charges de surface par rapport au temps. Dans certaines situations, ces résultats peuvent être corrélés aux mesures de courant d'absorption. Le DPS est le plus rapide sur le PA6T/66.GF50 car il possède la plus faible résistivité. Ces données seront utilisées plus tard pour évaluer l'influence des charges de surface lors d'expériences de décharges rampantes avec ces matériaux. Pour les mesures de claquage en "champ perpendiculaire" décrites plus loin, la géométrie du champ sera identique à celle qui existe lors des expériences de DPS (c'est-à-dire champ principal perpendiculaire à la surface). Par conséquent, le comportement du DPS observé ici peut être utilisé correctement pour analyser les résultats. Dans la deuxième configuration (mesures de claquage en "champ parallèle"), la

direction du champ sera différente, mais nous supposerons que la classification des solides en ce qui concerne leur capacité à stocker ou à dissiper les charges de surface demeure la même. Les valeurs de permittivité à 1MHz seront utilisées pour étudier l'influence de la permittivité sur la tension de claquage.

Chapitre 3: Influence de la nature du solide sur la tension de claquage

Dans ce chapitre, une large gamme de matériaux a été testée pour étudier l'influence de la nature des solides sur les mesures de claquage. Un système d'électrodes adéquat a été choisi pour que la tension de claquage ait une incidence sur la propagation des décharges et la transition au claquage, plutôt que sur l'initiation de la décharge (présence de décharges partielles à une tension inférieure au claquage).
Deux géométries de champ typiques ont été étudiées, le champ étant parallèle ou perpendiculaire à la surface solide. Le champ d'application réel se situe généralement entre ces deux situations extrêmes.

Il résulte de ces résultats que la tension de claquage est principalement fonction de la permittivité relative des matériaux. La nature chimique et la teneur en eau n'ont qu'une influence indirecte sur le claquage, en modifiant la permittivité. Dans toutes les géométries étudiées, une augmentation de la permittivité induit une réduction de la tension de claquage. Une seule exception a été observée avec des mesures en champ "parallèle" à 0,2 MPa.
En présence d'un solide, la pression a un impact positif principalement en géométrie de champ "parallèle", et presque aucune influence en champ "perpendiculaire". Comme de faibles tensions de claquage sont toujours mesurées dans cette géométrie, cette situation est clairement la plus critique.

L'influence de la teneur en eau de l'échantillon n'est démontrée que par son influence sur la permittivité. Cela indique que l'accumulation de charges sur le solide pendant les mesures de claquage a un impact négligeable sur le processus de claquage. Cette conclusion se fonde sur le fait que l'eau a un impact important sur le déclin de potentiel de surface (chapitre 2). La même conclusion peut être tirée des mesures de claquage effectuées avec différents matériaux ayant un déclin de potentiel de surface assez différent.
Dans le chapitre suivant, nous étudierons les phénomènes de pré-claquage. Cela permettra de mieux comprendre les processus réellement impliqués dans les expériences de claquage et l'influence des surfaces solides.

Chapitre 4 : Streamers de pré-claquage : étude de l'initiation et de la séquence des événements conduisant au claquage

Dans ce chapitre, nous avons étudié les phénomènes de pré-claquage. Des visualisations ont été effectuées pour décrire les étapes de développement de la décharge sans et avec solides. Avant le claquage, deux streamers se développent : un streamer de surface et un streamer de volume.

Les phénomènes de claquage sont complexes avec et sans solide. Plusieurs modes de claquage ont été observés selon la pression, le matériau et la géométrie de l'électrode. Avec notre configuration, les DP se produisent toujours avant le claquage, l'initiation de la décharge ne contrôle pas la tension de claquage. Les streamers se propagent jusqu'au plan sans claquage. On peut conclure que la propagation des streamers n'est pas le critère qui maîtrise le claquage. C'est lorsqu'il y a une transition entre le streamer et l'étincelle que le claquage se produit. Cependant, ce résultat n'est pas valide à 0,3 MPa sans solide. Dans ce cas, la propagation des streamers contrôle la tension de claquage.
En présence d'un solide, pour toutes les pressions testées, c'est la transition streamer à étincelle qui contrôle le claquage.

Dans la deuxième partie de ce chapitre, nous avons étudié l'initiation des streamers de surface et de volume. Cette initiation des streamers de surface dépend de la nature solide dans le cas du PP et du PTFE. Nous avons également pu observer qu'avec ces deux matériaux, le temps d'initiation est fortement retardé par rapport à l'époxy/silice. Ces résultats peuvent être significatifs et influer sur les tensions de claquage si les mesures sont effectuées avec des impulsions de choc de foudre standard.

Conclusions et perspectives

Dans le cadre de cette étude expérimentale, plusieurs propriété matériau ont été observées pour faire un lien avec le processus de décharge rampante. Différents modes de claquage ont été mis en évidence avec une description des étapes conduisant au claquage de 0,1 à 0,3 MPa. Cependant, un grand nombre d'expériences pourraient être réalisées pour mieux comprendre le processus physique et essayer de vérifier plusieurs hypothèses. Une liste non exhaustive de questions pourrait être abordée :

- Les mesures de claquage pourraient être effectuées avec un champ moins divergent (tel que le système sphère – plan utilisé ici), afin de documenter l'influence de la nature du solide sur l'initiation. Par exemple, avec des solides tels que le PP, on peut s'attendre à une augmentation de la tension de claquage par rapport à d'autres matériaux ;

- Dans quelles conditions se produit la transition de streamer à leader ? Plusieurs articles ainsi que les résultats obtenus ici à haute pression et haute permittivité suggèrent que ce processus pourrait expliquer les transitions au claquage dans ces conditions. La nature physique des événements de pré-claquage pourrait être documentée davantage par une étude spectroscopique de la lumière émise, ainsi que par des mesures à résolution temporelle des vitesses de propagation et des courants transitoires ;
- L'utilisation d'un choc de foudre standard (1,2/50 µs), plus proche des méthodes d'essai pour les applications, pourrait donner des résultats légèrement différents dans des conditions où de longs délais d'initiation ont été enregistrés (par exemple dans l'air seul ou avec du PP) ;
- D'autres solides connus pour avoir une forte affinité électronique (par exemple le PVC) pourraient être étudiés pour vérifier l'hypothèse d'une corrélation possible entre les propriétés triboélectriques et l'initiation.